# Investigation of Some Small Molecule-Protein and Protein-Protein Interactions in Nicotine Addiction, Opioid Use Disorder, and COVID-19

Thesis by

Stephen Nicholas Grant

In Partial Fulfillment of the Requirement

for the Degree of

Doctor of Philosophy


CALIFORNIA INSTITUTE OF TECHNOLOGY

Pasadena, California

2022

(Defended July 12, 2021)

ORCID: 0000-0003-0923-8886

*For my family*

# Acknowledgments

I would like to thank my two advisors, Professor Dennis Dougherty and Professor Henry Lester. Dennis and Henry are two of the smartest and nicest people I have ever met. Their mentoring styles were unique; while Dennis gave me free rein, Henry ensured that I was precise with my experiments. While Henry is incredibly detailed-oriented and will launch into discussions about anything, Dennis was exceptional at keeping the big picture in view. Despite their differences, they were my biggest supporters, both in the good and the bad. Through the years, I have increasingly grown more confident in my abilities. Although this is goodbye in a sense, I look forward to seeing what comes next from this dynamic duo.

Next, I would like to thank my other two committee members: Professor David Tirrell and Professor Jacqueline Barton. To call these two titans of chemistry is an understatement, and yet they always had time to talk to me. Whether I was a budding second year trying to understand my thesis or a G6 defending their it, each time they always had my best interests in mind, and I cannot thank them enough for their support.

The Lester lab has given me a place to do my work for the past three years. This includes Anand Muthusamy, Zach Blumenfeld, Dr. Aaron Nichols, Dr. Kallol Bera, Dr. Bruce Cohen, Theo Chin, Laura Luebbert, Zoe Beatty, Eve Fine, and Elaine Lin. Special thanks to “Team Menthol,” which included Dr. Selvan Bavan, Dr. Matt Mulcahy, Dr. Saidhbhe O’Riordan, and Charlene Kim. Extra special thanks to Purnima Despande for managing the lab, Jonathan Wang for giving me great oocytes, and Dr. Brandon Henderson for being a great post-doc mentor and an even better friend. Although our research often diverged, I appreciate the

atmosphere that was cultivated in the lab. These are tremendously talented individuals, and I look forward to the many biosensor papers in the coming years.

It was truly a privilege to get to work in the Dougherty lab for the first three years of my Ph.D. To the former members of the Dougherty lab that I had the pleasure of overlapping with (Dr. Clint Reagan, Dr. Oliver Shafaat, Dr. Mike Post, Dr. Matt Rienzo, Dr. Matt Davis, Dr. Betty Wong, Dr. Catie Blunt. Dr. David Paul Walton, Dr. John Bryce Jarman, Dr. Annet Blum, and Dr. Richard Mosesso, Gabby Tender, and Kate Kutzer), thank you for making this lab a home. I was immediately drawn to this lab because of how amazing the students were. While I made many mistakes as a first year, the best decision I made during that time was joining the Dougherty lab. Whether it was going to see Taylor Swift, running races, or a number of other shenanigans, you all really made graduate school fun, and I appreciate your friendship. I'd also like to acknowledge some Dougherty lab members I did not overlap with but have gotten to know quite well. Dr. Chris Marotta and Dr. Tim Miles have stayed close to Caltech, and it's always nice when we get to talk. Finally, I have to thank the present Dougherty lab members, Dr. Hailey Knox and Dr. Coni Maldefassi. Both of them arrived during a pandemic and brought back life to Crellin 247. It was a lot of fun to talk about nAChRs again with you two.

Thankfully, many have been people outside of the Lester and Dougherty labs have made my time at Caltech fun and enjoyable. Mona Shahgholi ensured that the mass spectrometry lab was always in working order. Dr. Annie Moradian ran the Protein Expression Laboratory flawlessly. Dr. Andres Collazo and Dr. Giada Spigolon made complex imaging experiments relatively easy and were always happy to talk to me about microscopy. Outside of the science, the folks in

the Office of Residential Experience have been incredible to me. Dr. Felicia Hunt has been a great boss. The RLCs (Vanessa Tejada, Steven Metzmaker, Erica Crawford, and Kenny Carter) were amazing mentors for me as an RA The other RAs have also been excellent. I am grateful that I can call them my friends.

Fortunately, I was able to get off campus on occasion, and I met some amazing people. The folks at the Glendale pick-up lacrosse games and the Los Angeles Rowing Club have given me something to look forward to doing on Sundays or at 5 AM in the morning. Special thanks from these groups go out to Joe Campbell, John Seaver, Ken Hudson, Gary Bell, and Lily Lee.

I would be remiss if I failed to mention the teachers and advisors I had before Caltech. Professor Isaac Carrico at Stony Brook University accepted me into his lab while I was a freshman with no idea of what research actually entailed. Indeed, I didn't even know what a graduate student was. Nonetheless, he trusted me with my own project. He gave me a sense of independence that gave me the confidence to continue my scientific journey at Caltech. I would also like to thank some of my high school science teachers, most notably Dr. Hemmick and Mr. Gambino. Dr. Hemmick cultivated a love of chemistry that continues to inspire me. Mr. Gambino, despite my hesitation to take AP science classes, insisted that I enroll in them. Needless to say, it was a good decision.

Family is incredibly important to me, and during my time at Caltech, I found an incredible family in Fleming. Although I was just their RA, and they were a bunch of undergrads, the "Flems" were easily my favorite part about Caltech. The house dinners, strange traditions, and annual trips to Big Bear and the Rose Bowl are some of my favorite memories of my time at Caltech. Whenever I had a bad time in lab or things were just awful, I could always count on the Flems to put a smile

on my face by just being there. Fleming is truly an amazing house with even better people. It's safe to say that the hardest part about leaving Caltech is that I would also be leaving Fleming. All of you are incredible, and remember me when some of you get a Nobel Prize.

Finally, I have to thank my actual family. My brothers, Kenny, Dennis, Gary, Eric, Jonathan, and David…, oh, and Zack, are some of the funniest and most interesting people in the world. I am always amazed by you guys' creativity and just everything you do. I can't believe that I get to call you my brothers, and I get to spend time with all of you. I really hope that I've inspired you, and I hope you know that no matter what happens, we are together, and we will be together forever.

And, of course, my parents, Jim and Liz Grant, deserve all the credit for everything I've done here. I could list off all the amazing things that all great parents do, but something unique about my parents is that they never told me that "the sky is the limit." Instead, they never let the idea of "limit" enter my brain. Sure, this sometimes causes me to bite more than I can chew, but it also allows me to strive to do ambitious things like go for a Ph.D. Their confidence and belief in me, through thick and thin, is how I got to this place and how I will get to wherever I wind up going. I love you so much, and thank you for everything.

# Abstract

Nicotine addiction, opioid use disorder, and COVID-19 have made lasting impacts on every aspect of society. These are complicated conditions, and studies in these fields will likely continue for decades, if not centuries. Here, we make contributions to each of these issues using electrophysiology and microscopy. The first chapter goes into the motivation behind this thesis and the major experiments I used in my graduate career. In the second chapter, we introduce a new amino acid into the mouse muscle nicotinic acetylcholine receptor in an attempt to understand the dynamics of receptor activation. In the third chapter, we continue the Lester lab's work on the neuroscientific effects of menthol and how it plays a role in nicotine addiction. We found the binding site for menthol on the α4β2 nicotinic acetylcholine receptor, which continues our hypothesis that the neuroscientific effects of menthol are detrimental to cigarette smokers. Fortunately, partly because of our studies, mentholated nicotine products are being phased out of the United States. The fourth and fifth chapters investigate μ-opioid receptor trafficking, both the trafficking from the endoplasmic reticulum and endocytosis from the plasma membrane. Both of these events play a role in inducing opioid use disorder and increasing the danger of using opioids. We hope that these studies will help other researchers understand opioid use disorder and fight the opioid epidemic. Finally, we studied the effects of SARS-COV-2 proteins on epithelial sodium channels. These channels are important for regulating lung fluid levels where their improper function may cause pulmonary edema. Pulmonary edema has been observed in COVID-19 patients. Altogether, we believe that we have made meaningful impacts on these important health concerns in this thesis. We look forward to how the scientific communities continue to build on our results.

# Published Content and Contributions

1. Henderson, B. J., S. Grant, B. K. Wong, R. Shahoei, S. M. Huard, S. S. M. Saladi, E. Tajkhorshid, D. A. Dougherty, and H. A. Lester. *eNeuro* Menthol Stereoisomers Exhibit Different Effects on α4β2 nAChR Upregulation and Dopamine Neuron Spontaneous Firing. **2019** doi: 10.1523/eneuro.0465-18.2018

B.J.H., E.T., D.A.D., and H.A.L. designed experiments; B.J.H., S.G., B.K.W.,R.S., S.M.H., and S.S.M.S. performed experiments; B.J.H., S.G., B.K.W., R.S., S.M.H., and S.S.M.S. analyzed data; B.J.H., S.G., E.T., and H.A.L. wrote the paper.

2. Grant, S.N. and Lester, H.A. Regulation of Epithelial Sodium Channel Activity by SARS-CoV-1 and SARS-CoV-2 Proteins. *Biophysical Journal*, **2021** doi: 10.1016/j.bpj.2021.06.005

S.G. and H.A.L. designed experiments. S.G. performed experiments. S.G. and H.A.L. analyzed the data and wrote the manuscript.

# Table of Contents

# List of Figures and Tables

# Chapter 1: Introduction

## 1.1 The Nicotinic Acetylcholine Receptors and Allosteric Modulators

Smoking is currently the leading cause of preventable death and costs the United States over $100 million in direct medical costs.[1] The nicotinic acetylcholine receptors (nAChR) play a large role in nicotine addiction and other central nervous system (CNS) diseases like Parkinson's and Alzheimer's disease. The nAChRs are a family of pentameric ligand-gated ion channels responsible for some of the signaling at the neuromuscular junction by acetylcholine (ACh) or several exogenous ligands such as nicotine. Smoking tobacco or using electronic nicotine delivery systems (ENDS) will introduce exogenous nAChR agonists. Initial reports suggest that ENDS use is harmful to humans. There is a long history demonstrating that smoking causes harm to the cardiovascular system and is a leading cause of cancer.[2-5] While anti-smoking campaigns have been very successful at preventing young adults from smoking conventional cigarettes, ENDS have recently made a major impact on the health of the youth as "vaping" is popular among high school students. We have witnessed an increase in nicotine consumption due to these products (**Figure 1.1**).[6]

While a key factor in the addictive potential in ENDS and conventional cigarettes is nicotine, several other compounds influence the action of the nAChRs. One class of these molecules is the allosteric modulators. Allosteric modulators are different from agonists or antagonists in that allosteric modulators do not bind at the orthosteric site. For the neuronal nAChRs, the orthosteric site is at the α-β or α-α interface. It is characterized by an aromatic box which allows for an important cation-π interaction to form.[7,8] However, allosteric modulators will bind to another location, and its binding will affect the energy landscape of the

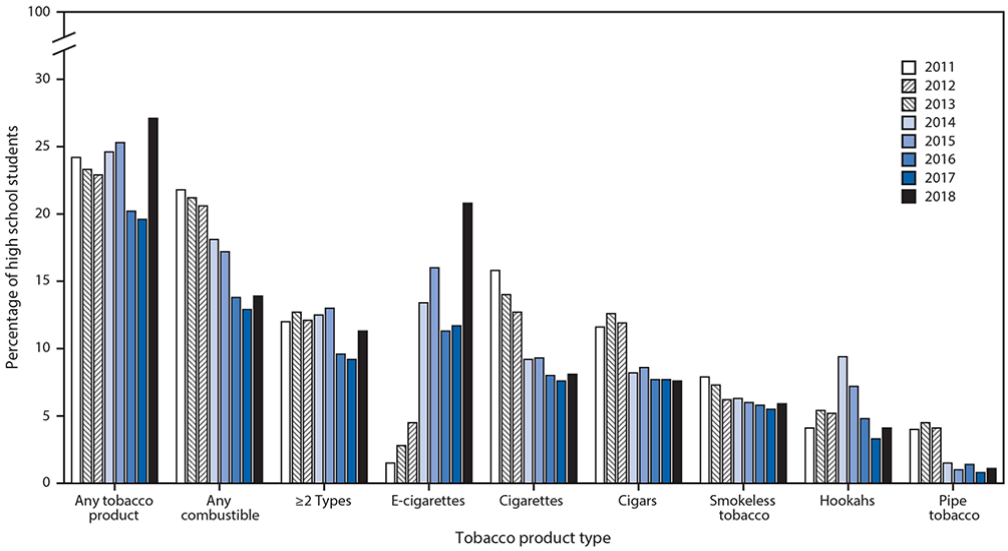


**Figure 1.1.** High School student tobacco product consumption increased drastically from 2017 to 2018, largely due to a rise in E-cigarette use. (Gentzke 2019)

nAChR (**Figure 1.2**). Positive allosteric modulators (PAMs) will shift the energy landscape to increase the stability of the active conformation, increase agonist affinity (shift the $EC_{50}$ for an agonist to a lower concentration), or increase the maximal current elicited by the receptor. A negative allosteric modulator (NAM) will increase the stability of an inactive conformation, decrease agonist affinity (shift the $EC_{50}$ for an agonist to a higher concentration), or reduce the maximal current elicited by the receptor. A neutral allosteric modulator will not affect agonist activity but may prevent other allosteric modulators from binding to that allosteric site. Nevertheless, just because two molecules are allosteric modulators does not mean they will bind to the same location. For example, the gamma-aminobutyric acid (GABA) receptor has more than one allosteric site.[9] One should also note that just because a molecule binds at an allosteric site does not mean it is an allosteric modulator. Finally, certain compounds can act as both PAMs and NAMs depending on the concentration. One example is $Zn^{2+}$, where the $EC_{50}$ for

potentiation is 168 μM, but the $IC_{50}$ for inhibition is 3.2 mM for the $(\alpha3)_2(\beta4)_3$ nAChR.[10]

The α4β2 nAChR is especially important as it is the most prominent heteromeric subtype in the brain.[11] The α4β2 nAChR can be found in two stoichiometries: the high-affinity $(\alpha4)_2(\beta2)_3$ or the low-affinity $(\alpha4)_3(\beta2)_2$ stoichiometry. The high-affinity stoichiometry will bind to ACh with an $EC_{50}$ of ~1 μM, while the low-affinity stoichiometry will bind with an $EC_{50}$ of ~ 83 μM.[12] The α4β2 receptor provides one of the main binding sites for nicotine in the brain.[13] Picciotto *et al*. found that the high-affinity binding sites were absent from mice where the β2 subunit was mutated and their thalamic neurons did not respond to nicotine.[14] Furthermore, the α4β2 nAChR has been implicated in perception, cognition, emotion, nicotine self-administration, reward, and dependence.[15]

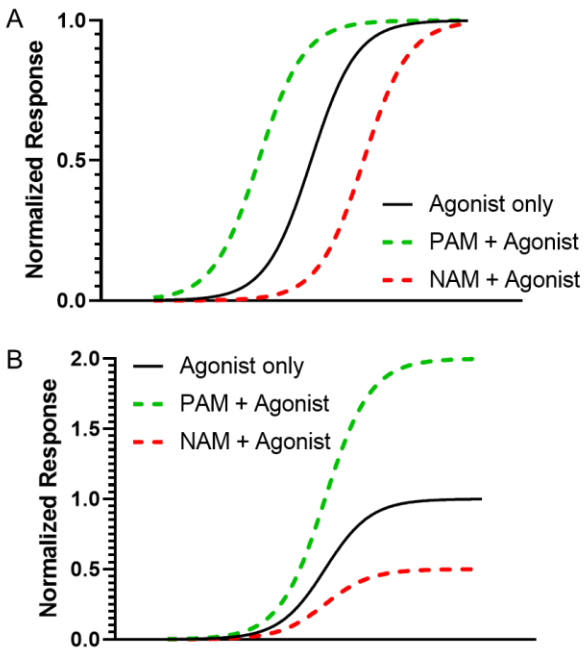


**Figure 1.2** How allosteric modulators effect $EC_{50}$ curves by *(A)* changing the $EC_{50}$ or *(B)* changing the maximal response

Clearly, α4β2 nAChR has a tremendous influence on a patient's response to nicotine, and likewise, anything that affects the α4β2 nAChR may also affect a person's susceptibility to nicotine addiction.

Unfortunately, recent work has shown that tobacco and ENDS flavorants are NAMs of the α4β2 nAChR.[12,16] The most prominent of these

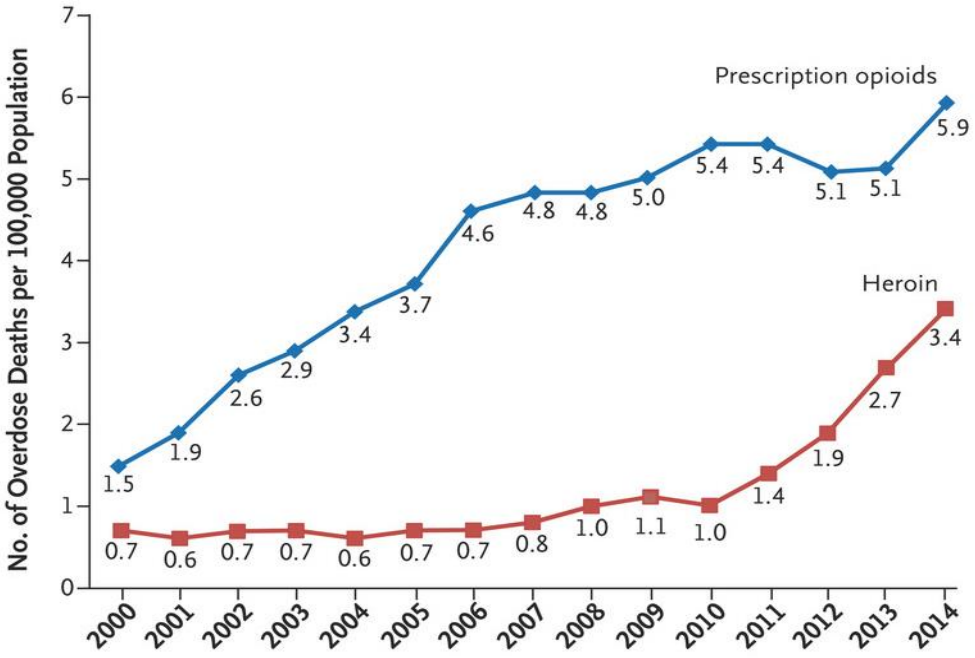


**Figure 1.3**. The opioid epidemic has grown the past two decades (Comptom 2016).

flavorants is menthol which is the only flavorant allowed in conventional cigarettes in the United States after the 2009 Family Smoking Prevention and Tobacco Control Act. However, due to our work and other studies demonstrating that flavors entice youth to start using nicotine products, flavorants are being phased out in many nicotine products. Already, Canada and San Francisco have banned the sale of menthol cigarettes. The popular ENDS manufacturer Juul has stopped producing many of its flavored oils to combat the spread of adolescent nicotine addiction. The third chapter of this thesis details my efforts on this issue.[12]

### 1.2 The Opioid Receptors and Protein Trafficking

The United States is currently facing an opioid abuse epidemic that is causing over 1000 emergency room visits and approximately 91 deaths every day (**Figure 1.3**).[17] Drug overdose is currently the leading cause of accidental death in the United States and opioids are the most common drug overdosed. The prevalence of opioids is largely a result of these compounds being exceptional treatments for

pain.[18] To this day, despite billions of dollars being spent looking for alternative pain medications, opioids remain the gold standard.[19] With approximately 100 million people suffering from some form of pain in the United States, opioids are among the most prescribed medications, having been dispensed 245 million times in 2014.[18,19] Public policy has attempted to combat the epidemic by monitoring prescriptions. However, the lack of a better option has left healthcare providers with few options other than prescribing these addictive substances. Indeed, these opioids, which include buprenorphine, fentanyl, hydromorphone, methadone, morphine, and oxycodone, will also cause respiratory depression, leading to death if any of these opioids are taken in excess.

The primary target for all of these opioids is the μ-opioid receptor (MOR). These receptors are expressed throughout the human body, but, consistent with its role in opioid use disorder, it is prominently expressed in the ventral tegmental area in the brain.[20] On a system level, MOR activation leads to dopamine release into the nucleus accumbens, giving rise to a pleasurable sensation. The rest of the brain creates conditioned associations with this feeling and the opioid. This association between pleasure and opioids drives the initial compulsions for opioid use, but eventually, secondary responses build as the body becomes accustomed to the chronic presence of opioids. These secondary effects can be broken down into tolerance and dependence. Tolerance involves the escalating doses required to elicit a certain response. Dependence refers to the body's need for the stimuli to function normally. When a patient that has developed dependence is taken off opioids, withdrawal symptoms occur. Both tolerance and dependence are induced with consistent opioid use and contribute to opioid use disorder.

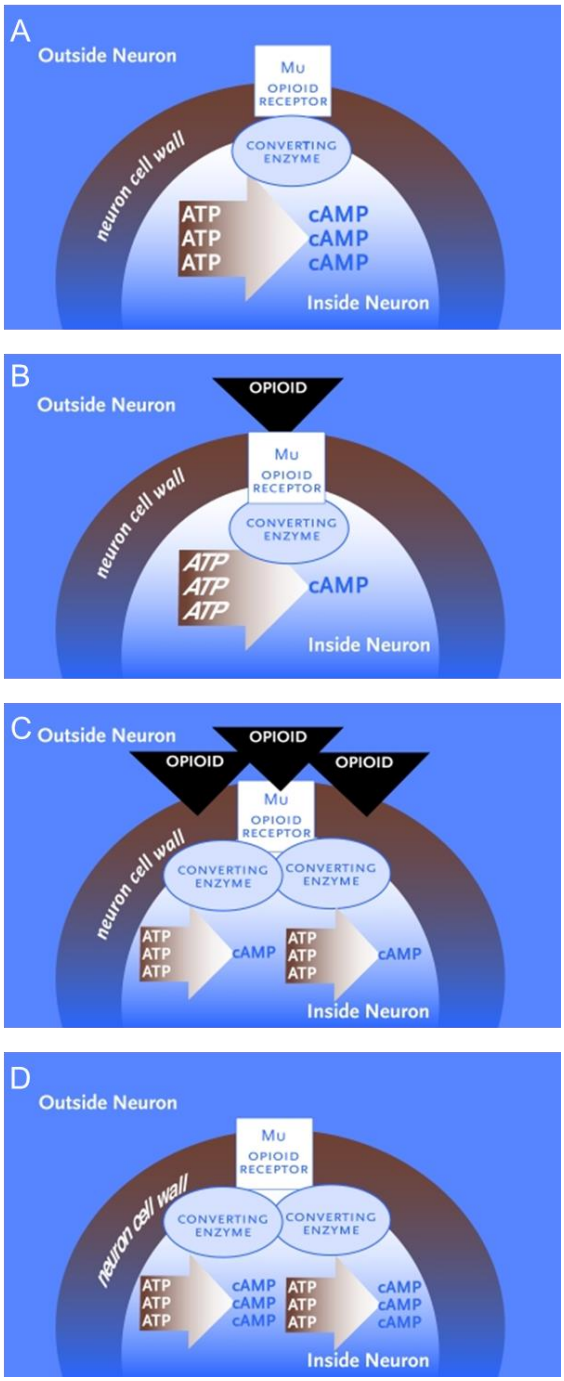


**Figure 1.4**. Overview of [cAMP] changes during *(A)* normal function, *(B)* upon initial opioid exposure, *(C)* upon development of tolerance, *(D)* during withdrawal. [cAMP] is directly related to noradrenaline release. (Kosten 2002)

On a molecular level, MOR activation causes several responses in neurons. First, the MORs are coupled to the $G_{i/o}$ proteins.[21] Upon activation, there is a decrease in the conversion of adenosine triphosphate (ATP) to cyclic adenosine monophosphate (cAMP), which leads to decreases in the release of noradrenaline; thus the subject experiences sedation and shallow breathing (**Figure 1.4**).[20] To combat this, the neuron will increase the intracellular concentration of adenyl cyclase, thus leading to an increase in [cAMP] and offsetting the effects of the opioids. Indeed, there are disadvantages to feeling drowsy, so humans are evolutionarily inclined to reverse these effects to some degree. When opioids are not present, these adjustments to adenyl cyclase expression cause the [cAMP] to be higher than normal and excessive amounts of noradrenaline to

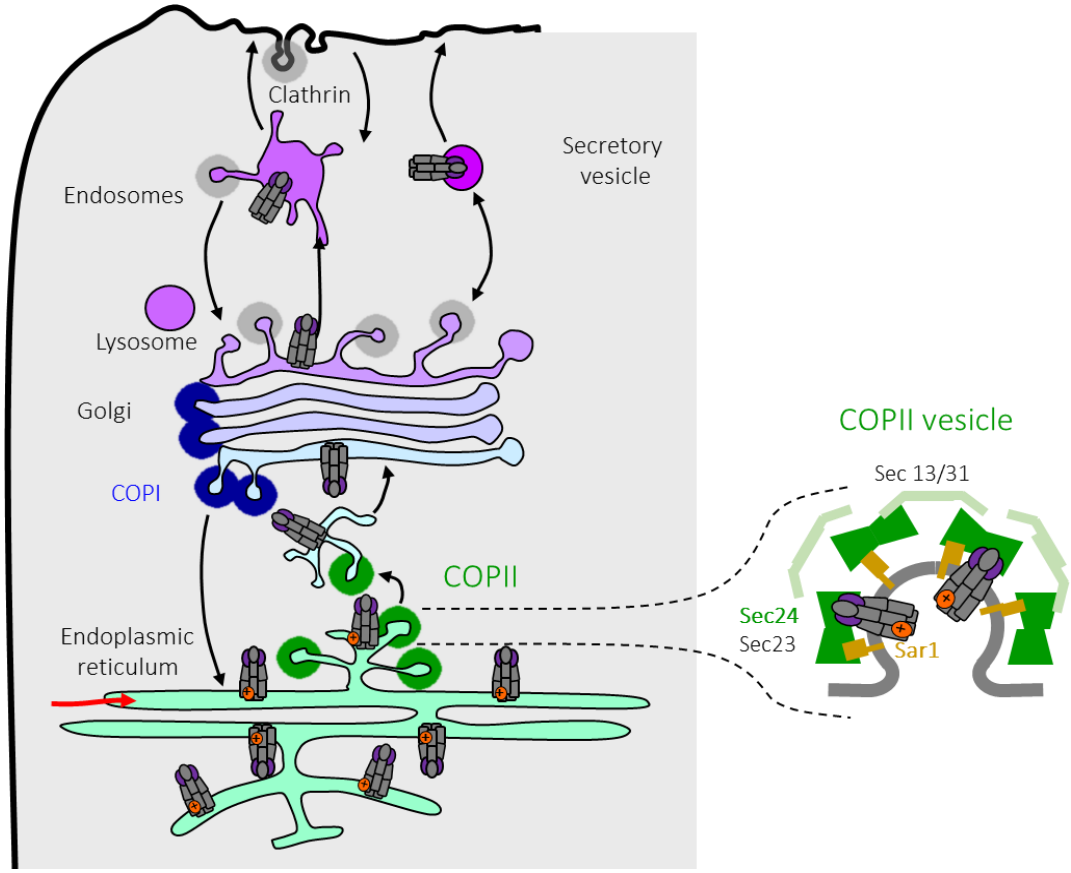


**Figure 1.5**. Overview of membrane protein trafficking with an expanded view of the COPII vesicle (Henderson 2015).

be produced, inducing feelings of anxiety, muscle cramps, and diarrhea. Essentially, one experiences withdrawal and these effects are abolished with time, but a subject can take more of the opioid to remove the withdrawal symptoms. Unfortunately, since tolerance is induced with dependence, the dose required to reverse withdrawal symptoms increases. Furthermore, with the escalating dosages, many subjects suffering from opioid use disorder eventually take a dose that causes severe respiratory depression (due to the large drop of noradrenaline) and death.

Several diseases can result from deficiencies in protein trafficking. The 2013 Nobel Prize in Physiology or Medicine went to James Rothman, Randy

Schekman, and Thomas Südhof “for their discoveries of machinery regulating vesicle traffic, a major transport system in our cells.”[22] In general, most membrane proteins will be translated by ribosomes and mature in the endoplasmic reticulum (ER). Proper folding will result in forming an endoplasmic reticulum exit site (ERES) that will guide the protein to the Golgi for further processing before finally being trafficked to the plasma membrane.

ERES formation has been studied extensively (**Figure 1.5**).[23-26] First, Sar1p, a Ras-like GTPase, phosphorylates GDP, and associates with the ER. This process leads to membrane curvature that will eventually generate a vesicle and detach from the rest of the ER.[27] Sar1p then recruits Sec23/Sec24 heterodimers, constituting the inner coat of ERES. Sec24 is also responsible for cargo binding. The four Sec24 subtypes (designated A-D) have unique binding motifs, and there have been reports that cargo can bind to one, two, three, or all four of these subtypes.[28-31] Then, the Sec13/Sec31 heterodimer is recruited to form the outer coat. Then, GTP hydrolysis by Sar1p causes the components to dissociate from the ER, and the entire complex and cargo will transport to the Golgi. Based on some calculations performed by Heinzer *et al*., 48 COPII complexes make up a COPII vesicle, and about 12 COPII vesicles make up a single ERES.[32] Within a mammalian cell, there can be hundreds of ERES, each with a diameter of approximately 500 nm.

The ERES are of particular interest to the Lester lab. Prior group members have found that nicotine’s ability to increase the membrane density of α4β2 nAChRs occurs through an ERES-dependent process.[33] By using fluorescently tagged Sec24 proteins and confocal microscopy, the Lester lab observed increases in the number of ERES in cells overexpressing α4 and α6 nAChRs when

the cells are treated with nicotine. The hypothesis to explain these observations is that nicotine serves as a pharmacological chaperone for these nAChRs.[34] Essentially, because nicotine will cross the plasma membrane, nicotine can target nAChRs in the cytoplasm. This includes the ER when the nAChRs are folded and assembled.[34] We believe that these ligands bind to the α4-containing (α4*) and α6-containing (α6*) nAChRs to promote a trafficking-enabled conformation, thus biasing them to the Golgi through ERES-mediated transport.

This thesis's fourth chapter will delve into how we applied these ideas to the opioid receptors and how antagonists pharmacologically chaperone the receptors to the plasma membrane. Much like the relationship between nicotine and nAChRs, naltrexone and naloxone will increase the surface density of the MOR.[35-38] While these papers hypothesize that pharmacological chaperoning is the mechanism, no direct intracellular experiments have been done to confirm these ideas. Expanding on the experiments of previous lab members, I do 3D image analysis to suggest that the opioid receptors are being chaperoned by the antagonists naltrexone (Ntx) and naloxone, but not agonists or allosteric modulators. I also show that this chaperoning event is dependent on the antagonists entering the cell. This discovery introduces a new way to approach the opioid epidemic by using “inside-out” pharmacology.

In terms of its localization in the cell, the MOR predominately localizes to the plasma membrane.[39] This contrasts with the δ- and κ-opioid receptors, which primarily localize within the cytoplasm.[40] Regulation of the surface density of the MOR has received tremendous attention because certain agonists, like fentanyl and the synthetic peptide DAMGO, will cause endocytosis of the MOR.[41] Morphine, on the other hand, has been shown to have different effects on MOR endocytosis

depending on the system used.[42,43] Along with the morphine story, what role agonist-induced MOR endocytosis has on opioid use disorder is hotly contested.[44-46] On the one hand, MOR endocytosis will diminish the available pool of receptors activated on the surface, so endocytosis is desired. On the other hand, studies have shown that endocytosis is followed by receptor recycling.[47] Endocytosis may be a mechanism for removing desensitized receptors and allowing them to resensitize through recycling. In this sense, if desensitization occurs in the absence of endocytosis and subsequent recycling, endocytosis is not desired. However, resensitization in the absence of recycling has also been observed.[48] There are studies where MOR activation has been observed at an intracellular site, so the importance of these intracellular activation events must be considered.[49] Ultimately, the trafficking of the MOR and its role in opioid use disorder is not completely understood.

In the fifth chapter, we conduct novel experiments investigating C-terminal phosphorylation's role on morphine- and fentanyl-induced endocytosis. Using a fluorescently tagged MOR and visualizing early endosomes with CellLight™ Early Endosome GFP, we can calculate the Pearson's correlation coefficient as a measure of MOR endocytosis. Our initial experiments demonstrate that in our system, both morphine and fentanyl will increase MOR endocytosis. However, we do not observe a significant increase in morphine-induced endocytosis in any receptor where the S375 residue is mutated to alanine. The S375 residue has been established as an important phosphorylation site, and our experiments are consistent with this hypothesis.[50-53] We could only prevent fentanyl-induced MOR endocytosis if we mutated T354, S355, S356, T357, S363, S364, T370, S375, T376, and T379 to alanine. These results suggest that C-terminal phosphorylation

is an important step to MOR endocytosis, and these particular residues are of special interest.

### 1.3 Epithelial sodium channels' role in COVID-19

For decades, we have that known species crossover events of diseases present major public health threats.[54] In December 2019, the first instance of SARS-CoV-2 infection in a human was documented. In roughly four months, a pandemic was declared, and millions of lives have been lost since. Fortunately, the global scientific community mobilized to learn more about this disease and find treatments. Nonetheless, it is unlikely that this will be the last crossover event, and it is important to continue to study SARS-CoV-2 to understand how to track and treat other pandemic-causing agents.

The symptoms of COVID-19 include severe respiratory distress that can lead to death. A specific form of respiratory distress is pulmonary edema, which has been observed in COVID-19 patients.[55] Pulmonary edema results from improper fluid regulation in the respiratory system, which may originate from malfunctioning epithelial sodium channels (ENaC).[56] ENaCs are partly responsible for regulating fluid levels because the flow of sodium ions will coincide with water flow via osmosis. If these channels do not function properly, then serious complications can develop, many of which have been observed in COVID-19 patients.

These symptoms were also observed in SARS patients, which is the disease caused by SARS-CoV-1. SARS-CoV-1 and SARS-CoV-2 are related beta-coronaviruses with many homologous proteins.[57] In 2009, Ji and co-workers explored how some of the SARS-CoV-1 proteins influenced ENaC activity.[58] Ji and co-workers found that SARS-CoV-1 spike (S) and envelope (E) protein decreased

ENaC activity in *Xenopus* oocytes. Ultimately, they found that this was a result of protein kinase C activation by these SARS-CoV-1 proteins.

Chapter six documents our efforts to investigate how SARS-CoV-2 E and S proteins affect ENaC activity. Although there is 96% and 76% sequence identity between the two SARS virus E and S proteins, respectively, there is still merit in measuring these potential effects. Indeed, while SARS and COVID-19 are similar diseases, they have significant differences in how humans and communities were affected by the diseases. Here, we find that the effects of the E protein are conserved, and, in our hands, inhibition was only observed for SARS-CoV-2 S protein, but not SARS-CoV-1 S protein. We believe this difference results from using different controls; Ji and co-workers compared their results to oocytes injected with ENaC mRNA only. We compared our results to oocytes injected with ENaC and a control mRNA (SARS-CoV-2 ORF8), which does not interact with ENaC. We believe that SARS-CoV-1 S protein appears to decrease ENaC currents in the Ji *et al*. experiments because the extra mRNA utilized translational resources in the oocyte that otherwise would have been used to generate more ENaC. We also found that the PKC inhibition experiments that could recover ENaC activity in the Ji *et al*. paper could not recover ENaC activity in our hands. Finally, we did some mechanistic work to look at one of the differences between the SARS-CoV-1 and SARS-CoV-2 S proteins: the introduction of a furin-cleavage motif. We know that ENaC function, specifically ENaC-α, requires furin cleavage. Suppose SARS-CoV-2 S protein is taking some of the available furin. In that case, this will decrease the amount of ENaC-α being cleaved and thus reduce active ENaC levels.[59] Here, we found that we could slightly recover ENaC activity by mutating this site. However, we did not observe complete recovery. Ultimately, these

findings are just one of many basic science discoveries that will help us fight the current and potential future pandemics.

## 1.4 Major Experiments

### *1.4.1 Two-electrode voltage-clamp electrophysiology on Xenopus oocytes*

The first electrophysiology experiment may be attributed to Luigi Galvani when he could cause a dead frog's leg to twitch with electricity. Since that famous experiment, we now understand how important electricity is to virtually every aspect of life. Indeed, life relies on being able to manipulate energy, and a great deal of it is stored as potential energy in the form of a voltage gradient across various lipid membranes. Galvani was probably changing the potential in some of these dead frog neurons, which despite being dead, were still able to transmit that change in the potential to other neurons and muscle fibers and induce muscle contraction. Since then, popular literature and frontier science have been fascinated with electrophysiology and what we can learn about life by understanding it from an electrical perspective.

While there are numerous ways to observe currents and potentials in a living system, the experiment I focused on during my graduate career was the two-electrode voltage clamp (TEVC) technique. Each electrode is typically made from a glass pipette and closed off at a sharp point that will eventually be impaled into the sample. The electrode is filled with a solution with a high concentration of KCl, and when impaled into the sample, they can form a high resistance seal so that most of the fluctuations in voltage or current result from a physiological response. Two electrodes are necessary as one will be used to measure the potential across the membrane, and the other will inject current into the sample to maintain the potential at a set voltage; thus, the voltage across the membrane is "clamped."

Using both of these electrodes with an appropriate rig and software will ultimately give a current reading across the membrane.

One way people have used TEVC electrophysiology is to study ion channels. The idea behind these experiments is that ion channel opening will allow ions to flow through these channels down their electrical gradient when there is a set potential across the membrane. This movement of charge will create a current, and one can measure these currents with TEVC techniques. From here, many different experiments can be done to investigate the various properties of ion channels. One way is to perform voltage jump experiments where the clamped voltage changes and the changes in current are recorded. These experiments were done to identify the M2 protein, made by an influenza virus, as a viroporin.[60] Further work leveraging M2's role as an ion channel lead to the development of the antiviral drugs amantadine and rimantadine.[61] Indeed, Wang *et al*. observed channel block with amantadine, and this observation lead to further experiments with amantadine and the related rimantadine as antiviral drugs. Another method is to use ligands to change the open-state probability of the ion channel. This is most popularly done with ligand-gated ion channels (LGIC) like the nAChRs. Using TEVC, one can test a series of compounds to determine if they are agonists, antagonists, or allosteric modulators of these LGICs by determining whether the compound will open, prevent the opening, or modulate activation, respectively. One can also rank these compounds by how well they act on these LGICs. For example, if compound A at low doses can induce the same currents as compound B at higher doses, then we can say that the channels are more sensitive to compound A.

Unfortunately, most mammalian cells are quite small and range between 10-100 μm in diameter.[62] From an experimental standpoint, it is possible to perform electrophysiology experiments on these cells, but it would be easier and faster to use a larger model, especially if one wants to use the TECV technique. Fortunately, the oocytes from the African frog species *Xenopus laevis* are quite ideal for these experiments. These oocytes are 1 mm in diameter, so one can easily impale them with the two electrodes. The oocytes also facilely assemble and traffic many membrane proteins to the plasma membrane, and their general lack of other ion channels makes them the perfect model system for most TEVC experiments.[63] Transfection of these oocytes typically involves injecting mRNA into the oocyte, and owing to its large size, it is a fairly easy procedure, and the oocytes tolerate this technique well. Additionally, one can simultaneously express many different proteins in each oocyte, making protein-protein interaction or heteromeric ion channel work possible.

In terms of nAChR research, the utility of the *Xenopus* oocyte and the TEVC technique is perfect for a range of questions. Since the nAChRs are a family of pentameric ion channels typically composed of different subunits, expressing several proteins is critical.[64] Additionally, currents from the α7 receptor can be enhanced when a protein chaperone, like Ric-3 or NACHO, is expressed, so expressing multiple proteins is useful even when one subunit is desired.[65,66] An additional benefit to injecting mRNA is that precise stoichiometries can be induced since transcription is done *in vitro* and translation efficiencies are easier to predict with direct mRNA injection than with more conventional transfection methods with cDNA. For example, fairly consistent expression of either $(\alpha4)_2(\beta2)_3$ or $(\alpha4)_3(\beta2)_2$ can be achieved by modulating the ratio of α4:β2 mRNA injected into the oocyte.[12]

Alternatively, one can observe a mix of stoichiometries using the same method. Lastly, the α5 subunit is an accessory subunit meaning that it cannot form functional receptors without other α subunits.[67,68] Therefore, any experiment with these channels will have to answer the question of how to differentiate between the α5* nAChRs from the non-α5* nAChRs. Fortunately, due to the ability to precisely control each subunit's expression, simply using a much larger ratio of α5 mRNA (>10-fold more) will nearly ensure that all receptors will form with an α5 subunit.[67]

Due to the large surface area that allows for potentially high surface densities of ion channels coupled with a highly sensitive technique like TEVC electrophysiology, even poorly expressed receptors can be detected. This becomes especially relevant in the next section, which discusses non-canonical amino acid (NCAA) mutagenesis.

### *1.4.2 NCAA mutagenesis*

There are twenty standard or canonical amino acids encoded by all organisms using the 64 possible codons, where three of these codons cause translation termination. Their side chains from the α-carbon characterize each amino acid, and the twenty canonical amino acids cover quite a variety of chemical moieties. However, for precise and extensive chemical biology experiments, these twenty residues are very limiting. At this point, chemical biologists have looked for ways to incorporate NCAAs to answer some of their questions. For example, in terms of phenyl groups, chemical biologists were limited to tyrosine or phenylalanine. While there are certainly NCAAs that can completely utilize the natural translation machinery, they are limited.[69] At the moment, there are two popular methods for

incorporating NCAAs into proteins: the orthogonal tRNA/synthetase method and the *in vitro* tRNA aminoacylation method.

The Schultz lab discovered the orthogonal tRNA/synthetase method in 2001.[70] Since then, chemical biologists have been pushing the boundaries of what is possible with proteins. Here, this group had to optimize the tRNA, the synthetase, and the NCAA. The synthetase had to charge the orthogonal tRNA with the NCAA selectively, and whatever proofreading mechanisms the organism has has to fail to recognize the NCAA as unnatural. Lastly, the NCAA could not be recognized by any of the endogenous synthetases or tRNAs. After a heroic effort, they were successful, and they generated a functional chloramphenicol acetyltransferase protein in *Escherichia coli* with an *O*-methyl-L-tyrosine incorporated at a specific location.[70] Since then, many NCAAs have been successfully incorporated into proteins in bacterial and mammalian cells for experiments involving photocrosslinking, click chemistry, microscopy, and post-translational manipulation.[71-77]

While the tRNA/synthetase method is incredibly useful, introducing novel NCAAs can be quite laborious and even impossible. Indeed, there is no guarantee that the NCAA one wants to use will not be recognized by endogenous synthetases, which will make a selective modification of a single residue quite difficult. To eliminate this barrier, one could charge the tRNA *in vitro* (**Figure 1.6**). This is the essence behind the second NCAA incorporation technique, in which, through chemical synthesis and *in vitro* transcription, the NCAA and tRNA can be facilely coupled.[78] Generally, the NCAA is made with a  dinucleotide on the carboxyl group (for efficient coupling to the rest of the tRNA) and a protecting group on the amine (to prevent the amine from hydrolyzing the tRNA). After the NCAA

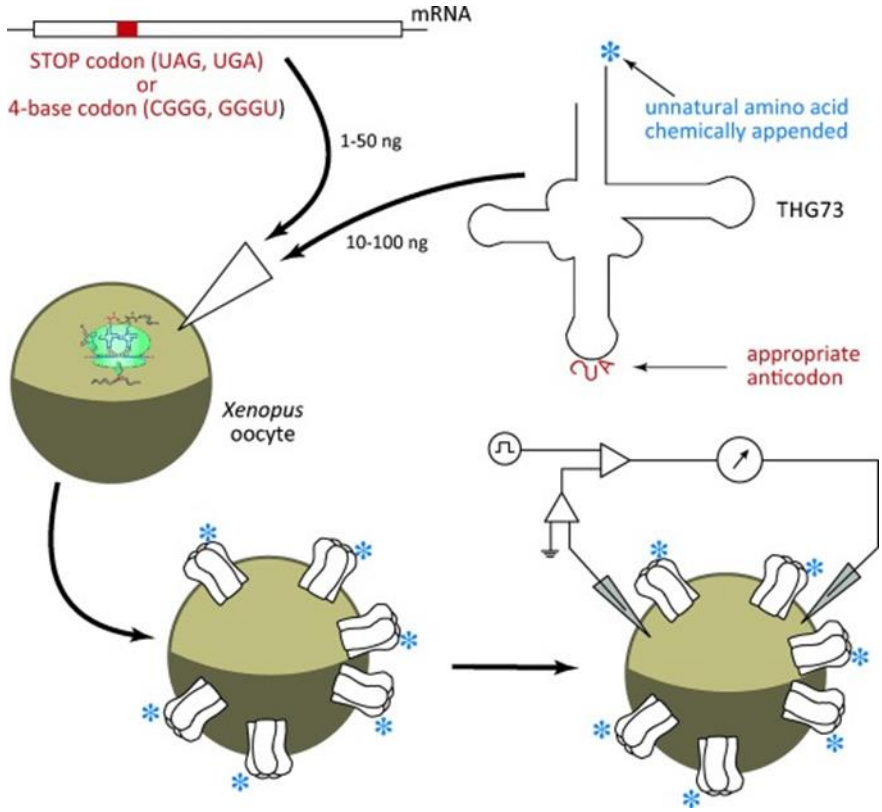


**Figure 1.6** Overview of the TECV and *in vitro* aminoacylation technique in *Xenopus* oocytes (Dougherty 2014).

has been charged onto the tRNA, the protecting group is removed, and it is ready to participate in translation at the appropriate codon designated by the tRNA's anticodon. Thus, in bypassing the amino acid selection stage of tRNA charging, even very small modifications to a canonical amino acid can be efficiently and selectively incorporated at a site of interest. One example is adding fluorine substituents in place of hydrogens. This is a fairly minor change in steric bulk, and it is unlikely that a phenylalanine residue decorated with fluorine will be distinguishable from native phenylalanine by the endogenous synthetases. However, by simply omitting phenylalanine from the reaction mixture, the tRNA will only be charged with whatever NCAA is in the reaction vessel. One could not do the same with the orthogonal tRNA/synthetase method because phenylalanine is

an essential amino acid, and substituting fluoro-phenylalanine in the media will cause all phenylalanine residues to be fluoro-phenylalanine, and the selectivity component is lost. Ultimately, if one very small modification is desired at just one residue, the *in vitro* aminoacylation method is superior to the orthogonal tRNA/synthetase method.

One of the main issues with the *in vitro* aminoacylation method is that, even under ideal circumstances, it requires stoichiometric amounts of tRNA-NCAA since the living system cannot charge the tRNA on its own.[78] Further, translation with the exogenously supplied tRNA-NCAA will not be perfect and some fraction of it will become uncharged, thus a greater than stoichiometric amount of material will be needed. However, TEVC electrophysiology is an incredibly sensitive technique in that <10 attomoles of functional protein are detectable on the oocyte surface.[78] This is well within reach of the *in vitro* aminoacylation technique, and this has allowed atomic level precision to be attained in experiments studying ion channels.[1,8,12,67,78-82]

In this thesis, we use this method extensively in Chapter Two in our attempts to incorporate a solvatochromic amino acid into the mouse muscle nAChR. The idea for the second chapter was to visualize protein conformation changes in real time using microscopy. While structural data on the nAChRs have been tremendously useful, they are ultimately just an image of the nAChR at a single time point. By observing changes in the fluorescent properties of a solvatochromic amino acid in a nAChR, we will understand when that residue and region of the protein enters a more hydrophobic or hydrophilic environment. Furthermore, this technique is used in the third chapter of this thesis to probe potential hydrogen bonding interactions between menthol and the α4β2 nAChR.

*1.4.3 ERES monitoring in SH-SY5Y cells*

Here, we became interested in membrane protein trafficking, much in line with the intracellular effects of menthol and nicotine on α4* nAChRs prior Lester lab members had found.[83] Our strategy centers around using fluorescently tagged Sec24 proteins to observe ERES under different conditions. Specifically, with our library of opioid agonists and antagonists, we were interested in how opioid receptors responded to these ligands. We already know that the surface density of opioid receptors increases with antagonists and decreases with some agonists, but intracellular examination has not been done yet.[36,43,84-88]

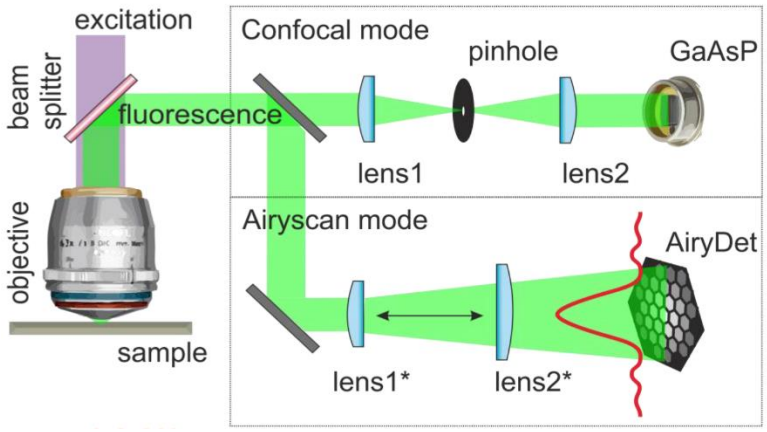


**Figure 1.7**. Basic schematic of the difference in image collection from conventional confocal microscopy and Airyscan microscopy (Korobchevskaya 2017)

While Henderson *et al*. and Srinivasan *et al.* did great work with ERES experiments, my projects sought to expand on these techniques.[83,89] The four most significant improvements in our experiments are: 1) we used human cells instead of mouse cells, 2) we analyzed 3D information after obtaining z-stacks, 3) we improved optical resolution by using a better microscope, and 4) we used objective as opposed to subjective thresholds for ERES designation. While switching cell lines on the surface is simple, Henderson *et al*. and Srinivasan *et al*. used neuro-2a cells because a transfection method with Lipofectamine 2000 had been optimized. Here, I optimized the transfection of a human neuroblastoma cell

line, the SH-SY5Y cells, with Lipofectamine 3000. Points two and three are related as z-stacks were only possible because we transitioned from a several decades-old Nikon microscope to a state-of-the-art Zeiss LSM 880 with a Fast Airyscan module (**Figure 1.7**).[90,91] The principle of Airyscan is that instead of simply rejecting any light not captured by the confocal pinhole, additional detector elements will collect this light and reconstruct the image with this light included to improve resolution. Combined with the LSM 880 with Fast Airyscan, we improved image quality and speed to get entire z-stacks in live cells before substantial ERES movement was observed. Zeiss introduced the Fast Airyscan module in May 2016, so Henderson *et al*. and Srinivasan *et al.* did not have access to this technology, seeing that their relevant papers came out in March 2016 and December 2010, respectively.[83,89,91] The final point was also a product of improved instrumentation as using objective thresholding was possible with the more consistently high-quality images produced by the LSM 880 with Fast Airyscan that was not possible on the old Nikon confocal microscope.

### 1.5 Summary of Dissertation Work

Improving public health is a major goal of many chemical biologists. This thesis demonstrates that the Lester lab is not an exception. I made contributions to three large contemporary public health issues throughout my graduate career: nicotine addiction, opioid use disorder, and COVID-19. In each, we utilized a unique set of skills and resources to understand new things about each of these issues. Like most things in science, we believe that this thesis builds on prior works and will serve as the foundation for further investigations. Comprehensive approaches to each of these problems are the best way to combat them, and we believe that this thesis makes a meaningful contribution to this effort.

## 1.6 References


1 Blom, A. E. M., Campello, H. R., Lester, H. A., Gallagher, T. & Dougherty, D. A. Probing binding interactions of cytisine derivatives to the α4β2 nicotinic acetylcholine receptor. *J Am Chem Soc* **141**, 15840-15849, doi:10.1021/jacs.9b06580 (2019).

2 Jamal, A. *et al.* Current cigarette smoking among adults - United States, 2005-2014. *MMWR-Morb. Mortal. Wkly. Rep.* **64**, 1233-1240 (2015).

3 Pankow, J. F. *et al.* Benzene formation in electronic cigarettes. *Plos One* **12**, 10, doi:10.1371/journal.pone.0173055 (2017).

4 Goniewicz, M. L., Boykan, R., Messina, C. R., Eliscu, A. & Tolentino, J. High exposure to nicotine among adolescents who use Juul and other vape pod systems ('pods'). *Tob. Control*, doi:10.1136/tobaccocontrol-2018-054565 (2018).

5 Willett, J. G. *et al.* Recognition, use and perceptions of Juul among youth and young adults. *Tob. Control*, doi:10.1136/tobaccocontrol-2018-054273 (2018).

6 Gentzke, A. S. *et al.* Vital signs: Tobacco product use among middle and high school students - United States, 2011-2018. *MMWR-Morb. Mortal. Wkly. Rep.* **68**, 157-164, doi:10.15585/mmwr.mm6806e1 (2019).

7 Jensen, A. A., Frolund, B., Lijefors, T. & Krogsgaard-Larsen, P. Neuronal nicotinic acetylcholine receptors: Structural revelations, target identifications, and therapeutic inspirations. *J. Med. Chem.* **48**, 4705-4745, doi:10.1021/jm040219e (2005).

8 Xiu, X., Puskar, N. L., Shanata, J. A., Lester, H. A. & Dougherty, D. A. Nicotine binding to brain receptors requires a strong cation-π interaction. *Nature* **458**, 534-537, doi:10.1038/nature07768 (2009).

9 Smith, G. B. & Olsen, R. W. Functional domains of $GABA_A$ receptors. *Trends in Pharmacological Sciences* **16**, 162-168, doi:10.1016/s0165-6147(00)89009-4 (1995).

10 Krashia, P. *et al.* Human α3β4 neuronal nicotinic receptors show different stoichiometry if they are expressed in Xenopus oocytes or mammalian HEK293 cells. *Plos One* **5**, 12, doi:10.1371/journal.pone.0013611 (2010).

11 Marks, M. J., Wageman, C. R., Grady, S. R., Gopalakrishnan, M. & Briggs, C. A. Selectivity of ABT-089 for α4β2* and α6β2* nicotinic acetylcholine receptors in brain. *Biochem Pharmacol* **78**, 795-802, doi:10.1016/j.bcp.2009.05.022 (2009).

12 Henderson, B. J. *et al.* Menthol stereoisomers exhibit different effects on α4β2 nAChR upregulation and dopamine neuron spontaneous firing. *eNeuro* **5**, eneuro.0465-0418.2018, doi:10.1523/eneuro.0465-18.2018 (2018).

13 Buisson, B., Gopalakrishnan, M., Arneric, S. P., Sullivan, J. P. & Bertrand, D. Human α4β2 neuronal nicotinic acetylcholine receptor in HEK 293 cells: A Patch-Clamp Study. *J. Neuroscience* **16**, 7880-7891, doi:10.1523/jneurosci.16-24-07880.1996 (1996).

14 Picciotto, M. R. *et al.* Abnormal avoidance learning in mice lacking functional high-affinity nicotine receptor in the brain. *Nature* **374**, 65-67, doi:10.1038/374065a0 (1995).

15 Eaton, J. B. *et al.* The unique α4+/-α4 agonist binding site in $(\alpha4)_3(\beta2)_2$ subtype nicotinic acetylcholine receptors permits differential agonist

desensitization pharmacology versus the $(\alpha4)_2(\beta2)_3$ subtype. *J. Pharmacol. Exp. Ther.* **348**, 46-58, doi:10.1124/jpet.113.208389 (2014).

16 Avelar, A. J. *et al.* Why flavored vape products may be attractive: Green apple tobacco flavor elicits reward-related behavior, upregulates nAChRs on VTA dopamine neurons, and alters midbrain dopamine and GABA neuron function. *Neuropharm.* **158**, 107729, doi:10.1016/j.neuropharm.2019.107729 (2019).

17 Schiller, E. Y., Goyal, A., Cao, F. & Mechanic, O. J. Opioid Overdose in *StatPearls* (StatPearls Publishing, StatPearls Publishing LLC., 2020).

18 Volkow, N. D. & McLellan, A. T. Opioid abuse in chronic pain — misconceptions and mitigation strategies. *NEJM* **374**, 1253-1263, doi:10.1056/NEJMra1507771 (2016).

19 Kaye, A. D. *et al.* New opioid receptor modulators and agonists. *Best Practice & Research. Clinical Anaesthesiology* **32**, 125-136, doi:10.1016/j.bpa.2018.06.009 (2018).

20 Kosten, T. R. & George, T. P. The neurobiology of opioid dependence: implications for treatment. *Science & Practice Perspectives* **1**, 13-20 (2002).

21 Bailey, C. P. & Connor, M. Opioids: Cellular mechanisms of tolerance and physical dependence. *Curr. Opin. Pharmacol.* **5**, 60-68, doi:10.1016/j.coph.2004.08.012 (2005).

22 Amara, J. F., Cheng, S. H. & Smith, A. E. Intracellular protein trafficking defects in human disease. *Trends Cell Biol* **2**, 145-149, doi:10.1016/0962-8924(92)90101-r (1992).

23 Antonny, B., Madden, D., Hamamoto, S., Orci, L. & Schekman, R. Dynamics of the COPII coat with GTP and stable analogues. *Nat Cell Biol* **3**, 531-537, doi:10.1038/35078500 (2001).

24 Antonny, B., Gounon, P., Schekman, R. & Orci, L. Self-assembly of minimal COPII cages. *EMBO Reports* **4**, 419-424, doi:10.1038/sj.embor.embor812 (2003).

25 Matsuoka, K. *et al.* COPII-coated vesicle formation reconstituted with purified coat proteins and chemically defined liposomes. *Cell* **93**, 263-275, doi:10.1016/s0092-8674(00)81577-9 (1998).

26 Matsuoka, K., Schekman, R., Orci, L. & Heuser, J. E. Surface structure of the COPII-coated vesicle. *PNAS* **98**, 13705-13709, doi:10.1073/pnas.241522198 (2001).

27 Lee, M. C. S. *et al.* Sar1p N-terminal helix initiates membrane curvature and completes the fission of a COPII vesicle. *Cell* **122**, 605-617, doi:10.1016/j.cell.2005.07.025 (2005).

28 Sucic, S. *et al.* The serotonin transporter is an exclusive client of the coat protein complex II (COPII) component SEC24C. *J. Biol. Chem.* **286**, 9, doi:10.1074/jbc.M111.230037 (2011).

29 Sucic, S. *et al.* Switching the clientele: A lysine residing in the C terminus of the serotonin transporter specifies its preference for the coat protein complex II component SEC24C. *J. Biol. Chem.* **288**, 5330-5341, doi:10.1074/jbc.M112.408237 (2013).

30 Kovalchuk, V. *et al.* Trafficking of the amino acid transporter $B^{0,+}$ (SLC6A14) to the plasma membrane involves an exclusive interaction with SEC24C for its exit from the endoplasmic reticulum. *Biochim.*

*Biophys. Acta-Mol. Cell Res.* **1866**, 252-263, doi: 10.1016/j.bbamcr.2018.11.005 (2019).

31 Zeyen, L., Döring, T., Stieler, J. T. & Prange, R. Hepatitis B subviral envelope particles use the COPII machinery for intracellular transport via selective exploitation of Sec24A and Sec23B. *Cell Microbiol.* **22**, 15, doi:10.1111/cmi.13181 (2020).

32 Heinzer, S., Worz, S., Kalla, C., Rohr, K. & Weiss, M. A model for the self-organization of exit sites in the endoplasmic reticulum. *J. Cell Science* **121**, 55-64, doi:10.1242/jcs.013383 (2008).

33 Srinivasan, R. *et al.* Nicotine up-regulates α4β2 nicotinic receptors and ER exit sites via stoichiometry-dependent chaperoning. *J. General Physiology* **137**, 59-79, doi:10.1085/jgp.201010532 (2011).

34 Henderson, B. J. & Lester, H. A. Inside-out neuropharmacology of nicotinic drugs. *Neuropharm.* **96**, 178-193, doi:10.1016/j.neuropharm.2015.01.022 (2015).

35 Yoburn, B. C., Kreuscher, S. P., Inturrisi, C. E. & Sierra, V. Opioid receptor upregulation and supersensitivity in mice: Effect of morphine sensitivity. *Pharmacology Biochemistry and Behavior* **32**, 727-731, doi:10.1016/0091-3057(89)90025-7 (1989).

36 Yoburn, B. C., Shah, S., Chan, K. W., Duttaroy, A. & Davis, T. Supersensitivity to opioid analgesics following chronic opioid antagonist treatment - relationship to receptor selectivity. *Pharmacology Biochemistry and Behavior* **51**, 535-539, doi:10.1016/0091-3057(94)00375-s (1995).

37 Patel, C. N., Rajashekara, V., Patel, K., Purohit, V. & Yoburn, B. C. Chronic opioid antagonist treatment selectively regulates trafficking and signaling proteins in mouse spinal cord. *Synapse* **50**, 67-76, doi:10.1002/syn.10246 (2003).

38 Sirohi, S., Kumar, P. & Yoburn, B. C. μ-opioid receptor up-regulation and functional supersensitivity are independent of antagonist efficacy. *Journal of Pharmacology and Experimental Therapeutics* **323**, 701-707, doi:10.1124/jpet.107.127019 (2007).

39 Sternini, C. *et al.* Agonist-selective endocytosis of μ opioid receptor by neurons in vivo. *PNAS* **93**, 9241-9246 (1996).

40 Wang, Y. L., Van Bockstaele, E. J. & Liu-Chen, L. Y. In vivo trafficking of endogenous opioid receptors. *Life Sci.* **83**, 693-699, doi:10.1016/j.lfs.2008.09.023 (2008).

41 Minnis, J. G. *et al.* Ligand-induced μ opioid receptor endocytosis and recycling in enteric neurons. *Neuroscience* **119**, 33-42, doi:10.1016/S0306-4522(03)00135-0 (2003).

42 Zadina, J. E., Chang, S. L., Ge, L. J. & Kastin, A. J. μ opiate receptor down-regulation by morphine and up-regulation by naloxone in SH-SY5Y human neuroblastoma cells. *Journal of Pharmacology and Experimental Therapeutics* **265**, 254 (1993).

43 Keith, D. E. *et al.* μ-opioid receptor internalization: opiate drugs have differential effects on a conserved endocytic mechanism *in vitro* and in the mammalian brain. *Mol. Pharmacol.* **53**, 377-384, doi:10.1124/mol.53.3.377 (1998).

44 Finn, A. K. & Whistler, J. L. Endocytosis of the mu opioid receptor reduces tolerance and a cellular hallmark of opiate withdrawal. *Neuron* **32**, 829-839, doi:10.1016/s0896-6273(01)00517-7 (2001).

45 Martini, L. & Whistler, J. L. The role of mu opioid receptor desensitization and endocytosis in morphine tolerance and dependence. *Curr. Opin. Neurobiol.* **17**, 556-564, doi:10.1016/j.conb.2007.10.004 (2007).

46 Molinari, P. *et al.* Morphine-like opiates selectively antagonize receptor-arrestin interactions. *J. Biol. Chem.* **285**, 12522-12535, doi:10.1074/jbc.M109.059410 (2010).

47 Bowman, S. L. *et al.* Cell-autonomous regulation of μ-Opioid receptor recycling by substance P. *Cell Reports* **10**, 1925-1936, doi:10.1016/j.celrep.2015.02.045 (2015).

48 Dang, V. C. & Christie, M. J. Mechanisms of rapid opioid receptor desensitization, resensitization and tolerance in brain neurons. *Br. J. Pharmacol.* **165**, 1704-1716, doi:10.1111/j.1476-5381.2011.01482.x (2012).

49 Stoeber, M. *et al.* A genetically encoded biosensor reveals location bias of opioid drug action. *Neuron* **98**, 963-+, doi:10.1016/j.neuron.2018.04.021 (2018).

50 Grecksch, G. *et al.* Analgesic tolerance to high-efficacy agonists but not to morphine is diminished in phosphorylation-deficient S375A μ-opioid receptor knock-in mice. *J Neurosci* **31**, 13890-13896, doi:10.1523/jneurosci.2304-11.2011 (2011).

51 Just, S. *et al.* Differentiation of opioid drug effects by hierarchical multi-site phosphorylation. *Mol. Pharm.* **83**, 633-639, doi:10.1124/mol.112.082875 (2013).

52 Yousuf, A. *et al.* Role of phosphorylation sites in desensitization of μ-opioid receptor. *Mol. Pharm.* **88**, 825-835, doi:10.1124/mol.115.098244 (2015).

53 Mouledous, L., Froment, C., Burlet-Schiltz, O., Schulz, S. & Mollereau, C. Phosphoproteomic analysis of the mouse brain mu-opioid (MOP) receptor. *FEBS Lett.* **589**, 2401-2408, doi:10.1016/j.febslet.2015.07.025 (2015).

54 Parrish, C. R. *et al.* Cross-species virus transmission and the emergence of new epidemic diseases. *Microbiology and Molecular Biology Reviews* **72**, 457-470, doi:10.1128/MMBR.00004-08 (2008).

55 Zwaveling, S., Gerth van Wijk, R. & Karim, F. Pulmonary edema in COVID-19: Explained by bradykinin? *Journal of Allergy and Clinical Immunology*, doi:10.1016/j.jaci.2020.08.038 (2020).

56 Fronius, M. Treatment of pulmonary edema by ENaC activators/stimulators. *Current Molecular Pharmacology* **6**, 13-27, doi:10.2174/1874467211306010003 (2013).

57 Gordon, D. E. *et al.* Comparative host-coronavirus protein interaction networks reveal pan-viral disease mechanisms. *Science* **370**, eabe9403, doi:10.1126/science.abe9403 (2020).

58 Ji, H. L. *et al.* SARS-CoV proteins decrease levels and activity of human ENaC via activation of distinct PKC isoforms. *American Journal of Physiology. Lung Cellular and Molecular Physiology* **296**, L372-383, doi:10.1152/ajplung.90437.2008 (2009).

59 Szabó, G. T., Kiss, A., Csanádi, Z. & Czuriga, D. Hypothetical dysfunction of the epithelial sodium channel may justify neurohumoral blockade in coronavirus disease 2019. *ESC Heart Failure* **8**, 171-174, doi:10.1002/ehf2.13078 (2021).

60 Wang, C., Takeuchi, K., Pinto, L. H. & Lamb, R. A. Ion-channel activity of influenza-A virus M(2) protein - characterization of the amantadine block. *Journal of Virology* **67**, 5585-5594, doi:10.1128/jvi.67.9.5585-5594.1993 (1993).

61 To, J. & Torres, J. Chapter 15 in *Virus Protein and Nucleoprotein Complexes* Vol. 88 *Subcellular Biochemistry* (eds J. R. Harris & D. Bhella) 329-377 (Springer, 2018).

62 Puck, T. T., Marcus, P. I. & Cieciura, S. J. Clonal growth of mammalian cells in vitro; growth characteristics of colonies from single HeLa cells with and without a feeder layer. *J. Experimental Medicine* **103**, 273-283, doi:10.1084/jem.103.2.273 (1956).

63 Papke, R. L. & Smith-Maxwell, C. High throughput electrophysiology with Xenopus oocytes. *Comb Chem High Throughput Screen* **12**, 38-50, doi:10.2174/138620709787047975 (2009).

64 Dani, J. A. Neuronal nicotinic acetylcholine receptor structure and function and response to nicotine. *Int Rev Neurobiol* **124**, 3-19, doi:10.1016/bs.irn.2015.07.001 (2015).

65 Matta, J. A. *et al.* NACHO mediates nicotinic acetylcholine receptor function throughout the brain. *Cell Reports* **19**, 688-696, doi:10.1016/j.celrep.2017.04.008 (2017).

66 Crespi, A., Colombo, S. F. & Gotti, C. Proteins and chemical chaperones involved in neuronal nicotinic receptor expression and function: An update. *Br. J. Pharmacol.* **175**, 1869-1879, doi:10.1111/bph.13777 (2018).

67 Marotta, C. B., Dilworth, C. N., Lester, H. A. & Dougherty, D. A. Probing the non-canonical interface for agonist interaction with an α5 containing nicotinic acetylcholine receptor. *Neuropharmacology* **77**, 342-349, doi:10.1016/j.neuropharm.2013.09.028 (2014).

68 Ramirez-Latorre, J. *et al.* Functional contributions of α5 subunit to neuronal acetylcholine receptor channels. *Nature* **380**, 347-351, doi:10.1038/380347a0 (1996).

69 Calve, S., Witten, A. J., Ocken, A. R. & Kinzer-Ursem, T. L. Incorporation of non-canonical amino acids into the developing murine proteome. *Sci Rep* **6**, 32377-32377, doi:10.1038/srep32377 (2016).

70 Wang, L., Brock, A., Herberich, B. & Schultz, P. G. Expanding the genetic code of *Escherichia coli*. *Science* **292**, 498-500, doi:10.1126/science.1060077 (2001).

71 Ai, H. W., Shen, W. J., Sagi, A., Chen, P. R. & Schultz, P. G. Probing protein-protein interactions with a genetically encoded photo-crosslinking amino acid. *ChemBioChem* **12**, 1854-1857, doi:10.1002/cbic.201100194 (2011).

72 Hino, N. *et al.* Protein photo-cross-linking in mammalian cells by site-specific incorporation of a photoreactive amino acid. *Nat. Methods* **2**, 201-206, doi:10.1038/nmeth739 (2005).

73 Majmudar, C. Y. *et al.* Impact of nonnatural amino acid mutagenesis on the in vivo function and binding modes of a transcriptional activator. *J Am Chem Soc* **131**, 14240-14242, doi:10.1021/ja904378z (2009).

74 Majmudar, C. Y., Wang, B., Lum, J. K., Hakansson, K. & Mapp, A. K. A High-resolution interaction map of three transcriptional activation domains with a key coactivator from photo-cross-linking and multiplexed mass spectrometry. *Angew. Chem.-Int. Edit.* **48**, 7021-7024, doi:10.1002/anie.200902669 (2009).

75 Krishnamurthy, M. *et al.* Caught in the act: Covalent cross-linking captures activator-coactivator interactions in vivo. *ACS Chemical Biology* **6**, 1321-1326, doi:10.1021/cb200308e (2011).

76 Kiick, K. L., Saxon, E., Tirrell, D. A. & Bertozzi, C. R. Incorporation of azides into recombinant proteins for chemoselective modification by the Staudinger ligation. *PNAS* **99**, 19-24, doi:10.1073/pnas.012583299 (2002).

77 Plass, T., Milles, S., Koehler, C., Schultz, C. & Lemke, E. A. Genetically encoded copper-free click chemistry. *Angewandte Chemie International Edition* **50**, 3878-3881, doi:10.1002/anie.201008178 (2011).

78 Dougherty, D. A. & Van Arnam, E. B. In vivo incorporation of non-canonical amino acids by using the chemical aminoacylation strategy: A broadly applicable mechanistic tool. *Chembiochem* **15**, 1710-1720, doi:10.1002/cbic.201402080 (2014).

79 Dahan, D. S. *et al.* A fluorophore attached to nicotinic acetylcholine receptor βM2 detects productive binding of agonist to the αδ site. *PNAS* **101**, 10195-10200, doi:10.1073/pnas.0301885101 (2004).

80 Lester, H. A. *et al.* Nicotine is a selective pharmacological chaperone of acetylcholine receptor number and stoichiometry. implications for drug discovery. *AAPS J.* **11**, 167-177, doi:10.1208/s12248-009-9090-7 (2009).

81 Pantoja, R., Rodriguez, E. A., Dibas, M. I., Dougherty, D. A. & Lester, H. A. single-molecule imaging of a fluorescent unnatural amino acid incorporated into nicotinic receptors. *Biophysical Journal* **96**, 226-237, doi:10.1016/j.bpj.2008.09.034 (2009).

82 Marotta, C. B., Rreza, I., Lester, H. A. & Dougherty, D. A. Selective ligand behaviors provide new insights into agonist activation of nicotinic acetylcholine receptors. *ACS Chem Biol* **9**, 1153-1159, doi:10.1021/cb400937d (2014).

83 Henderson, B. J. *et al.* Menthol alone upregulates midbrain nAChR, alters nAChR subtype stoichiometry, alters dopamine neuron firing frequency, and prevents nicotine reward. *J Neurosci* **36**, 2957-2974, doi:10.1523/JNEUROSCI.4194-15.2016 (2016).

84 De Vries, T. J., Tjon Tien Ril, G. H. K., Van der Laan, J. W., Mulder, A. H. & Schoffelmeer, A. N. M. Chronic exposure to morphine and naltrexone induces changes in catecholaminergic neurotransmission in rat brain without altering μ-opioid receptor sensitivity. *Life Sci.* **52**, 1685-1693, doi:10.1016/0024-3205(93)90476-J (1993).

85 Zadina, J. E., Harrison, L. M., Ge, L. J., Kastin, A. J. & Chang, S. L. Differential regulation of mu and delta opiate receptors by morphine, selective agonists and antagonists and differentiating agents in sh-sy5y human neuroblastoma-cells. *J. Pharmacology and Experimental Therapeutics* **270**, 1086-1096 (1994).

86 Belcheva, M. M., Barg, J., McHale, R. & Coscia, C. J. Naltrexone induces down- and upregulation of δ opioid receptors in rat brain regions. *Brain Research Bulletin* **35**, 69-72, doi:10.1016/0361-9230(94)90218-6 (1994).

87 Li, J., Chen, C., Huang, P. & Liu-Chen, L.-Y. Inverse agonist up-regulates the constitutively active D3.49(164)Q mutant of the rat μ-opioid receptor by stabilizing the structure and blocking constitutive internalization and down-regulation. *Mol. Pharmacol.* **60**, 1064-1075, doi:10.1124/mol.60.5.1064 (2001).

88 Petaja-Repo, U. E. *et al.* Ligands act as pharmacological chaperones and increase the efficiency of delta opioid receptor maturation. *Embo J.* **21**, 1628-1637, doi:10.1093/emboj/21.7.1628 (2002).

89 Srinivasan, R. *et al.* Nicotine up-regulates α4β2 nicotinic receptors and ER exit sites via stoichiometry-dependent chaperoning. *J. Gen. Physiol.* **137**, 59-79, doi:10.1085/jgp.201010532 (2011).

90 Korobchevskaya, K., Lagerholm, B. C., Colin-York, H. & Fritzsche, M. Exploring the potential of airyscan microscopy for live cell imaging. *Photonics* **4**, 19, doi:10.3390/photonics4030041 (2017).

91 Huff, J. *et al.* The new 2D superresolution mode for ZEISS airyscan. *Nature Methods* **14**, 1223-1223, doi:10.1038/nmeth.f.404 (2017).

# Chapter 2: Synthesis and incorporation of a solvatochromic amino acid into the mouse muscle nAChR

## 2.1 Abstract

Given the difficultly of acquiring ion channel structural information, we need creative solutions to understand the movements involved in activation. One of these solutions involves using solvatochromism. Solvatochromism refers to when fluorescent emission is modulated by the polarity of the fluorophore's environment. Here, we decided to use non-canonical amino acid (NCAA) mutagenesis to incorporate an NCAA with these solvatochromic properties. We synthesized 4-*N, N*-dimethylamino-1,8-naphthalimide (4-DMN) and successfully incorporated it into the mouse muscle nAChR. The incorporation was achieved by injecting orthogonal tRNA that we aminoacylated *in vitro* with 4-DMN. Following verification of its incorporation with electrophysiology, we moved into imaging experiments. Specifically, we tried to observe 4-DMN fluorescence using total internal reflection fluorescence (TIRF) microscopy to visualize the plasma membrane selectively. Unfortunately, we could not observe 4-DMN fluorescence. The low incorporation efficiency inherent in the *in vitro* aminoacylation method prevented us from discriminating between 4-DMN in the receptors from unincorporated 4-DMN. In future studies, improved NCAA incorporation efficiency or a protocol that prevents visualization of unincorporated NCAAs will be required for success in this project.

## 2.2 Introduction

Structure determination is more complicated for membrane proteins than for soluble proteins because membrane proteins traverse a hydrophilic and hydrophobic environment.[1] While detergents work well for soluble proteins, the hydrophilic/hydrophobic duality of membrane proteins makes detergents less

useful. It was only recently that any of the human heteromeric nAChR structures were experimentally solved by Ryan Hibbs and co-workers.[2-4] Although these structures are valuable in nAChR research, structures are limited. They only capture one state of the receptor and are usually captured in unnatural environments. Since there is value in looking at protein movement in biologically relevant systems, researchers have been creative in their experimental design to fill this curiosity.

One exciting solution is to incorporate NCAAs into proteins at specific sites. This chapter will exclusively focus on the *in vitro* aminoacylation strategy that we explained in Chapter 1. This strategy will allow us to quickly incorporate residues with various functions without evolving different synthetases and optimizing them for selectivity versus canonical amino acids. One example is introducing fluorescent NCAAs.[5-7] Fluorescent NCAAs are superior to fluorescent protein tags or cysteine-reactive dyes because NCAAs are significantly smaller than fluorescent proteins and more selective than cysteine-reactive dyes. Ultimately, NCAAs allow for the fluorescent detection of these proteins with minimal perturbation.

Going further with the fluorescent NCAAs, we focus specifically on using solvatochromic NCAAs. Solvatochromism refers to a special physical property where a fluorescent species undergoes a shift in their dipole moment upon excitation (**Figure 2.1**). These molecules differ from conventional fluorescent species in that their dipole moment significantly changes following excitation. The lifetime of the excited state is long enough that the molecules surrounding the fluorophore can readjust to decrease the entire system's energy. Then the fluorophore emits a photon, returns to the ground state, and the surrounding

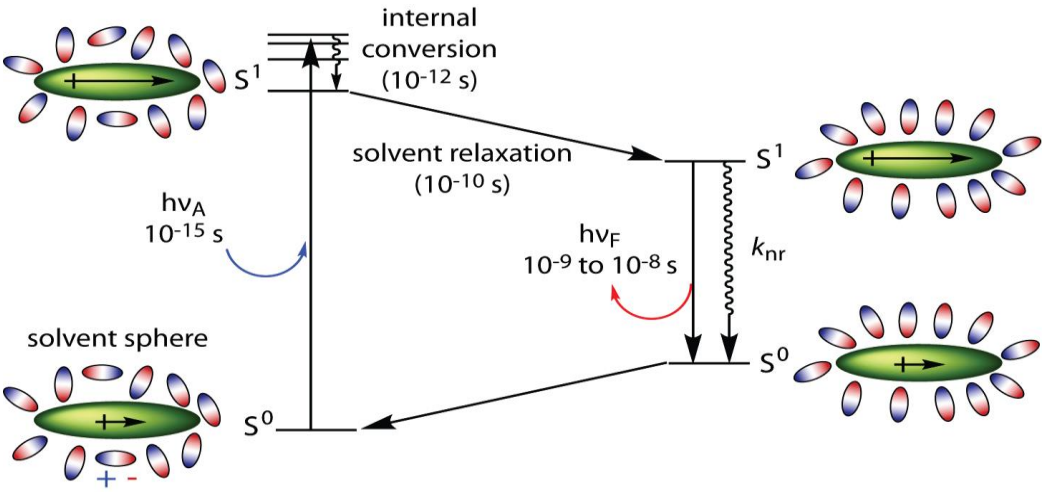


**Figure 2.1** Scheme depicting solvatochromism. Excitation of the fluorophore causes a change in the molecule's dipole moment (bottom-left to top-left). The surrounding environment will react to this change in dipole moment so that the excited fluorophore is in a more relaxed state (top-left to top-right). Fluorescent emission then occurs in this rearrangement environment (top-right to bottom-right). The emission wavelength is based on the environment since it directly influences the energy gap between the excited and ground state. Adopted from Loving, 2010.

environment returns to its ground state arrangement around the fluorophore. The unique aspect of this particular fluorescent cycle is that there is a significant shift in the fluorophore's dipole moment such that the surrounding environment will shift to accommodate it. The polarity of the surrounding environment will determine the wavelength of the photon emitted by the fluorophore. In general, the emitted wavelength will increase (the photon's energy will decrease) as the environment's polarity increases because it will lower the excited state's new dipole better than a less polar environment.[8-10] By measuring these emission shifts, one can determine if the solvatochromic molecule is in a polar or non-polar environment.

Bringing solvatochromism into biology can be tremendously useful. We know that all proteins have regions that are in polar or non-polar environments. Generally, the polar environments are "exposed" regions that interact with the aqueous solution in the cell. On the other hand, the non-polar environments are "buried" regions surrounded by other amino acids and have relatively lower polarity

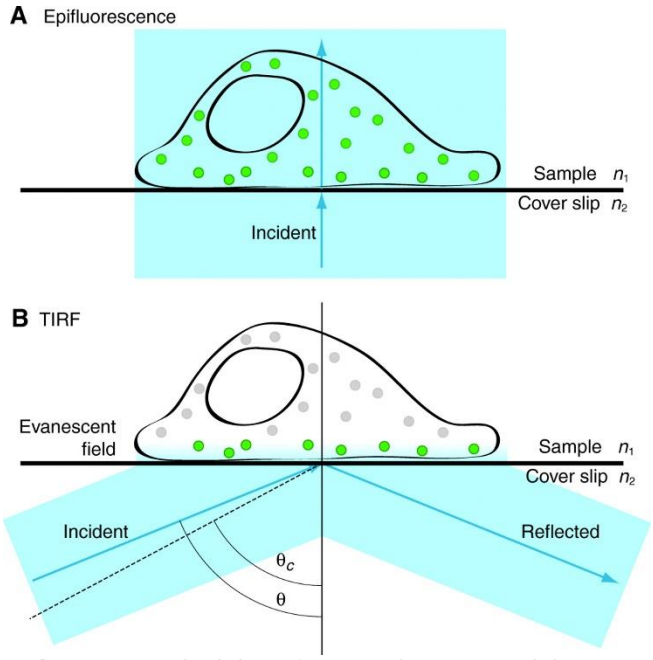


**Figure 2.2** Principles of TIRF microscopy. *(A)* In epifluorescence microscopy, the excitation light hits the sample at a 90° angle, allowing for maximum sample penetration. *(B)* Conversely, TIRF microscopy uses total internal reflection so that excitation penetration is only ~100 nm. This typically only allows visualization of the plasma membrane and anything very close to it. We decide to use TIRF microscopy because it will remove much of the autofluorescence that comes from inside the *Xenopus* oocyte and makes them difficult to use in conventional microscopy. Adopted from Mattheyses 2010.

than an aqueous solution. A particular residue is not necessarily always in an exposed or buried site since proteins can adopt an infinite number of conformations. Detecting if a specific residue is in a polar or non-polar environment in real-time is important to understanding a protein's mechanism, but it is also a difficult experiment to design. Fortunately, solvatochromic NCAAs react to changes in polarity rapidly, and fluorescent excitation and emission happen within a millisecond, so real-time detection of an environment's polarity is achievable.

To observe fluorescent NCAAs, we decided to use the *in vitro* aminoacylation technique in *Xenopus* oocytes. Unfortunately, this system is not well suited to most microscopy experiments because of the intense autofluorescence from the oocyte's cytoplasm. Since we are interested in visualizing receptors on the surface, we decided to utilize total internal reflection fluorescence (TIRF) microscopy (**Figure 2.2**).[11] Instead of directly irradiating the sample, the excitation light is directed at an angle to reflect all photons away from

the sample. However, the evanescent wave produced can penetrate the sample and excite molecules. However, the evanescent wavefront will decay exponentially with distance such that only ~100 nm of the sample will be illuminated. This roughly corresponds to the width of the coverslip and the plasma membrane. Therefore, this illumination section is perfect for our experiments because this will not excite the oocyte cytoplasm.

Here, we incorporated a solvatochromic amino acid, 4-DMN, into the mouse muscle nicotinic acetylcholine receptor (mm nAChR) to visualize protein conformation changes. The mm nAChR is made up of 5 subunits. From the extracellular side, the subunits have a counterclockwise order of αγαδβ.[12] The Imperiali group observed a shift in the emission spectrum when there is a shift in the polarity of 4-DMN's environment.[13] We were able to aminoacylate 4-DMN onto THG73, an orthogonal tRNA, *in vitro* for NCAA incorporation into *Xenopus laevis* oocytes. Using *in vitro* aminoacylation is substantially easier than developing a novel synthetase for 4-DMN.[14] Using two-electrode voltage-clamp electrophysiology, we were able to verify that 4-DMN was incorporated into the mm nAChR. Unfortunately, the transition to microscopy was unsatisfactory due to low incorporation rates and high fluorescence from the plasma membrane due to unincorporated 4-DMN.

## 2.3 Results and Discussion

### *2.3.1 Synthesis of 4-DMN and ligation onto THG73*

To incorporate 4-DMN into mm nAChR, we had to synthesize and append the amino acid onto an orthogonal tRNA. Fortunately, Loving and co-workers have already synthesized 4-DMN, and the remaining steps to ligate it onto THG73 have

been carried out numerous times with a wide range of amino acids.[5,13,15-17] The synthetic scheme is shown in **Figure 2.3**.

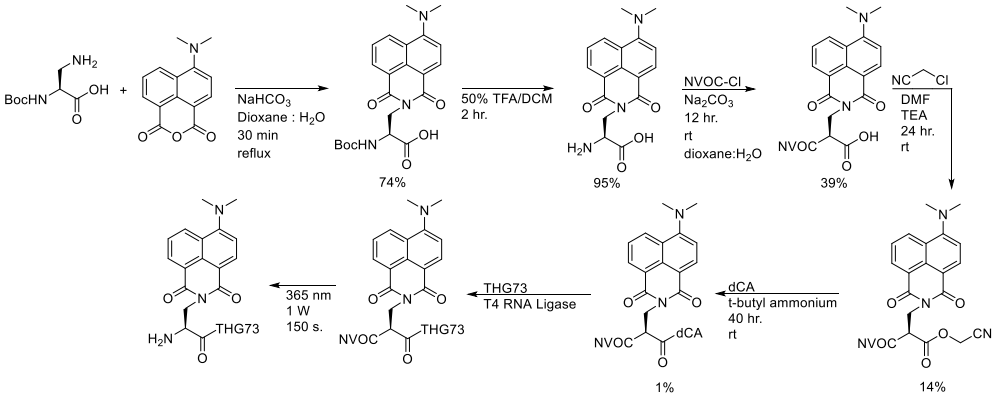


**Figure 2.3** Synthesis of 4-DMN and ligation onto the orthogonal tRNA, THG73.

While the organic chemistry was straightforward, we wanted to confirm the photochemical properties of 4-DMN, particularly after a mock 4,5-dimethoxy-2-nitrobenzyl (NVOC) deprotection. Since NVOC deprotects under ultraviolet (UV) light, we needed to confirm that the fluorescent properties of 4-DMN survived as some fluorophores will be damaged by UV light. We performed these experiments before conjugation to cytosine-adenine dinucleotide (dCA) since NVOC deprotection will cause hydrolysis of the dCA. We found that we still observe solvatochromism, and there is no significant drop in fluorescence after UV irradiation (**Figure 2.4**).

We then completed the dCA and THG73 conjugation and confirmed that 4-DMN was ligated onto the tRNA via mass spectrometry.

### *2.3.2 Confirming 4-DMN incorporation in mm nAChR*

Although the end goal for this project is to observe 4-DMN on the mm nAChR through a microscope, microscopy is not the most sensitive method to confirm that 4-DMN is being incorporated into the protein. Instead, we use TEVC

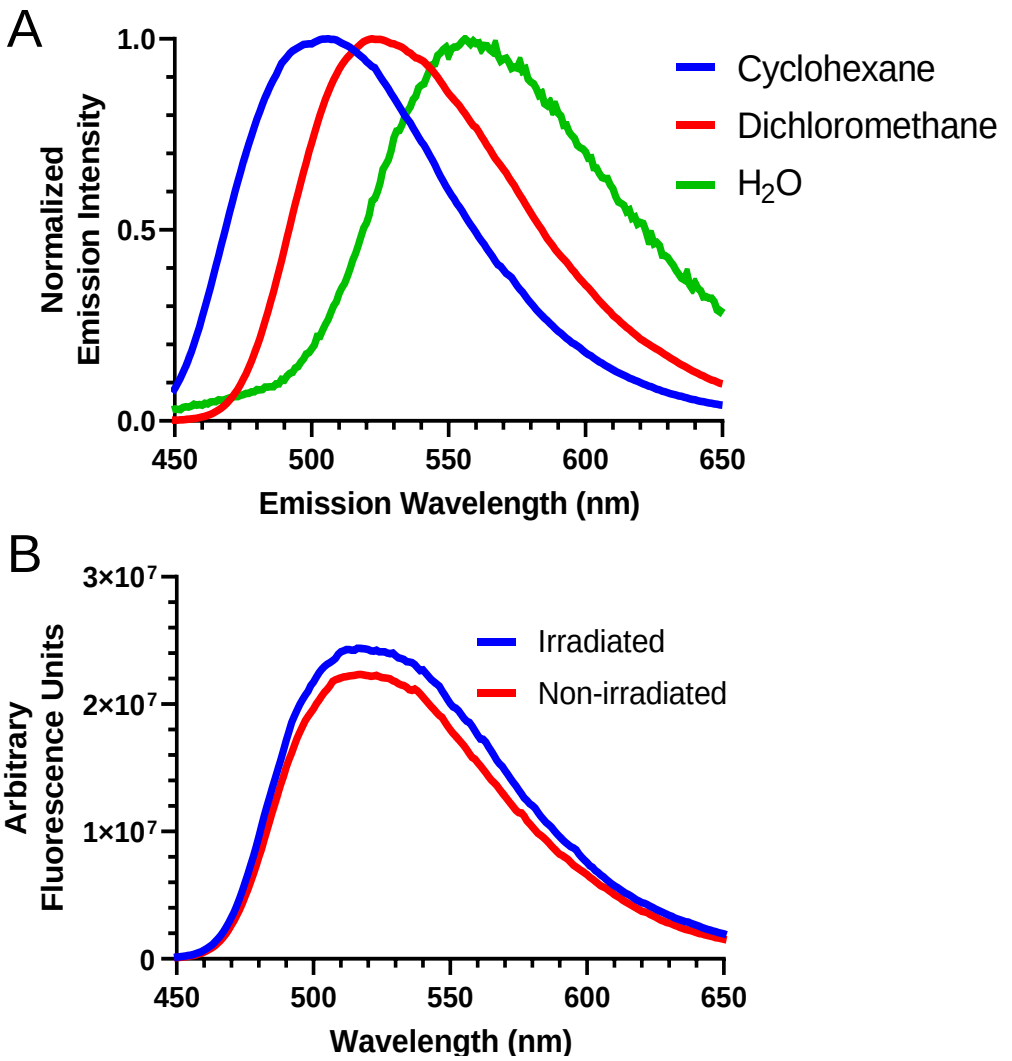


**Figure 2.4** The photochemical properties of 4-DMN. As the solvent (environment) becomes more polar, the emission wavelength increases. *(A)* 4-DMN was excited by the absorbance maxima in each solvent, which also red-shifted as solvent polarity increased (cyclohexane = 402 nm, dichloromethane = 430 nm, $H_2O$ = 444 nm. *(B)* Contrary to expectations of a decreased fluorescent intensity, we observed a slight increase in fluorescence after UV irradiation.

electrophysiology. In our experience, differentiating between signal and noise is easier in electrophysiology than in microscopy. Using THG73 charged with 4-DMN, we could selectively incorporate 4-DMN at a specific residue.[14]

We tested several different sites to see if 4-DMN could be successfully incorporated into the mm nAChR. Some sites are very sensitive to changes and

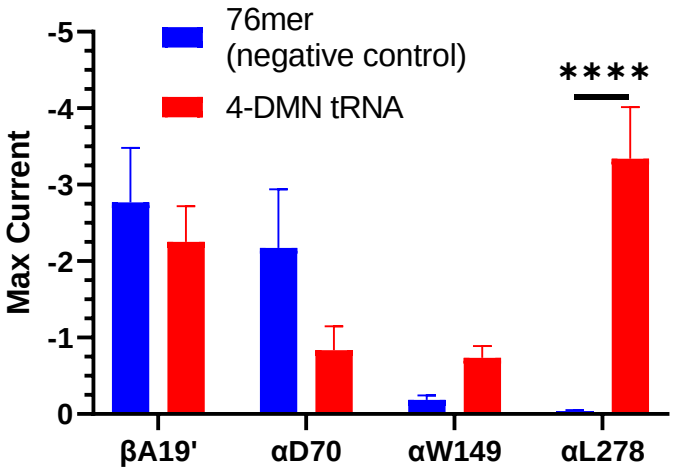


**Figure 2.5** Integrity of the different residues for amber codon suppression. *Xenopus* oocytes were injected with 25 ng mRNA with the amber stop codon incorporated at the site listed at the bottom of each column along with 40 ng of tRNA. The only significant difference between the 76mer and the 4-DMN samples were when the αL278 site was suppressed.

thus would be poor candidates for incorporating 4-DMN. Likewise, certain sites will have greater than average read-through events.[16] Since 4-DMN is larger than any of the canonical amino acids, we decided to begin with sites that have already been used to incorporate fluorophores either directly via NCAA mutagenesis or via tethering through a cysteine residue. These residues are A19' (the prime notation is used to number residues going up a transmembrane helix where numbering starts on the intracellular side of the helix) on the β subunit and D70 on the α subunit.[5,12] Unfortunately, both of these sites produced larger currents with our negative controls, suggesting that read-through may have been too high.

Going away from the more promiscuous sites, we next tested the TrpB site (W149) on the α subunit and L9' (L278) on the α subunit.[18-20] We decided to go with these sites because we know they have significant roles in channel activation, thus read-through at these residues will be more drastic than at the A19' or D70 site. Both of these residues had higher currents when we used a 4-DMN-charged tRNA over the 76mer control, with the L9' site giving a significant difference (**Figure 2.5**). Although it was surprising that so many sites gave currents with the

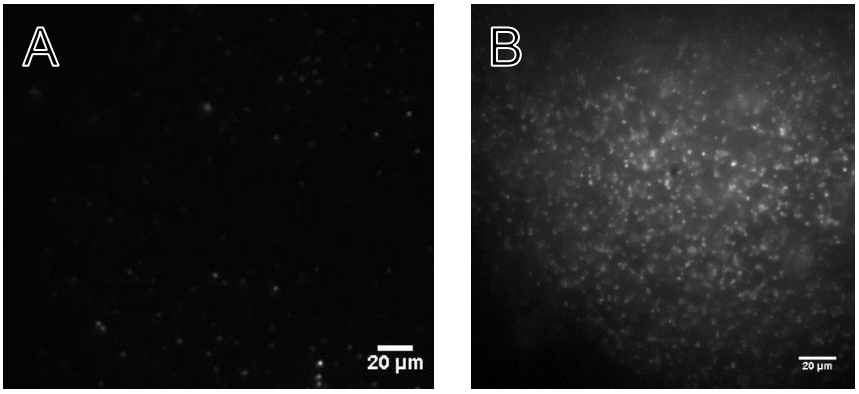


**Figure 2.6** Preliminary TIRF experiments to see if unincorporated 4-DMN gave substantial signal at the plasma membrane. *(A)* An uninjected oocyte. *(B)* An oocyte injected with 4-DMN-charged tRNA and no mRNA. The intense signal from panel *(B)* suggests that we would not be able to differentiate between incorporated and unincorporated 4-DMN.

76mer control, it is reassuring that we could incorporate 4-DMN at the L9' site. Further, in terms of the goals of this project, we should see changes in the polarity surrounding this site. The L9' residue is expected to occlude the pore in the inactive states (hydrophilic environment) and rotate to face the other transmembrane helices upon activation (hydrophobic environment).[20]

*2.3.3 Efforts to observe 4-DMN incorporated into mm nAChRs in Xenopus oocytes*

Since we successfully incorporated 4-DMN into mm nAChR, we decided to move into microscopy experiments to see if we could visualize these receptors using 4-DMN fluorescence. At this point, we exclusively utilized TIRF microscopy because the autofluorescence from the *Xenopus* oocyte yolk will overwhelm any signal from 4-DMN.

First, we wanted to see what oocytes looked like when we just injected 4-DMN-charged tRNA. This is an important negative control since we expect incorporation efficiency to be less than 100%, thus we want to know what an oocyte would look like if 4-DMN is not incorporated into the mm nAChR. Unfortunately,

there is intense fluorescence from the plasma membrane after 4-DMN-charged tRNA injection (**Figure 2.6**). This finding is consistent with the structure of 4-DMN as it is a hydrophobic molecule that will localize to hydrophobic regions. Indeed, when we performed experiments looking at where 4-DMN localizes in HEK293T cells, we found that it did localize in the plasma membrane (**Figure 2.7**).

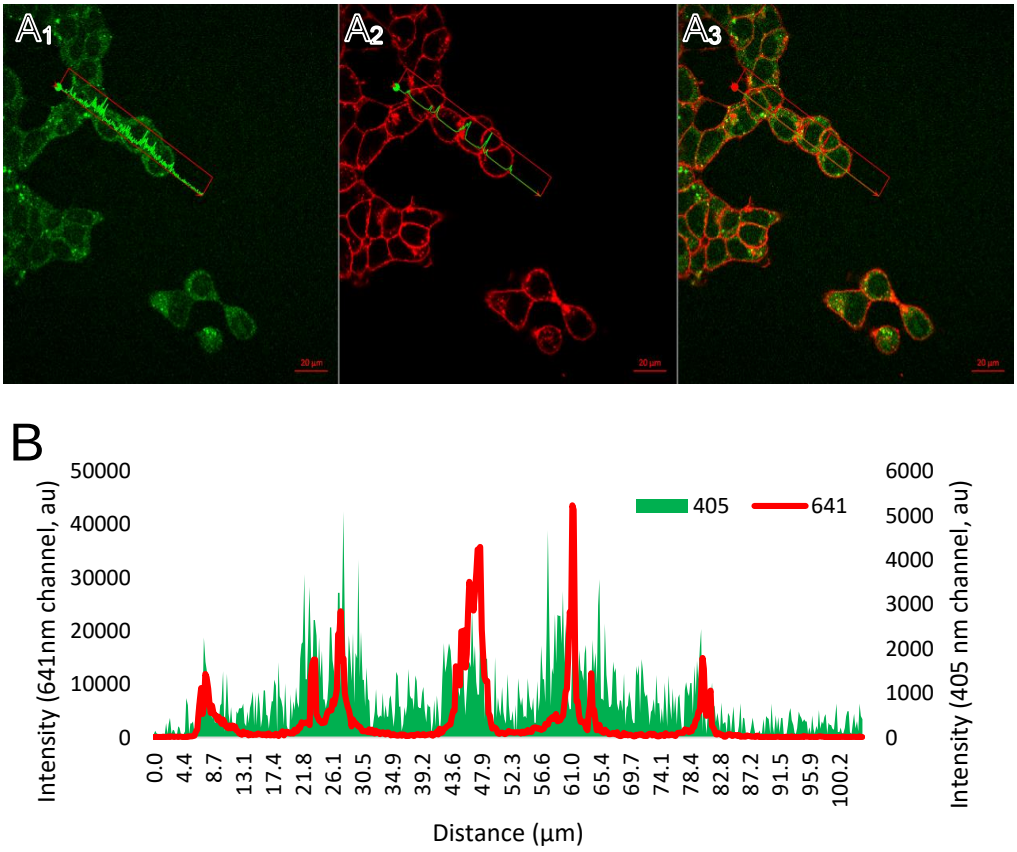


**Figure 2.7** 4-DMN localizes to the plasma membrane. *(A)* Confocal images of HEK293T cells. *($A_1$)* 4-DMN channel *($A_2$)* Plasma membrane marker. *($A_3$)* Merged. *(B)* Co-linearization line analysis showing that the peaks coincide, suggesting that 4-DMN localizes to the plasma membrane. The specific line used is depicted in ($A_1$).

Unfortunately, despite our attempts to use other solvatochromic amino acids, we could not overcome this barrier.

## 2.4 Conclusions

Despite our best attempts at this ambitious project, we ultimately came short of our goal of visualizing mm nAChRs using a solvatochromic amino acid. Unlike previous attempts performed by Rigo Pantoja and co-workers, we could not definitively observe receptors with a fluorescent amino acid.[5] While we were both able to incorporate the NCAA, in Pantoja *et al*., they observed ~10-fold more fluorescent puncta in their experimental samples than in their negative controls (without mRNA). Unfortunately, we were not able to replicate these results with 4-DMN.

Nonetheless, the project was not entirely for naught. We were able to synthesize and incorporate 4-DMN into the mm nAChR. Additionally, the insights with 4-DMN cellular localization will guide further efforts with this project. More hydrophilic fluorophores should be preferred to avoid plasma membrane localization of unincorporated NCAA. Furthermore, more *in vitro* methods could be explored. Miles *et al*. isolated the plasma membrane to restrict their observations to the plasma membrane.[21] While TIRF microscopy is good at limiting excitation to near the coverslip, it is not perfect. By isolating membranes, it leaves no doubt that we would exclusively observe signals from the plasma membrane. Additionally, using plasma membrane isolates, we could wash the plasma membrane and potentially remove unincorporated 4-DMN. Alternatively, one could explore developing an orthogonal synthetase/tRNA for 4-DMN to move into mammalian cell cultures.[22] These systems lend themselves more easily to microscopy and will not be restricted to membrane-bound targets. However, evolving a synthetase/tRNA is a monumental task. Lastly, other photochemical properties could be examined. Fluorescent lifetime measurements have become routine

recently, and depending on how the lifetime changes between 4-DMN in the lipid bilayer versus the mm nAChR, one could isolate the mm nAChR signal.[23-25]

## 2.5 Materials and Methods

### *2.5.1 Synthesis*

All reagents and solvents were procured from Sigma-Aldrich unless otherwise stated, and used as received. All organic reactions were carried out under an argon atmosphere in a flame-dried flask with a sealed rubber septum.

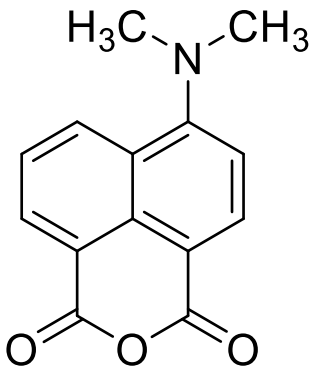


**4-N,N-dimethylamino naphthalic anhydride (4DMNA)** Synthesis was largely based on the protocol used by Kollar et al.[26] A solution of 4-bromo-1,8-napthalic anhydride (1.12 g, 4.0 mmol) in 3-methyl-1-butanol (28 mL) was heated to 132°C and stirred.[26] To this solution, 3-dimethlyaminopropionitrile (1.6 g, 16 mmol) was added and allowed to stir at 132°C for 12 hours. Crystals formed and were filtered and washed with water and cold hexanes to yield 0.7 g of orange product (73%) $^{1}$H-NMR (300 MHz, CDCl3): δ 3.18 (s, 6H), 7.11 (d, 8.4 Hz, 1H), 7.67 (t, 7.3 Hz, 1H), 8.47 (m, 2H), 8.57 (d, 7.3 Hz, 1H). LC-MS m/z: 242 [M+H]

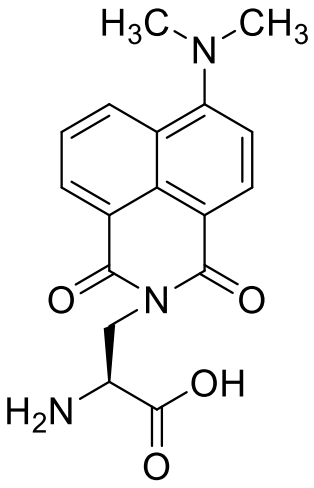

**$NH_2$-4DMN-COOH** Synthesis was largely based on the protocol used by Loving et al.[13] Briefly, (S)-3-amino-2- (Boc-amino)-propionic acid (200 mg, 0.98 mmol) and $NaHCO_3$ (400 mg, 4.9 mmol) were dissolved in 5 mL $dH_2O$. A separate flask was used to dissolve 4DMNA (0.26 g, 1.1 mmol) in dioxane (25 mL) which was evacuated of air, charged with $N_2$, stirred, and brought to reflux. Once at reflux, the amino acid solution was slowly added to the 4DMNA solution. The reaction was allowed to proceed at reflux for 30 minutes before allowing to cool to room temperature. The solution was then concentrated via a rotary evaporator, diluted with $dH_2O$ (20 mL), and washed with diethyl ether (3x20 mL). The aqueous layer was acidified and extracted with dichloromethane (3x30 mL). Organic layers were combined, dried over $MgSO_4$, filtered, and concentrated. The solid was then dissolved in 50% trifluoroacetic acid in dichloromethane and stirred for 90 minutes at room temperature. The solution was then concentrated by azeotroping with toluene to yield 230 mg (70%) of an orange solid. $^1$H NMR (300 MHz, Methanol-*d*4) δ 8.58 (m, 2H), 8.47 (d, 8.0 Hz, 1H), 7.75 (t, 8.0 Hz, 1H), 7.24 (d, 8.4 Hz, 1H), 4.74 (s, 1H), 4.68 – 4.56 (m, 1H), 4.32 (s, 1H), 3.22 – 3.12 (m, 6H). LC-MS: 328 [M+H]

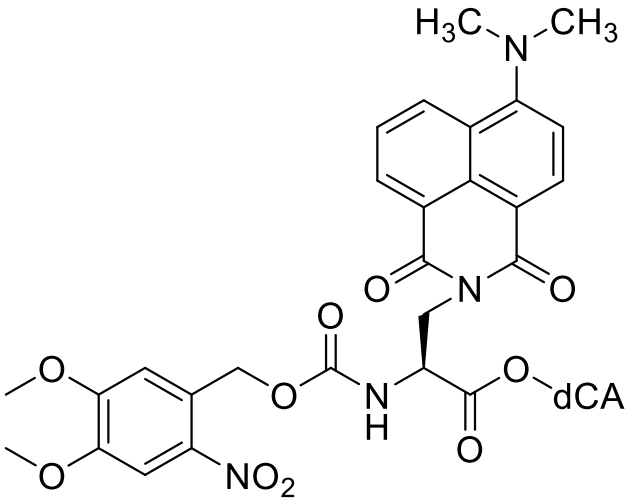


**Nvoc-4DMN-dCA** To $NH_2$-4DMN-COOH (164 mg, 0.5 mmol) was added 4,5-dimethoxy-2-nitrobenzyl chloroformate (Nvoc-Cl) (162 mg, 0.59 mmol), $Na_2CO_3$ (62 mg, 0.59 mmol), dioxane (50 mL) and water (34 mL), and stirred overnight at room temperature. The resulting solution was then concentrated and not purified further. Dimethylformamide (3.25 mL), 2-chloroacetonitrile (3.25 mL), and trimethylamine (0.23 mL) were added and stirred for 36 hours at room temperature. The resulting solution was concentrated, dissolved in acetonitrile, and purified via reverse-phase HPLC. Positive fractions were identified by ESI-MS and lyophilized. The solid Nvoc-4DMN-cyanomethyl ester was then dissolved in dimethylformamide (1 mL), added to a vial containing 5 mg tertbutyl-ammonium and 5 mg dCA, and stirred for 36 hours. The resulting solution was diluted to 10ml 1:1 acetonitrile/water and purified via reverse-phase HPLC. ESI-MS: 1185 [M+H].

*2.5.2 Mouse Muscle nAChR Molecular Biology*

Nvoc-4DMN-dCA was ligated onto a THG73 74mer using T4 RNA ligase to generate Nvoc-4DMN-THG73 (MALDI-MS, m/z= 24857.7, calc: 24845). Before injection, Nvoc-4DMN-THG73 was decaged using a 365 nm LED rated for 1 W for

150 s. The formation of $NH_2$-4DMN-THG73 was verified by MALDI and immediately injected into oocytes along with the appropriated mRNA. Mutated mRNA strands were generated from pAMV plasmid expressing the mouse muscle nAChR subunits and subjecting them to QuikChange PCR (Stratagene) to insert the mutations into the plasmid. The PCR product is then electroporated into *E. coli* and grown on a LB Agar plate at 37°C for 18 hours. Colonies were then picked and grown up in 2XYT media at 37°C for 12 hours. Bacteria was then subjected to a MiniPrep (Qiagen) and sequenced to confirm the mutation. Positive results were then linearized using the NotI restriction enzyme and translated to mRNA using a T7 mMessage mMachine kit (Thermo Fisher).

*2.5.3 Microinjection*

Stage V-VI *Xenopus laevis* oocytes were injected with mRNA and tRNA as described previously.[27,28] Each oocyte was injected with approximately 50 nL of solution with 10-25 ng mRNA and approximately 40 ng tRNA. Oocytes were injected twice over a 48 hours incubation time and either recorded in a two-electrorode voltage clamp on a OpusXpress 6000A or devitallinized and imaged using TIRF microscopy on a Zeiss Elyra microscope at the Translational Imaging Center at the University of Southern California.

**2.6 References**

1 Vinothkumar, K. R. & Henderson, R. Structures of membrane proteins. *Q Rev Biophys* **43**, 65-158, doi:10.1017/S0033583510000041 (2010).

2 Morales-Perez, C. L., Noviello, C. M. & Hibbs, R. E. X-ray structure of the human α4β2 nicotinic receptor. *Nature* **538**, 411-415, doi:10.1038/nature19785 (2016).

3 Walsh, R. M. *et al.* Structural principles of distinct assemblies of the human α4β2 nicotinic receptor. *Nature* **557**, 261-265, doi:10.1038/s41586-018-0081-7 (2018).

4 Gharpure, A. *et al.* Agonist selectivity and ion permeation in the α3β4 ganglionic nicotinic receptor. *Neuron* **104**, 501-511.e506, doi:10.1016/j.neuron.2019.07.030 (2019).

5 Pantoja, R., Rodriguez, E. A., Dibas, M. I., Dougherty, D. A. & Lester, H. A. Single-molecule imaging of a fluorescent unnatural amino acid incorporated into nicotinic receptors. *Biophysical Journal* **96**, 226-237, doi:10.1016/j.bpj.2008.09.034 (2009).

6 Cohen, B. E. *et al.* Probing protein electrostatics with a synthetic fluorescent amino acid. *Science* **296**, 1700-1703, doi:10.1126/science.1069346 (2002).

7 Turcatti, G. *et al.* Probing the structure and function of the tachykinin neurokinin-2 receptor through biosynthetic incorporation of fluorescent amino acids at specific sites. *J. Biol. Chem.* **271**, 19991-19998 (1996).

8 Niko, Y., Kawauchi, S. & Konishi, G.-i. Solvatochromic pyrene analogues of prodan exhibiting extremely high fluorescence quantum yields in apolar and polar solvents. *Chemistry – A European Journal* **19**, 9760-9765, doi:10.1002/chem.201301020 (2013).

9 Rácz, D., Nagy, M., Mándi, A., Zsuga, M. & Kéki, S. Solvatochromic properties of a new isocyanonaphthalene based fluorophore. *Journal of Photochemistry and Photobiology A: Chemistry* **270**, 19-27, doi:10.1016/j.jphotochem.2013.07.007 (2013).

10 Greiner, R., Schlücker, T., Zgela, D. & Langhals, H. Fluorescent aryl naphthalene dicarboximides with large Stokes shifts and strong solvatochromism controlled by dynamics and molecular geometry. *J. Materials Chemistry C* **4**, 11244-11252, doi:10.1039/C6TC04453K (2016).

11 Mattheyses, A. L., Simon, S. M. & Rappoport, J. Z. Imaging with total internal reflection fluorescence microscopy for the cell biologist. *J. Cell Science* **123**, 3621-3628, doi:10.1242/jcs.056218 (2010).

12 Dahan, D. S. *et al.* A fluorophore attached to nicotinic acetylcholine receptor βM2 detects productive binding of agonist to the αδ site. *PNAS* **101**, 10195-10200, doi:10.1073/pnas.0301885101 (2004).

13 Loving, G. & Imperiali, B. A versatile amino acid analogue of the solvatochromic fluorophore 4-N,N-dimethylamino-1,8-naphthalimide: A powerful tool for the study of dynamic protein interactions. *J Am Chem Soc* **130**, 13630-13638, doi:10.1021/ja804754y (2008).

14 Dougherty, D. A. & Van Arnam, E. B. In vivo incorporation of non-canonical amino acids by using the chemical aminoacylation strategy: a broadly applicable mechanistic tool. *ChemBioChem* **15**, 1710-1720, doi:10.1002/cbic.201402080 (2014).

15 Saks, M. E. *et al.* An engineered tetrahymena tRNA(Gln) for in vivo incorporation of unnatural amino acids into proteins by nonsense suppression. *J. Biol. Chem.* **271**, 23169-23175 (1996).

16 Rodriguez, E. A., Lester, H. A. & Dougherty, D. A. In vivo incorporation of multiple unnatural amino acids through nonsense and frameshift suppression. *PNAS* **103**, 8650-8655, doi:10.1073/pnas.0510817103 (2006).

17 Tavares Xda, S. *et al.* Variations in binding among several agonists at two stoichiometries of the neuronal, α4β2 nicotinic receptor. *J Am Chem Soc* **134**, 11474-11480, doi:10.1021/ja3011379 (2012).

18 Xiu, X. A., Puskar, N. L., Shanata, J. A. P., Lester, H. A. & Dougherty, D. A. Nicotine binding to brain receptors requires a strong cation-π interaction. *Nature* **458**, 534-U510, doi:10.1038/nature07768 (2009).

19 Van Arnam, E. B., Blythe, E. E., Lester, H. A. & Dougherty, D. A. An unusual pattern of ligand-receptor interactions for the α7 nicotinic acetylcholine receptor, with implications for the binding of varenicline. *Mol Pharmacol* **84**, 201-207, doi:10.1124/mol.113.085795 (2013).

20 Labarca, C. *et al.* Channel gating governed symmetrically by conserved leucine residues in the M2 domain of nicotinic receptors. *Nature* **376**, 514-516, doi:10.1038/376514a0 (1995).

21 Miles, T. F., Dougherty, D. A. & Lester, H. A. The 5-$HT_3$AB receptor shows an $a_3b_2$ stoichiometry at the plasma membrane. *Biophysical Journal* **105**, 887-898, doi:10.1016/j.bpj.2013.07.015 (2013).

22 Ellman, J., Mendel, D., Anthonycahill, S., Noren, C. J. & Schultz, P. G. Biosynthetic method for introducing unnatural amino acids site-specifically into proteins. *Method Enzymol.* **202**, 301-336, doi:10.1016/0076-6879(91)02017-4 (1991).

23 Berezin, M. Y., Lee, H., Akers, W. & Achilefu, S. Near infrared dyes as lifetime solvatochromic probes for micropolarity measurements of biological systems. *Biophysical Journal* **93**, 2892-2899, doi:10.1529/biophysj.107.111609 (2007).

24 Elder, A. D. *et al.* A quantitative protocol for dynamic measurements of protein interactions by Förster resonance energy transfer-sensitized fluorescence emission. *J R Soc Interface* **6**, S59-S81, doi:10.1098/rsif.2008.0381.focus (2009).

25 Levitt, J. A., Chung, P. H. & Suhling, K. Spectrally resolved fluorescence lifetime imaging of Nile red for measurements of intracellular polarity. *J. Biomed. Opt.* **20**, 11, doi:10.1117/1.jbo.20.9.096002 (2015).

26 Kollar, J., Hrdlovic, P., Chmela, S., Sarakha, M. & Guyot, G. Synthesis and transient absorption spectra of derivatives of 1,8-naphthalic anhydrides and naphthalimides containing 2,2,6,6-tetramethylpiperidine; triplet route of deactivation. *J. Photochem. Photobiol. A-Chem.* **170**, 151-159, doi:10.1016/j.jphotochem.2004.07.021 (2005).

27 Marotta, C. B., Dilworth, C. N., Lester, H. A. & Dougherty, D. A. Probing the non-canonical interface for agonist interaction with an α5 containing nicotinic acetylcholine receptor. *Neuropharmacology* **77**, 342-349, doi:10.1016/j.neuropharm.2013.09.028 (2014).

28 Nichols, W. A. *et al.* Mutation linked to autosomal dominant nocturnal frontal lobe epilepsy reduces low-sensitivity α4β2, and increases α5α4β2, nicotinic receptor surface expression. *PLoS One* **11**, e0158032, doi:10.1371/journal.pone.0158032 (2016).

# Chapter 3: Identification and biophysical analysis of the menthol binding site in the α4β2 nicotinic acetylcholine receptor

**This chapter is partly adapted from*: Brandon J. Henderson, Stephen Grant, *et al.* Menthol stereoisomers exhibit different effects on α4β2 nACh upregulation and dopamine neuron spontaneous firing. *eNeuro*, **2018.**

## 3.1 Abstract

Smoking is the leading cause of preventable death, with tobacco being responsible for over 7 million deaths each year. The addictive compound in tobacco, nicotine, will bind to several receptors in the brain to elicit pleasurable sensations that lead to addiction. However, inhaling burning gas during smoking can be uncomfortable. To overcome these unpleasant burning sensations, tobacco companies make cigarettes with menthol, a cooling agent, to make their products more attractive. For decades, menthol was thought to be a flavorant without any significant effects on the brain. Unfortunately, recent work has demonstrated that not only does menthol have a neurobiological effect, but it may accentuate nicotine addiction. One explanation for this observation is that menthol upregulates α4-containing (α4*) nAChRs, the proteins most responsible for the effects of nicotine. Additionally, menthol is a negative allosteric modulator of the α4β2 nAChRs. However, the binding site for menthol on α4β2 had not been determined. Here, using molecular dynamics (MD) and TEVC electrophysiology, we determine that menthol is binding to α4β2 at the pore and mutating the L9' site alters menthol's potency as a negative allosteric modulator. These results confirm that menthol can bind to α4β2. Furthermore, we determine that the effect is

primarily based on the size at the 9' residue and one menthol molecule is sufficient for receptor inhibition. Together, the menthol binding site's experimental determination on α4β2 gives further proof that menthol is not an innocent bystander in nicotine addiction.

**3.2 Introduction**

Humans have consumed tobacco for millennia, but it was only in the past few decades that we have come to terms with its adverse health effects. In 1964, the United States Surgeon General issued a warning about smoking's health hazards.[1] Since then, scientists and politicians have worked together to protect people from tobacco's harmful effects. Nevertheless, millions of people and hundreds of billions of dollars are lost globally due to tobacco. A primary challenge in addressing nicotine addiction, from a scientific standpoint, is that it is a neuronal condition. The brain remains one of the most mysterious things that we know. Nonetheless, we are making progress in understanding the brain, and we certainly know more about nicotine addiction than we did even a year ago.

One of the most important discoveries was finding the neuronal nAChRs. These are pentameric ligand-gated ion channels that are composed of α and β subunits.[2] Given that there are six unique α subunits and three unique β subunits found in the brain, there is incredible diversity in the types of nAChRs that can assemble in the brain. Of the hundreds of possible nAChR combinations, perhaps the most important one to nicotine addiction is the nAChR composed of α4 and β2 subunits, the α4β2 nAChR.[3,4] Activation of α4* nAChRs is sufficient for reward and tolerance and nicotine self-administration is attenuated in β2-knock out mice.[5,6]

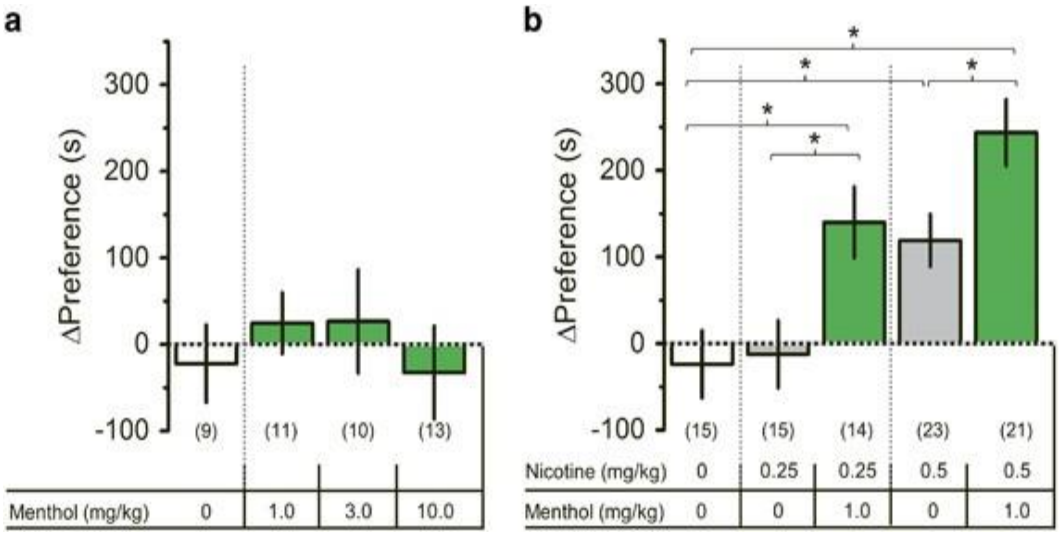


**Figure 3.1** Menthol alone does not change place preference *(a)*, but will increase nicotine-related reward *(b)*. (Henderson 2017)

Combined with the prominence of α4β2 nAChRs in the brain, we decided to focus specifically on the α4β2 nAChR.

While unflavored cigarettes are in high demand, a large portion of nicotine consumers prefer a flavored product. For most of its history, tobacco flavors were not regulated, but this ended in 2009 when the Family Smoking Prevention and Tobacco Control Act limited flavors to just menthol. Menthol provides a cooling sensation from the activation of the transient receptor potential cation channel subfamily melastatin member 8 (TRPM8).[7] Menthol cigarettes control a large portion of the market (currently, approximately 25% of all smokers use menthol cigarettes) and was thought to have no meaningful impact on addiction.[8] Unfortunately, the latter statement proved to be incorrect. Firstly, menthol cigarette smokers have a harder time quitting and have a greater dependence on their cigarettes than non-mentholated cigarette smokers.[9,10] There are three potential reasons for these observations (and indeed they may all play a role): menthol makes the cigarettes taste better than non-mentholated cigarettes, menthol

decreases nicotine metabolism, and menthol has a neurobiological effect on menthol cigarette smokers.[11] Recent work gives credence to the third reason as injected menthol will enhance the nicotine-related reward (**Figure 3.1**).[12] Further studies revealed that dopaminergic neurons treated with menthol and nicotine would have more α4* and α6* receptors on the plasma membrane, and these receptors will be biased towards the higher sensitivity confirmation.[12] We also see α4* receptors upregulated when the dopaminergic neurons are treated with only menthol, although menthol alone will bias towards the less sensitive confirmation.[13]

In addition to menthol's cellular effects, menthol has been found to affect several neuronal receptors directly, including α4β2.[14] Menthol is a negative allosteric modulator for many of these receptors.[15-20] Specifically, menthol will inhibit currents through these receptors without affecting agonist $EC_{50}$, demonstrating that menthol will not compete for the agonist binding site. Although these results are not tremendously physiologically relevant because the $IC_{50}$ for menthol is several orders of magnitude higher than the concentrations found in a menthol smoker's brain, they show a direct interaction between menthol and these important neuroreceptors. Nonetheless, other methods for channels modulation do not involve direct binding to the receptor. For example, the lipid environment can play a major role in membrane protein function, so a small molecule can induce changes to a membrane protein by altering the surrounding lipids.[21-23] Since menthol will partition primarily out of solution and into the lipid bilayer, altering the membrane environment is a possible mechanism for altering channel activity.

Here, we tested our hypothesis that menthol was binding to α4β2 by looking for the menthol binding site for α4β2. We turned to our collaborators in the Clemons (Caltech) and Tajkhorshid (UIUC) labs for MD simulations to give us

insight into where menthol may interact with α4β2. Using the crystal structure solved by the Hibbs group in 2016, we could predict the residues that menthol would likely explore.[24] Although the MD simulations predict the most of the menthol will enter the lipid bilayer, one of the trajectories predicts that menthol will enter the channel and populate an area around the 9' (the prime numbering system starts numbering residues from the cytoplasmic side of the helix) site on the M2 helix.[25] Going forward with this prediction, we experimentally tested the 9' site by mutating it to different residues to see if it affected menthol's $IC_{50}$. Indeed, menthol's $IC_{50}$ depended on the residue's size at the 9' site, where larger residues gave a lower $IC_{50}$. We also found that one menthol molecule was sufficient for channel inhibition, consistent with our MD simulations. The identification of the menthol binding site, thus proving that menthol directly interacts with neuronal proteins, supports why menthol is a dangerous molecule to include in nicotine products.

## 3.3 Results and Discussion

### *3.3.1 Changing the residue at the 9' site in the M2 helix alters menthol's $IC_{50}$*

At a set concentration of agonist, the presence of menthol will cause fewer ions to pass through the α4β2 nAChR than when menthol is absent. This inhibition is directly related to the concentration of menthol in the solution, where a higher concentration of menthol will inhibit the channel more. Plotting the concentration of menthol against the number of ions passing through the channel (the current) and fitting to the Hill equation:

$$Normalized\ Current = \frac{1}{1+\left(\frac{IC_{50}}{[menthol]}\right)^{n}} \quad (1)$$

where n is the Hill coefficient, we can measure the menthol's ability to inhibit the α4β2 nAChR using TEVC electrophysiology.[26] When we have a candidate site for the menthol binding site, we would mutate it and then remeasure the $IC_{50}$ for

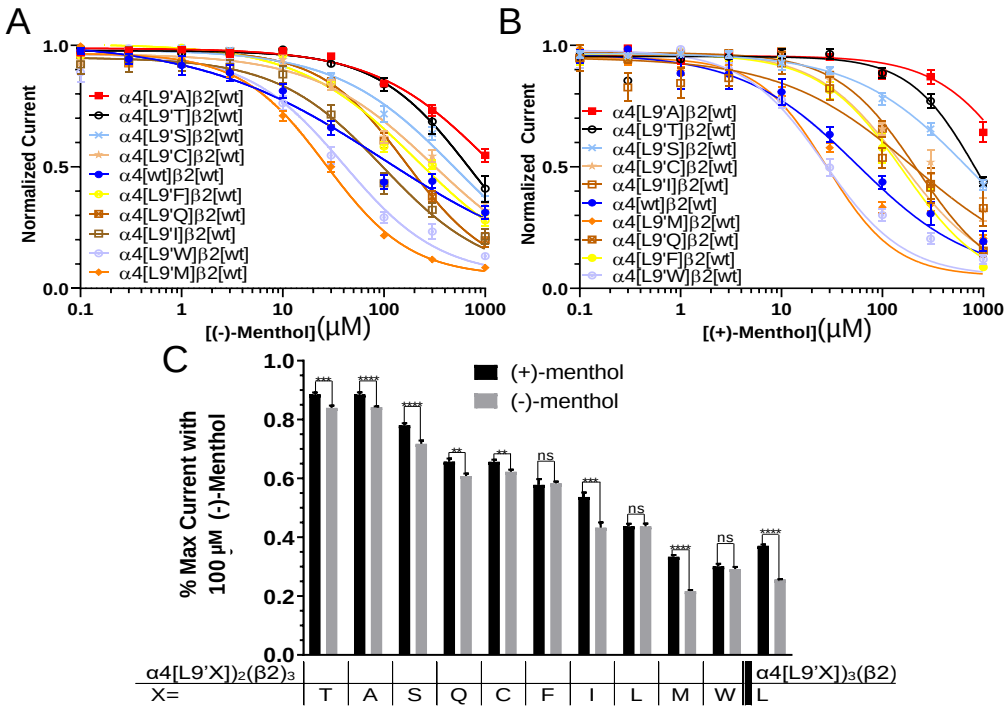


**Figure 3.2** Changing the residue at the 9' site on the M2 helix changes the $IC_{50}$ curve for *(A)*(-)-menthol and *(B)* (+)-menthol for the $(\alpha4)_2(\beta2)_3$ receptor. *(C)* Inhibition with 100 μM (-)-menthol is higher than inhibition with 100 μM (+)-menthol. P-values are calculated from a Student's t-test. ****, $p < 0.001$; ***, $p<0.005$, **, $p<0.01$.

menthol to see if the mutation changed menthol's ability to negatively modulate the α4β2 nAChR.

After several unsuccessful attempts to alter menthol's $IC_{50,}$ we finally generated a significant shift by mutating the 9' site on the M2 helix (**Figure 3.2**). We find that this site is the same for both enantiomers of menthol, with (-)-menthol being more potent than (+)-menthol. This finding is consistent with a calculation performed by Rezvan Shahoei of the Tajkhorshid group (**Figure 3.3**). These results suggest that menthol can enter the pore and essentially block the channel, thus preventing ions from flowing through it. Channel block is a common strategy to antagonize ion channels, although many of them are large cations that utilize the cell membrane's negative potential, ensuring that the large cation stays in the

pore and prevents smaller ions from passing through the membrane.[27-29] Here, menthol seems to be engaging with the pore because it is more stable near the pore's hydrophobic residues than in the bulk water.

*3.3.2 Menthol inhibition is directly related to the length of the 9' residue*

Since each mutant gave a unique menthol $IC_{50}$ value, we had a decent data set to do structure-function analysis. The amino acids vary in their polarity, size, and functional groups, which allows us to probe for various trends. In addition to the reduced AA index produced by Kibinge and co-workers, we also probed for end-to-end residue length, determined with a Hartree-Fock calculation.[30] Here, we find the best correlation with the end-to-end residue length (**Figure 3.4**). This observation is consistent with our hypothesis that menthol is simply blocking the pore. We believe that we do not see a dependence

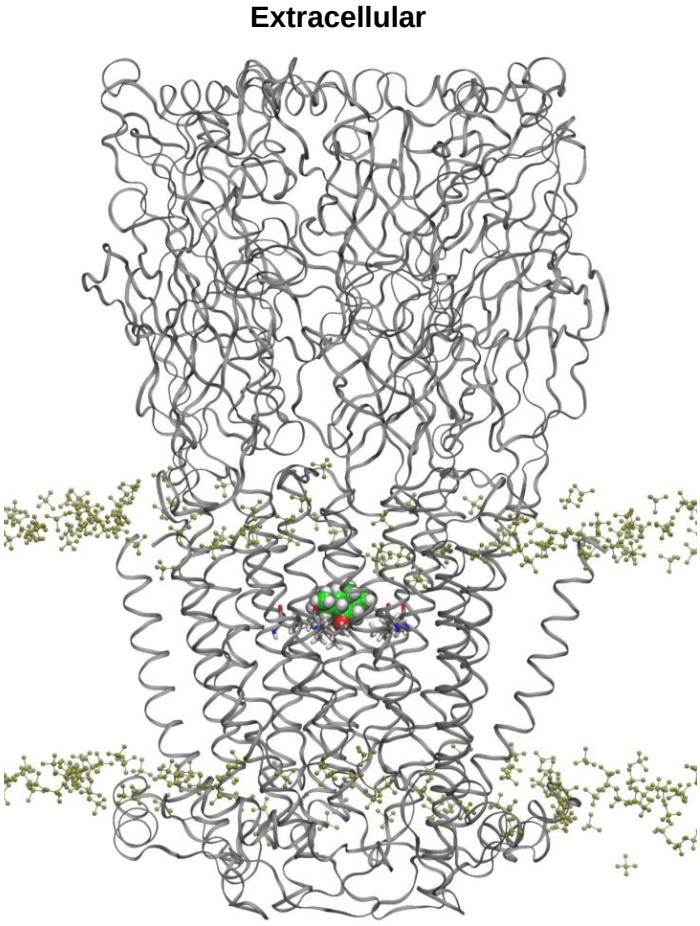


**Figure 3.3** MD simulation where menthol (space-filling model) binds to the channel pore in the α4β2 nAChR (ribbons). The sticks surrounding the α4β2 nAChR represent the polar head groups of the lipid bilayer.

on polarity because all residues provide a more nonpolar environment than water. Instead, the residue must be large enough (so that the pore is small enough) for menthol to plug the pore.

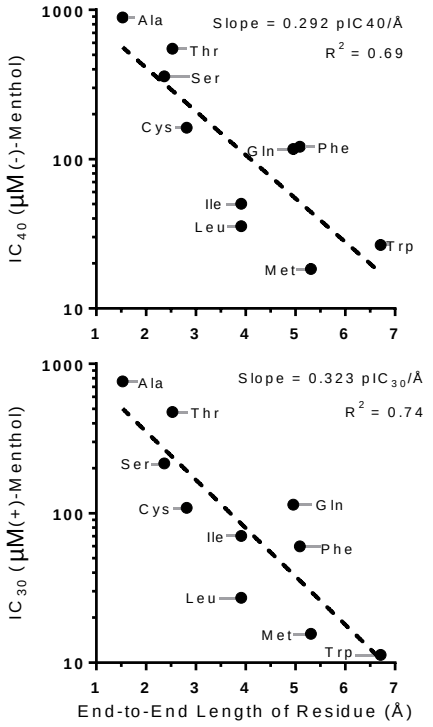


**Figure 3.4** Menthol's potency is directly related to the residue's length

Arguably the most important intermolecular interaction in proteins is the hydrogen bond, and we wanted to ensure that menthol will not bond to the 9' residue through a hydrogen bond. Since there are no canonical amino acids that differ in just the presence or absence of a hydrogen bond, we turned to NCAAs. Here, we will pick residues that will be very close to the same size but differ in the replacement of methylene for oxygen, thereby allowing this residue to become a hydrogen bond acceptor with a minimal change in sterics. Specifically, we compared the $IC_{50}$ values between a receptor with isoleucine at the 9' position with a receptor with O-methyl threonine at the 9' position (**Figure 3.5**). Since there is no difference between the $IC_{50}$'s in these two receptors, we are confident that hydrogen bonding is not important for menthol to inhibit the α4β2 nAChR.

*3.3.3 Only one menthol molecule is required for receptor inhibition*

In addition to measuring potency, the Hill equation can predict relative cooperativity between ligand binding events through the Hill coefficient.[26] For

menthol and α4β2, we can use the Hill coefficient to estimate the number of menthol molecules required for receptor inhibition. We averaged the Hill coefficient between all of the mutants we made and found that for both enantiomers of

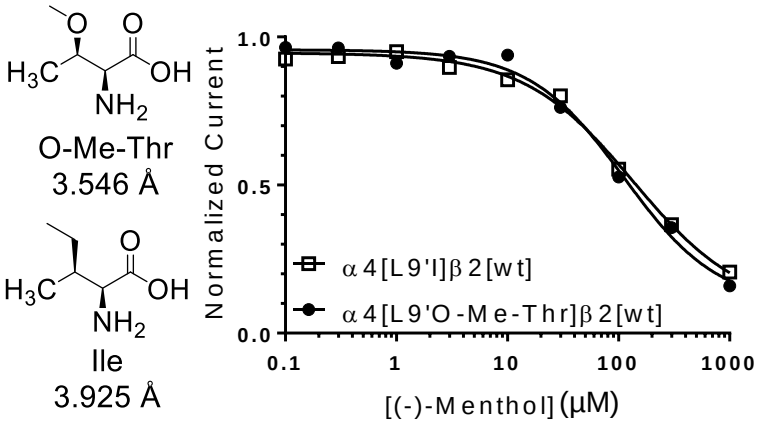


**Figure 3.5** The presence of a hydrogen bond acceptor does not change menthol's $IC_{50}$

menthol, the mean Hill coefficient is one, suggesting that one menthol molecule is sufficient for α4β2 inhibition (**Figure 3.6**).

*3.3.4 (-)-menthol is more potent than (+)-menthol*

There are eight stereoisomers of menthol, but tobacco products almost exclusively contain (-)-menthol.[31] Additionally, (-)-menthol is the most common stereoisomer found in plants and has the lowest $EC_{50}$ for TRPM8.[32] Previous work in our lab demonstrated that (-)-menthol will upregulate plasma membrane levels of α4β2, reduce the firing frequency of dopamine neurons, and decrease dopamine neuron excitability, while (+)-menthol does not.[25] Since the binding mechanism appears to be entirely based on sterics, we decided to compare the inhibitory potencies of (-)-menthol and (+)-menthol. We find that there is not a substantial difference between (-)-menthol and (+)-menthol in terms of inhibiting α4β2 (**Figure 3.7**). This contrasts with what others have observed for the $GABA_A$ receptor, where

(+)-menthol was more potent than (-)-menthol.[15] These results suggest that the origin of menthol's effects on plasma membrane α4β2 levels and dopaminergic neurons is not based on its ability to inhibit α4β2 since (+)-menthol inhibits α4β2, but it does not affect dopaminergic neurons or α4β2 plasma membrane levels.

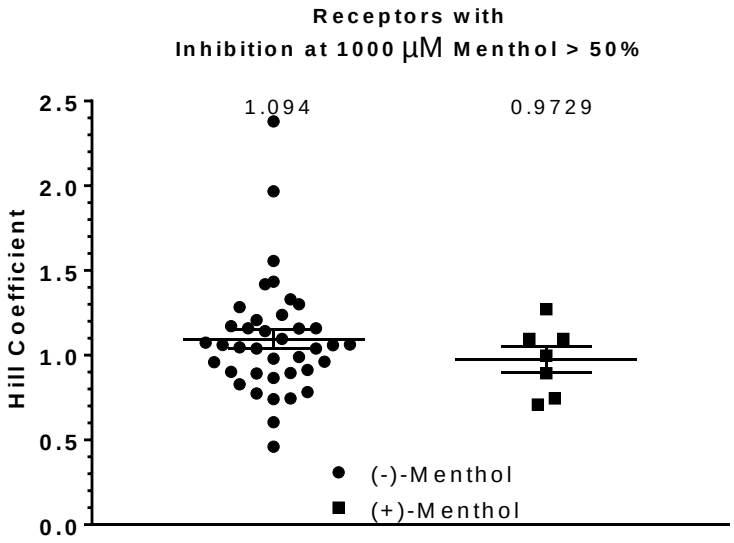


**Figure 3.6** The average Hill coefficient for the menthol concentration-response curves is ~1, suggesting that one molecule of menthol is sufficient to inhibit each α4β2 receptor.

### *3.4 Conclusions*

The increased consumption of nicotine in the past few years is troubling. Major components of the tobacco market are products that are flavored with menthol. For decades, this ingredient was thought to be inactive in the brain, but recent work shows that menthol will alter the dopaminergic neurons and increase nicotine-related reward. Our work in this chapter expands our understanding of menthol. The α4β2 nAChRs are major players in nicotine addiction, and knowing how menthol binds to these receptors gives further evidence that menthol is not an innocuous flavorant. Menthol directly interacts with the α4β2 nAChRs by binding to the pore and essentially preventing ions from flowing through the channel. There are still many questions surrounding the mechanism of menthol's

neurobiological effects, and learning more about menthol is paramount to addressing nicotine addiction.

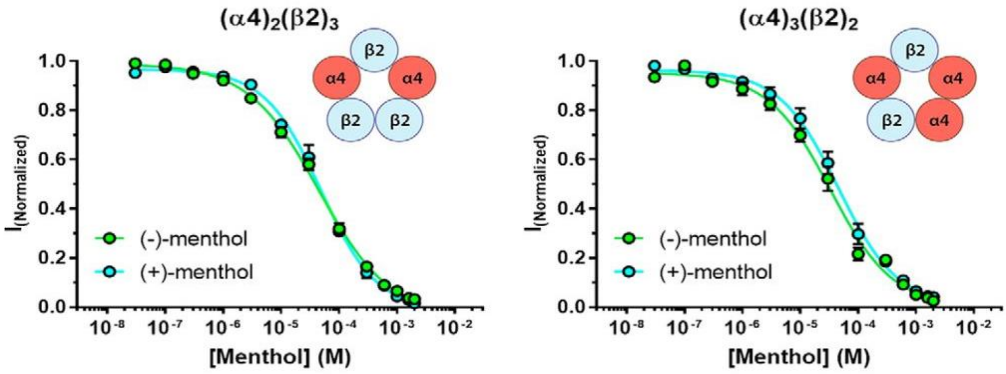


**Figure 3.7** (-)-menthol and (+)-menthol inhibit both stoichiometries of α4β2 to a similar extent

### *3.5 Materials and Methods*

#### *3.5.1 Reagents*

(-)-Menthol (product number 63658), (+)-menthol (product number M2780), and acetylcholine (ACh) chloride (product number A6625) were obtained from Sigma-Aldrich.

#### *3.5.2 Oocyte preparation and injection*

Rat α4 and β2 nAChR subunits were in pGEMhe vectors. The mRNAs were prepared from linearized DNA, using a T7 mMessage mMachine kit (Ambion), and were purified with the RNeasy Mini Kit (Qiagen). Xenopus laevis stage V and VI oocytes were harvested via standard protocols.[33] The α4 and β2 mRNAs were mixed in a 10:1 ratio to obtain the $(\alpha4)_3(\beta2)_2$ receptor or 1:10 ratio to obtain the $(\alpha4)_2(\beta2)_3$ receptor. For unnatural amino acid incorporation, a TAG codon was incorporated into the site of interest, and 40 ng of unnatural amino acid-coupled THG73 tRNA was added to the injection solution. The α4 and β2 mRNAs were

mixed in a 100:1 ratio by mass to obtain the $(\alpha4)_3(\beta2)_2$ receptor for these unnatural amino acid experiments. A total of 50 nL of the RNA mixture were injected into each oocyte, delivering an mRNA mass total of 22 ng for wild-type or conventional mutant experiments. After injection, the oocytes were incubated at 18°C in ND96 medium (96 mM NaCl, 2 mM KCl, 1 mM MgCl2, and 5mM HEPES at pH 7.5) enriched with theophylline, sodium pyruvate, and gentamicin for 48 h before recording.

*3.5.3 Oocyte electrophysiology*

The OpusXpress 6000A (Molecular Devices) in two-electrode voltage-clamp mode was used for all electrophysiological recordings. ACh was dissolved to 1 M stock solutions in ND96 $Ca^{2+}$ free buffer. The holding potential was set to -60 mV, and the running buffer used was ND96 $Ca^{2+}$ free buffer for all experiments. Drug applications used 1 mL of drug solution applied over 15 s followed by a 5 min buffer wash at a rate of 3 mL/min. Data were sampled at 50 Hz and low-pass filtered at 5 Hz. Averaged and normalized data were fit to the Hill equation to generate Hill coefficient ($n_H$) and $EC_{50}$ or $IC_{50}$ values. All currents for the activity testing were normalized to the maximum current ($I_{max}$) produced by the oocyte. Error bars represent S.E.M. values.

**3.6 References**


1 Jamal, A. *et al.* Current cigarette smoking among adults - United States, 2005-2014. *MMWR-Morb. Mortal. Wkly. Rep.* **64**, 1233-1240 (2015).

2 Pons, S. *et al.* Crucial Role of α4 and α6 Nicotinic Acetylcholine Receptor Subunits from Ventral Tegmental Area in Systemic Nicotine Self-Administration. *J. Neurosci.* **28**, 12318-12327, doi:10.1523/jneurosci.3918-08.2008 (2008).

3 Xiao, C. *et al.* Chronic nicotine selectively enhances α4β2*nicotinic acetylcholine receptors in the nigrostriatal dopamine pathway. *J. Neurosci.* **29**, 12428-12439, doi:10.1523/jneurosci.2939-09.2009 (2009).

4 Xiu, X., Puskar, N. L., Shanata, J. A., Lester, H. A. & Dougherty, D. A. Nicotine binding to brain receptors requires a strong cation-π interaction. *Nature* **458**, 534-537, doi:10.1038/nature07768 (2009).

5 Picciotto, M. R. *et al.* Acetylcholine receptors containing the β2 subunit are involved in the reinforcing properties of nicotine. *Nature* **391**, 173-177 (1998).

6 Tapper, A. R. *et al.* Nicotine activation of alpha 4*receptors: Sufficient for reward, tolerance, and sensitization. *Science* **306**, 1029-1032, doi:10.1126/science.1099420 (2004).

7 Andersson, D. A., Chase, H. W. N. & Bevan, S. TRPM8 activation by menthol, icilin, and cold is differentially modulated by intracellular pH. *J. Neurosci.* **24**, 5364-5369, doi:10.1523/jneurosci.0890-04.2004 (2004).

8 Thompson, M. F. *et al.* Menthol enhances nicotine-induced locomotor sensitization and in vivo functional connectivity in adolescence. *J. Psychopharmacol.* **32**, 332-343, doi:10.1177/0269881117719265 (2018).

9 Ahijevych, K. & Garrett, B. E. The role of menthol in cigarettes as a reinforcer of smoking behavior. *Nicotine Tob. Res.* **12**, S110-S116, doi:10.1093/ntr/ntq203 (2010).

10 Gandhi, K. K., Foulds, J., Steinberg, M. B., Lu, S. E. & Williams, J. M. Lower quit rates among African American and Latino menthol cigarette smokers at a tobacco treatment clinic. *Int. J. Clin. Pract.* **63**, 360-367, doi:10.1111/j.1742-1241.2008.01969.x (2009).

11 Benowitz, N. L., Herrera, B. & Jacob, P., 3rd. Mentholated cigarette smoking inhibits nicotine metabolism. *J. Pharmacology and Experimental Therapeutics* **310**, 1208-1215, doi:10.1124/jpet.104.066902 (2004).

12 Henderson, B. J. *et al.* Menthol enhances nicotine reward-related behavior by potentiating nicotine-induced changes in nAChR function, nAChR upregulation, and da neuron excitability. *Neuropsychopharmacology* **42**, 2285-2291, doi:10.1038/npp.2017.72 (2017).

13 Henderson, B. J. *et al.* Menthol alone upregulates midbrain nAChR, alters nAChR subtype stoichiometry, alters dopamine neuron firing frequency, and prevents nicotine reward. *J Neurosci* **36**, 2957-2974, doi:10.1523/jneurosci.4194-15.2016 (2016).

14 Pandya, A. & Yakel, J. L. Allosteric modulators of the α4β2 subtype of neuronal nicotinic acetylcholine receptors. *Biochem. Pharmacol.* **82**, 952-958, doi:10.1016/j.bcp.2011.04.020 (2011).

15 Hall, A. C. *et al.* Modulation of human $GABA_A$ and glycine receptor currents by menthol and related monoterpenoids. *Eur. J. Pharmacol.* **506**, 9-16, doi:10.1016/j.ejphar.2004.10.026 (2004).

16 Hans, M., Wilhelm, M. & Swandulla, D. Menthol suppresses nicotinic acetylcholine receptor functioning in sensory neurons via allosteric modulation. *Chem. Senses* **37**, 463-469, doi:10.1093/chemse/bjr128 (2012).

17 Ashoor, A. *et al.* Menthol binding and inhibition of α7-nicotinic acetylcholine receptors. *PLoS One* **8**, e67674, doi:10.1371/journal.pone.0067674 (2013).

18 Ashoor, A. *et al.* Menthol Inhibits 5-$HT_3$ Receptor-Mediated Currents. *J. Pharmacol. Exp. Ther.* **347**, 398-409, doi:10.1124/jpet.113.203976 (2013).

19 Ton, H. T. *et al.* Menthol enhances the desensitization of human α3β4 nicotinic acetylcholine receptors. *Mol Pharmacol* **88**, 256-264, doi:10.1124/mol.115.098285 (2015).

20 Oz, M., Lozon, Y., Sultan, A., Yang, K. H. S. & Galadari, S. Effects of monoterpenes on ion channels of excitable cells. *Pharmacol. Ther.* **152**, 83-97, doi:10.1016/j.pharmthera.2015.05.006 (2015).

21 Brannigan, G., LeBard, D. N., Henin, J., Eckenhoff, R. G. & Klein, M. L. Multiple binding sites for the general anesthetic isoflurane identified in the nicotinic acetylcholine receptor transmembrane domain. *PNAS* **107**, 14122-14127, doi:10.1073/pnas.1008534107 (2010).

22 Henault, C. M. *et al.* The role of the M4 lipid-sensor in the folding, trafficking, and allosteric modulation of nicotinic acetylcholine receptors. *Neuropharmacology* **96**, 157-168, doi:10.1016/j.neuropharm.2014.11.011 (2015).

23 Yin, Y. & Lee, S. Y. Current view of ligand and lipid recognition by the menthol receptor TRPM8. *Trends Biochem.Sci.* **45**, 806-819, doi:10.1016/j.tibs.2020.05.008 (2020).

24 Morales-Perez, C. L., Noviello, C. M. & Hibbs, R. E. X-ray structure of the human α4β2 nicotinic receptor. *Nature* **538**, 411-415, doi:10.1038/nature19785 (2016).

25 Henderson, B. J. *et al.* Menthol stereoisomers exhibit different effects on α4β2 nAChR upregulation and dopamine neuron spontaneous firing. *eNeuro* **5**, eneuro.0465-0418.2018, doi:10.1523/eneuro.0465-18.2018 (2018).

26 Prinz, H. Hill coefficients, dose–response curves and allosteric mechanisms. *Journal of Chemical Biology* **3**, 37-44, doi:10.1007/s12154-009-0029-3 (2010).

27 Pascual, J. M. & Karlin, A. Delimiting the binding site for quaternary ammonium lidocaine derivatives in the acetylcholine receptor channel. *J. Gen. Physiol.* **112**, 611-621, doi:10.1085/jgp.112.5.611 (1998).

28 Charnet, P. *et al.* An open-channel blocker interacts with adjacent turns of α-helices in the nicotinic acetylcholine receptor. *Neuron* **4**, 87-95, doi:10.1016/0896-6273(90)90445-l (1990).

29 Wang, C., Takeuchi, K., Pinto, L. H. & Lamb, R. A. Ion-channel activity of influenza-A virus M(2) protein - characterization of the amantadine block. *Journal of Virology* **67**, 5585-5594, doi:10.1128/jvi.67.9.5585-5594.1993 (1993).

30 Kibinge, N., Ikeda, S., Ono, N., Altaf-Ul-Amin, M. & Kanaya, S. Integration of residue attributes for sequence diversity characterization of terpenoid enzymes. *BioMed Research International* **2014**, 10, doi:10.1155/2014/753428 (2014).

31 Chen, C., Luo, W. T., Isabelle, L. M., Gareau, K. D. & Pankow, J. F. The stereoisomers of menthol in selected tobacco products. A brief report. *Nicotine Tob. Res.* **13**, 741-745, doi:10.1093/ntr/ntr031 (2011).

32 Sherkheli, M. A. *et al.* Characterization of selective TRPM8 ligands and their structure activity response (SAR) relationship. *J. Pharm. Pharm. Sci.* **13**, 242-253, doi:10.18433/j3n88n (2010).

33 Marotta, C. B., Dilworth, C. N., Lester, H. A. & Dougherty, D. A. Probing the non-canonical interface for agonist interaction with an α5 containing

nicotinic acetylcholine receptor. *Neuropharmacology* **77**, 342-349, doi:10.1016/j.neuropharm.2013.09.028 (2014).

# Chapter 4: Opioid receptor antagonists pharmacologically chaperone a mutant μ-opioid receptor via an endoplasmic reticulum exit site-dependent pathway

*This work was done in collaboration with Anand K. Muthusamy and Dr. Matthew J. Mulcahy*

## 4.1 Abstract

Some opioid-related drug overdoses occur during relapse after naltrexone (Ntx) or naloxone treatment. These opioid receptor antagonists induce supersensitivity to μ-opioid receptor (MOR) agonists *in vivo,* thereby increasing the risk of overdose. The effects of opioid ligands on trafficking from the endoplasmic reticulum (ER) have been insufficiently studied. Endoplasmic reticulum exit sites (ERES) are a component in the trafficking of membrane proteins. Using fluorescently tagged Sec24 to visualize ERES and a highly ER-retained MOR point mutant, MOR[N190K], we measured ERES levels after incubation in various opioid receptor ligands. Data from sensitized emission Förster resonance energy transfer (FRET) show that MOR[N190K] interacts with Sec24D. By expressing MOR[N190K] and Sec24D-eGFP to visualize ERES in SH-SY5Y cells fluorescently, we observe that antagonists increase the fraction of the cytoplasm occupied by ERES. In contrast to the antagonists, the agonists, morphine, fentanyl, buprenorphine, and methadone, have no significant effect on ERES levels. Mutating S375, an important phosphorylation site for MOR internalization, did not cause morphine or fentanyl to become pharmacological chaperones. Two MOR allosteric modulators had no significant effect on ERES levels. Ntx did not change intracellular cyclic adenosine monophosphate (cAMP) concentrations. We also

find that pharmacological chaperoning depends on functional coat protein I (COPI) vesicles. N-methylnaltrexone (Me-Ntx), a permanently charged analog, did not act as a pharmacological chaperone, suggesting that Me-Ntx would be safe if used more widely for its approved indications. Thus, understanding of chaperoning could lead to improved use of opioids.

**4.2 Introduction**

The MOR is the primary target for most clinically used analgesic opioids.[1] Understanding how the MOR enters and exits the plasma membrane is critical to understanding the causes of opioid use disorder.[1-6] Chronic application of certain agonists results in decreased MORs on the plasma membrane. In the prevailing view (not challenged in this study), these agonists cause phosphorylation at the C-terminus via G-protein receptor kinases, which induce β-arrestin binding and endocytosis.[7] The opioid peptides and some synthetic alkaloid agonists, like fentanyl, broadly cause rapid endocytosis.[8] In turn, researchers have tried to develop biased agonists that maintain analgesic properties while reducing dependence and tolerance.[9]

In contrast, chronic doses of the two most common opioid antagonists, naltrexone (Ntx) and naloxone,[10] decrease the number of MORs on the cell surface. This upregulation of surface levels of opioid receptors in response to antagonists causes supersensitivity *in vivo.*[11] Supersensitivity is a health concern because these antagonists are prescribed for individuals recovering from opioid use disorder. This treatment is intended to prevent relapse from causing euphoria. However, if antagonists are not present and the patient relapses to opioid use, the supersensitivity causes a more potent effect than expected, increasing the risk of overdose. These increased MOR levels may last weeks after the final

administration of the antagonist.[12] If researchers find a way to prevent opioid receptor surface level upregulation, the health risks involved in prescribing opioid antagonists will decrease dramatically.

Several mechanisms could underlie upregulation. Since certain agonists induce endocytosis, perhaps the prevention of basal MOR activation decreases basal endocytosis and increases MOR plasma membrane levels.[3,8,13,14] Alternatively, after endocytosis, the antagonists could be increasing the recycling of the receptors. Following endocytosis, the MORs can be degraded or recycled to the surface, and there is evidence that some opioid ligands, like fentanyl, can bias towards the recycling pathway.[15] There is also a cAMP hypothesis: recent work demonstrated that increases in intracellular [cAMP] coincide with increases in protein trafficking[16]. MOR activation decreases [cAMP], so perhaps decreasing basal MOR activity will increase [cAMP] and increase trafficking.[17]

This study examines the pharmacological chaperoning hypothesis.[18] Pharmacological chaperoning occurs when a pharmacophore binds to a nascent protein and promotes proper folding, thus aiding its exit from the ER.[19] Pharmacological chaperoning participates in therapeutic approaches when sub-optimal protein levels reach the plasma membrane.[19-22] Agonists and antagonists are capable of chaperoning in various systems, and several studies show that ligands promote trafficking of δ-opioid receptors.[23,24]

Research investigating pharmacological chaperoning has not yet examined key early events in MOR surface expression, in part because MORs traffic rather efficiently to the plasma membrane. We have therefore investigated the MOR[N190K] mutant, which is substantially retained in the ER.[25] We established that Ntx and naloxone could increase the plasma membrane density

of this mutant. In previous experiments with nicotinic receptors, pharmacological chaperoning produces increases in ERES levels.[26,27] We established that Sec24D, one of four Sec24 isoforms that can participate in ERES formation, does interact with MORs, suggesting that Sec24D shuttles MORs. We used Sec24D-eGFP to visualize ERES and observe changes in the fraction of the cytoplasm that ERES occupy in response to drug treatment. Heinzer *et al*. reasoned that increasing the size of ERES is a more advantageous strategy for increasing secretory flux than increasing the number of ERES, thus measuring the fraction of the cytoplasm occupied by ERES is more appropriate than measuring the total number of ERES.[28] The possibility that antagonists induce supersensitivity by pharmacologically chaperoning opioid receptors could suggest innovative approaches for opioid abuse disorder.

## 4.3 Results

### *4.3.1 MOR[N190K] reaches wild-type plasma membrane densities after Ntx or naloxone treatment*

In contrast to the other opioid receptor subtypes, MORs are primarily localized on the plasma membrane.[3] This lack of ER-localized MORs vitiates systematic studies of chaperoning. To increase the pool of MORs in the ER, we generated the MOR[N190K] mutant [25]. This N190K mutation impairs trafficking: most MOR[N190K] is retained in the ER. Prior reports state that wild-type plasma membrane expression is rescued by treating the MOR[N190K] expressing cells with Ntx.[25] Here, we generated the MOR[N190K] mutant with mCherry on the C-terminus to visualize the receptor. After antagonist treatment, we did observe fluorescent intensity outlining the cell, suggesting an increase in plasma membrane localization compared to vehicle-treated cells (**Figure 4.1**).

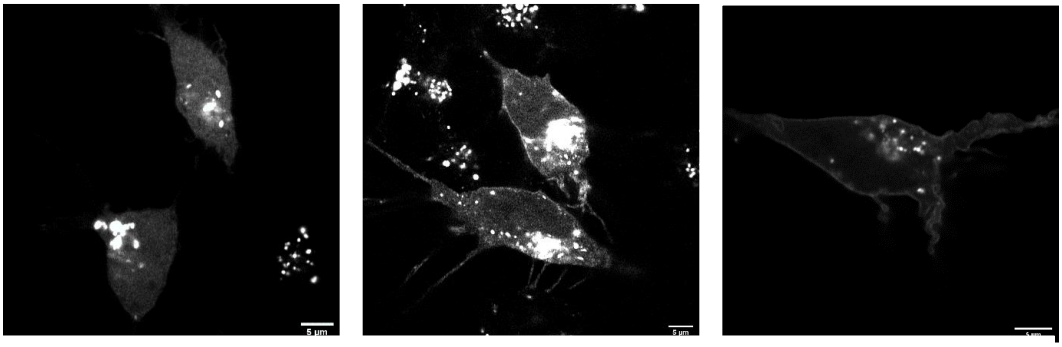

**Figure 4.1** MOR[N190K] appears on the plasma membrane after 24 h incubation in 10 μM Ntx or naloxone. SH-SY5Y cells were transfected with MOR[N190K]-mCherry and treated with **(A)** vehicle, **(B)** 10 μM Ntx, or **(C)** 10 μM naloxone for 12 h. The vehicle-treated samples show no plasma membrane localization of MOR[N190K]-mCherry while both the Ntx and naloxone treated cells are outlined with fluorescent signal, suggesting an increase in plasma membrane localization.

*4.3.2 MOR interacts with Sec24D*

There are four Sec24 isoforms, so it is imperative to validate that a specific isoform interacts with the MOR. In order to verify that the MOR and Sec24D interact with each other, we performed sensitized emission FRET experiments.[29] The donor was eGFP attached to Sec24D and the acceptor was mCherry attached to MOR[N190K]. The MOR[N190K] mutant was used to ensure that a large pool of receptors would be in the ER, available to interact with Sec24D. As a negative control, we used Rab5-eGFP as a donor. Rab5 localizes to early endosomes, thus we would not expect Rab5 to interact extensively with the MOR[N190K].[30] We quantified cFRET, a sensitized emission FRET method that corrects for spectral bleed-through from the donor excitation to acceptor emission in the absence of FRET (see Methods). We found that the Sec24D-MOR[N190K] FRET pair results in significantly greater cFRET intensity and FRET efficiency than the Rab5-MOR[N190K] FRET pair (**Figure 4.2**). These results suggest that the MOR interacts with Sec24D. The MOR[N190K]-mCherry + Rab5-eGFP samples serve

as an additional negative control to rule out spectral bleed-through from the donor excitation wavelength to the acceptor excitation spectrum.

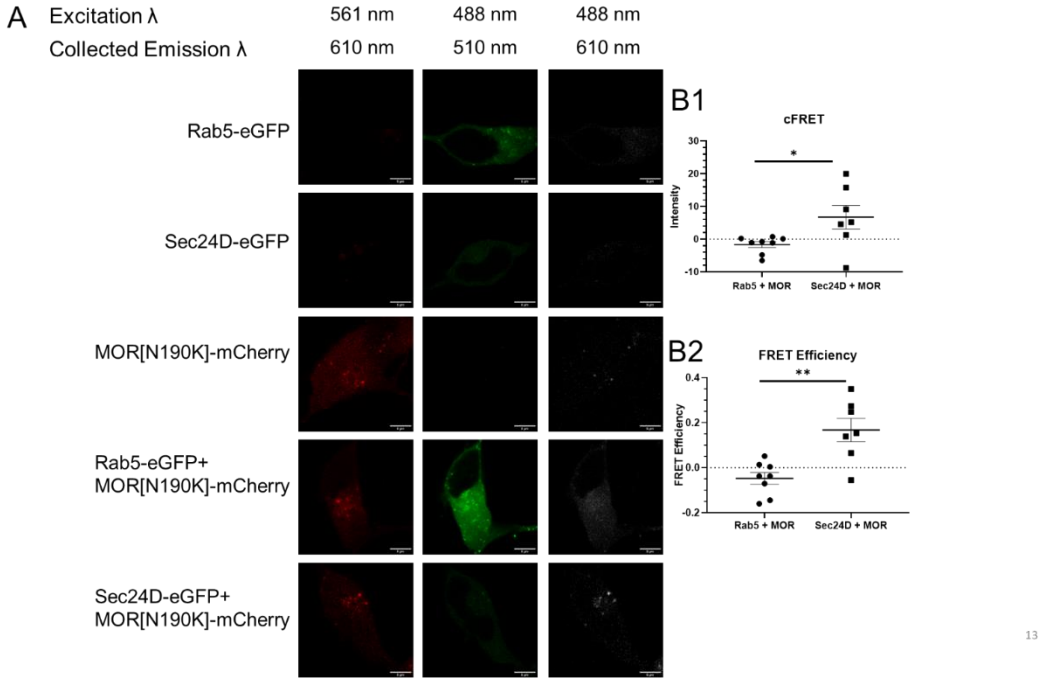


**Figure 4.2.** FRET analysis shows that in living cells, MOR is close to Sec24D. **(A)** Representative images of SH-SY5Y cells expressing Rab5-eGFP, Sec24D-eGFP, MOR[N190K]-mCherry, Rab5-eGFP and MOR[N190K]-mCherry, or Sec24D-eGFP and MOR[N190K]-mCherry. Left column, samples are excited at 561 nm excitation filter and imaged at 610 nm to reveal mCherry. Center column, samples are excited with at 488 nm excitation filter and imaged at 510 nm to reveal eGFP. Right column, samples are excited at 488 nm excitation filter and imaged at 610 nm to reveal sensitized emission. **(B1)** The cFRET intensities and (**B2)** FRET efficiency from the two FRET samples (Rab5-eGFP and MOR[N190K]-mCherry or Sec24D-eGFP and MOR[N190K]-mCherry. P-values are calculated from a Student's t-test. *, $p < 0.05$; ***, $p < 0.0005$.

### *4.3.3 Ntx and naloxone, but not agonists, induce increases in ERES in SH-SY5Y cells overexpressing MOR[N190K]*

To observe ERES specifically upregulated due to MOR chaperoning, we overexpress the ER-retained MOR mutant, MOR[N190K], in SH-SY5Y cells.[25] First, the percentage of the cytoplasm occupied by ERES was measured in SH-SY5Y cells transfected with MOR[N190K] and Sec24D-eGFP after 12 h incubation

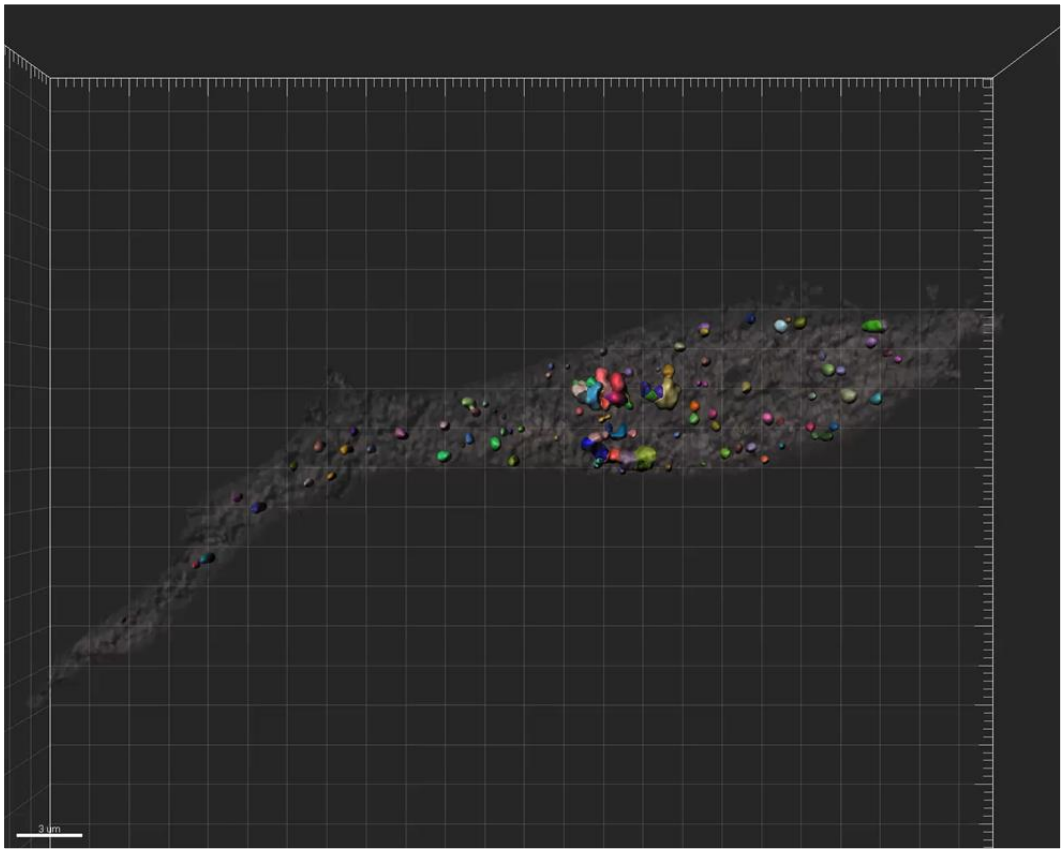


**Figure 4.3.** Representative image of a 3D rendering of the z-stacks obtained for ERES analysis. Each slice of the z-stack is 0.1 µm apart. The transparent grey region represents the cytoplasm. The opaque structures represent ERES. Each color represents a separate ERES. The analysis distinguishes individual ERES within a cluster, based on the assumption measurements that the average ERES is 500 nm in diameter (Heinzer *et al)*. However, this distinction is not used to calculate the fraction of cytoplasm occupied by ERES.

in 10 µM Ntx or naloxone. We chose to analyze the z-stacks to investigate ERES levels in the entire cell (**Figure 4.3**). Both Ntx and naloxone treatments showed a significant increase in ERES levels (**Figure 4.3**). Together, these results suggest that the antagonists are increasing ERES levels by binding and chaperoning ER-localized MORs. In contrast, among the full and partial agonists tested, none caused a significant increase in ERES levels (**Figure 4.3**).

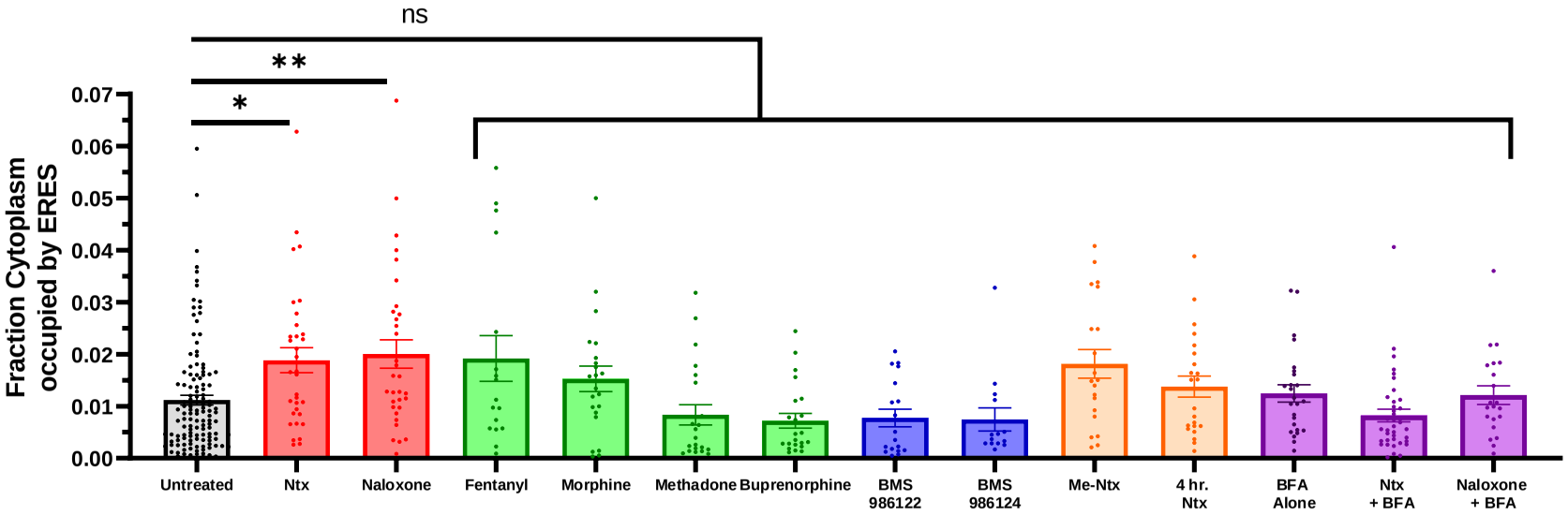


**Figure 4.4.** ERES levels are significantly higher after antagonist exposure. All incubation times are 12 h. at 10 µM concentration in SH-SY5Y cells transfected with MOR[N190K] and Sec24D-eGFP. The black data are untreated samples. The red bars are cells treated with an antagonist (Ntx or naloxone). The green bars represent cells treated with an agonist (fentanyl, morphine, methadone, or buprenorphine). The blue bars represent cells treated with an allosteric modulator (BMS 986122 or BMS 986124). The orange bars represent cells treated with either a modified Ntx (Me-Ntx) or Ntx with a briefer incubation. The purple bars represent cells treated with a COPI inhibitor, brefeldin A (BFA). p-values are calculated from an ANOVA and post-hoc Tukey test comparing to the untreated cells. *, $p < 0.05$; **, $p < 0.01$; ns, $p > 0.05$.

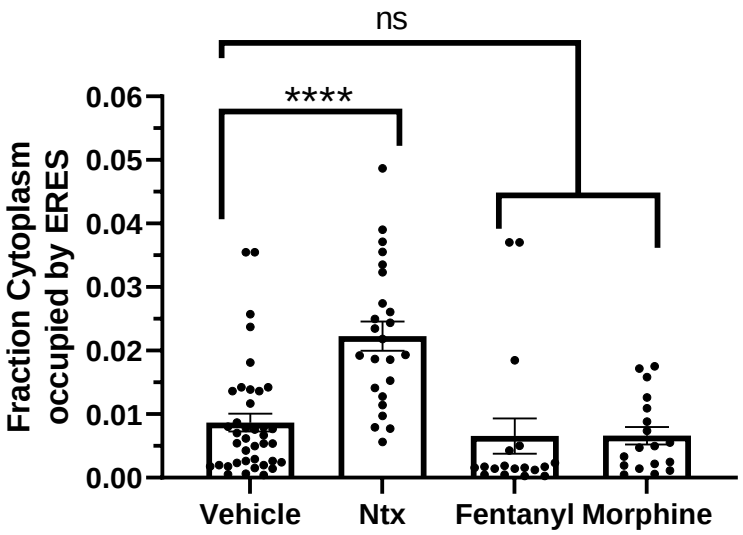


**Figure 4.5.** Ntx, but not agonists, increase ERES levels in SH-SY5Y cells despite abolition of the S375 phosphorylation site. SH-SY5Y cells were transfected with MOR[N190K][S375A] and Sec24D-eGFP. p-values are calculated from an ANOVA and post-hoc Tukey test. ****, $p < 0.0001$; ns, $p > 0.05$.

*4.3.4 N-methyl-naltrexone does not cause a significant shift in ERES levels*

To test the dependence of antagonist entry into the cytoplasm for ERES level increases, we used N-methyl-naltrexone (Me-Ntx), a permanently charged derivative of Ntx.[31] Me-Ntx crosses the plasma membrane at a substantially lower rate than Ntx. Since Me-Ntx will not reach the ER, the pharmacological chaperoning hypothesis predicts that Me-Ntx would not induce a rise in ERES levels. Indeed, unlike Ntx, Me-Ntx did not cause a significant shift in ERES levels in SH-SY5Y cells overexpressing MOR[N190K] (**Figure 4.4**). These results support the hypothesis that the antagonists work in an “inside-out” manner as pharmacological chaperones for MORs in the ER.

*4.3.5 Observation of ERES upregulation requires 12 h incubation with Ntx*

Next, we tested the temporal dependence of the ERES upregulation event. To observe the increase in MORs on the surface, it typically requires ~24 h

incubation with the antagonist to reach peak MOR surface densities.[32] We also tested 4 h incubations with Ntx. The significant shift in ERES levels did not occur after 4 h but did occur after 12 h (**Figure 4.4**). These results suggest that approximately 12 h is required for increased ERES levels to be observed.

*4.3.6 The lack of significant chaperoning by agonists is not due to phosphorylation at S375*

When MORs become activated, they undergo a series of phosphorylation events before arrestin recruitment and endocytosis.[33] One of the key residues for phosphorylation is S375: point mutations at this site are most effective for reducing receptor internalization.[34-36] If antagonists increase ERES levels via preventing phosphorylation, then perhaps using a mutant that cannot be phosphorylated at S375 might allow agonists to increase ERES levels. Ntx continues to induce a rise in ERES levels in SH-SY5Y cells overexpressing MOR[N190K][S375A], providing a positive control for these experiments (**Figure 4.5**). However, morphine and fentanyl do not significantly increase ERES levels in SH-SY5Y cells overexpressing MOR[N190K][S375A](**Figure 4.5**). While it is not clear whether S375 is becoming phosphorylated by agonists in the ER, mutating this residue to alanine does not enhance the chaperoning effects of agonists.

*4.3.7 Ntx does not induce a rise in [cAMP]*

An increase in intracellular [cAMP] occurs when cargo export increases in fibroblasts or HeLa cells.[16] It is not known whether there is an increase in [cAMP] with Ntx treatment without prior MOR activation. Here we tested whether Ntx increases [cAMP] in SH-SY5Y cells overexpressing MOR[N190K]. An ELISA

competition assay was used to measure relative concentrations of cAMP in SH-SY5Y cells transfected with MOR[N190K] after 12 h incubation with 10 µM Ntx, 15 min incubation with 10 µM forskolin (positive control for increases in [cAMP]), or vehicle. Our results suggest that Ntx does not increase [cAMP] (**Figure 4.6**). This

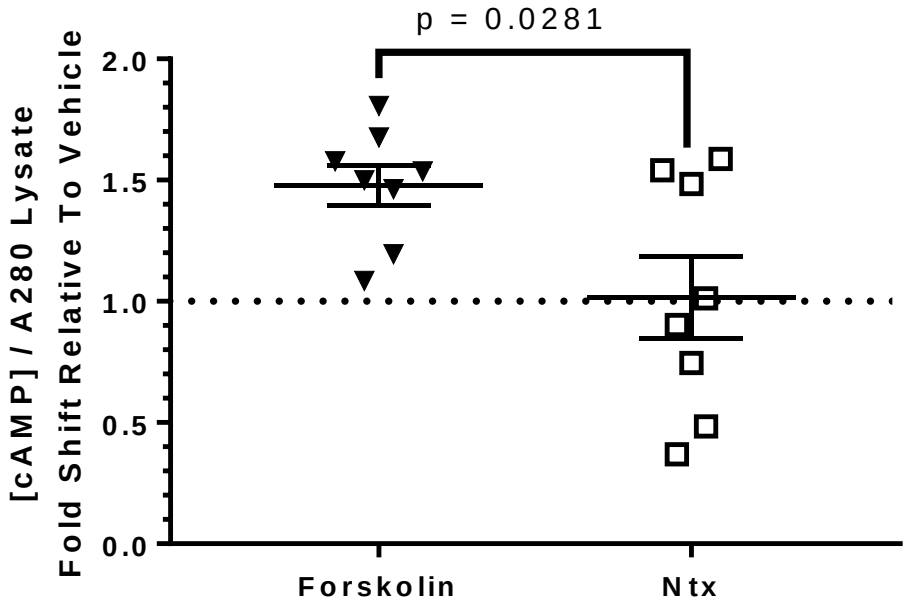


**Figure 4.6** [cAMP] levels do not change in cells treated with Ntx. SH-SY5Y cells were transfected with MOR[N190K] as in ERES imaging experiments. These cells were then treated with either 10 µM Ntx for 12 h, vehicle for 12 h followed by 10 µM forskolin for 15 min, or vehicle for 12 h. Forskolin-treated cells serve as a positive control for [cAMP] increases. Measurements for [cAMP] were normalized to vehicle-treated samples (represented by the dotted line). These results show that [cAMP] increases in forskolin-treated but not in NTx-treated cells, relative to vehicle-treated samples. p-values are calculated from an unpaired Student's t-test where $p < 0.05$ is considered significant for the ELISA assays.

is not surprising because the most likely way for Ntx to increase [cAMP] is by further inhibiting the MOR below its basal activity. The activity of MORs requires activation with agonists; thus observing a significant increase in [cAMP] by further inhibiting MORs is unlikely.[37,38] Since cAMP concentration changes have been ruled out as the cause of MOR upregulation, the chaperoning hypothesis remains the leading explanation for how Ntx and naloxone increase ERES levels.

*4.3.8 Ntx pharmacological chaperoning depends on COPI*

Coat protein I (COPI) vesicles [39-41] are retrotransport cargo from the Golgi to the ER to aid in sorting and protein quality control.[42] COPI vesicles are composed of seven core subunits, α-COP, β'-COP, ε-COP, βCOP, δ-COP, γ-COP, and ζ-COP and are thus distinct from ERES. Prior work in our lab and others have demonstrated that COPI vesicles can play a role in pharmacological chaperoning.[18,43] Here, we find a similar dependence as Ntx and naloxone no longer increase ERES levels if the cells are co-treated with brefeldin A (BFA), a COPI inhibitor (**Figure 4.4, purple**).[18,32,44] These results suggest that some of the ERES observed in the non-BFA treated cells have already traveled to the Golgi. This suggests that MORs must undergo multiple rounds of ER-Golgi trafficking before final maturation and presentation on the plasma membrane. This retrograde trafficking dependence is not uncommon for some cargos, and it appears that the MORs also depend on some ER-Golgi cycling before they are completely ready to go to the plasma membrane.

**4.4 Discussion**

Although efforts continue to reduce pain by actions on non-MOR targets such as the voltage-gated sodium channels and some nicotinic receptors, at present the MOR continues to be the primary target for analgesic drugs.[45,46] MOR trafficking is important to the development of opioid use disorder. If we can understand MOR trafficking and manipulate MOR surface densities in predictable ways, we may better treat opioid use disorder. Until now, there have been no studies done on ERES and MORs.

Here we show that, for a mutant MOR that builds to observable levels in the ER, the antagonists Ntx and naloxone increase the fraction of the cytoplasm

occupied by ERES. This is likely an early event in the pathway that results in increased opioid receptor surface densities and supersensitivity (**Figure 4.4**). By demonstrating that this adverse effect of antagonist treatment is manifested through ERES, we show that ERES can be considered a component in opioid use disorder.

Many agonists cause some endocytosis, but whether these drugs also cause chaperoning is not clear. We find that morphine, fentanyl, buprenorphine, and methadone do not cause a significant change in ERES levels. Our work suggests that the conformation induced by these agonists is less favorable for chaperoning than the conformation induced by the antagonists. In one hypothesis, this may be due to the lack of S375 phosphorylation when an antagonist is bound.[36] To test this, we made MOR[N190K][S375A], a MOR mutant that is highly-ER retained and could not be phosphorylated at S375. Despite the inability to phosphorylate S375, ERES levels did not significantly change using this mutant after 12 h incubation in 10 μM morphine or fentanyl (**Figure 4.5**).

We ruled out that the increases in ERES arise from increases in [cAMP] by measuring [cAMP] in MOR[N190K]-overexpressing SH-SY5Y cell lysates after incubation in Ntx, vehicle, or forskolin using a competitive ELISA assay. We overexpress MOR[N190K] to most closely replicate cells used in the imaging experiments. SH-SY5Y cells endogenously express the MOR, thus there will be MORs exhibiting basal activity at the plasma membrane that could be reduced by antagonist exposure.[47] Despite decreasing the basal activity of the MORs, we did not observe a significant change in [cAMP] in cells treated with Ntx (**Figure 4.6**). Since [cAMP] rises are no longer a viable reason for the increase in ERES levels, this experiment further supports the chaperoning hypothesis.

Our work does not challenge the prevailing view that, for the wild type MOR, agonists affect MOR via endocytosis at the plasma membrane—a much later stage than studied here.[48] The lack of substantial chaperoning by agonists is consistent with prior observations that several of the key steps in ERES formation could well be suppressed by the effects of MOR activation (such as increases in [cAMP]).[16,49] The endocytosed MOR plays a role in the cellular response to membrane-permeant opioids since the MOR can signal within recycling endosomes; in addition, MOR may also signal within the Golgi. [50] Fentanyl increases the recycling of MORs after endocytosis.[15] This observation, along with our results that antagonists can control trafficking from the ER to the Golgi, emphasizes how the earlier mechanisms that deliver MORs to the plasma membrane from the ER are regulated differently than the later mechanisms that traffic MORs from endosomes.[15] Pathways to the plasma membrane vary among MORs, and one may target one route over the other.

These results also give insight into how the mutant MOR matures in the ER and Golgi. The lack of ERES increases with COPI inhibition suggests some recycling between the ER and the Golgi. This observation is consistent with the ~24 hour incubation with naltrexone before observing increased MOR plasma membrane levels.[32] We also observe some time dependence with our ERES experiments (**Figure 4.4**). We hypothesize that after 4 hours, the mutant MOR has not had an opportunity to enter the Golgi-ER pathway, and only after 12 hours do we observe this transition as an increase in ERES levels. Furthermore, these COPI experiments are consistent with prior reports demonstrating the importance of retrograde transport for pharmacological chaperoning.[18,43]

Our results provide key information regarding MOR trafficking. We find that the antagonists can increase ERES levels, showing that in this case ERES exit events are rate-limiting for downstream MOR plasma membrane densities. Meanwhile, agonists do not increase ERES levels, consistent with their inability to increase MOR plasma membrane densities. Pharmacological chaperoning starts at the ER in many cases, and our work provides further evidence that Ntx and naloxone are pharmacological chaperones for the MOR.

Our work also continues to make a case for pharmacological chaperoning as an important part of a drug's efficacy profile.[22] This part of "inside-out pharmacology" involves using ligands to increase the trafficking of receptors.[51]

Our study applies only to the rare MOR[N190K] mutant; in pilot experiments, we found neither upregulation nor effects on ERES levels with wild type MOR. This limits our ability to explain the mechanism of upregulation/supersensitivity of MOR found in studies on intact animals with WT MORs treated with antagonists.[11,52,53] Superresolution experiments like those described here cannot yet be applied to native neurons of intact neural pathways.

One would need to invoke additional, unknown aspects of chaperoning to generalize its usefulness as a mechanism for upregulation / supersensitivity. This point resembles the uncertainties about mechanisms that allow nicotine to upregulate nicotinic receptors of only some cells types and only at some subcellular regions.[51]

To the extent that pharmacological chaperoning does govern upregulation / supersensitivity by naltrexone, we note that Me-Ntx is FDA-approved to suppress opioid-induced constipation (OIC) when opioids are used for chronic noncancer pain. OIC is a major discomfort. We can now suggest that Me-Ntx and other

membrane-impermeant antagonists, unlike membrane-permeant antagonists such as naltrexone and naloxone, are unlikely to cause upregulation / supersensitivity. This difference would arise from the same mechanism that allows Me-Ntx to block peripheral but not CNS MOR: it does not permeate across membranes.[54] Perhaps Me-Ntx deserves wider use for its approved indications.

## 4.5 Materials and Methods

### *4.5.1 Reagents*

All reagents were obtained from Sigma-Aldrich (St. Louis, MO). The MOR plasmid was a gift from Dr. Brigitte Kieffer. The MOR-mCherry plasmid was purchased from VectorBuilder (The vector ID is VB181109-1086uuu, which can be used to retrieve detailed information about the vector on vectorbuilder.com). The eGFP-Sec24D plasmid was used as previously described. All other mutants were generated using site-directed mutagenesis using standard protocols.

### *4.5.2 SH-SY5Y cell culture and transfection*

SH-SY5Y cells were purchased from the ATCC® (CRL-2266™). Cells were cultured according to the protocols specified by the ATCC, except Opti-Mem was used instead of EMEM/F12. Cells were cultured in 35 mm dishes with a glass coverslip on the bottom and allowed to reach 90% confluency before transfection. Transfection was carried out using Lipofectamine™ 3000 (Thermo Fisher) using the standard protocols. Typical DNA loads were between 0.5 and 1.0 µg per dish. Transfection media was replaced 24 h post-transfection with growth media. Drugs were added to the cell media to give a total drug concentration of 10 µM, 12 h before imaging. Before imaging, the cells were washed once with phosphate-buffered saline (PBS) and then remained in fresh PBS for imaging.

*4.5.3 Z-stack confocal microscopy*

The Zeiss LSM 880 with “Fast Airyscan” was used. The pixel dwell time was ~ 0.2 µs. Each slice was taken 0.1 µm from the previous one. All images and z-stacks were processed using Airyscan processing in the Zen Blue software package (Zeiss).

*4.5.4 Sensitized Emission Förster resonance energy transfer (FRET)*

FRET experiments were performed following a procedures described by Elder and co-workers [29] and previously used in this lab [55,56] to calculate sensitized emission FRET with corrections for donor bleed-through into the acceptor channel, and vice versa, SH-SY5Y cells were transfected with either Sec24D-eGFP, Rab5-eGFP, or MOR[N190K]-mCherry to establish the acceptor emission ratio (AER) or donor emission ratio (DER). These ratios were calculated using the equations:

$$AER = \frac{I^{AD}}{I^{AA}} \quad (1)$$

$$DER = \frac{I^{DA}}{I^{DD}} \quad (2)$$

where $I^{AD}$ is mCherry fluorescence intensity in the mCherry channel with 488 nm excitation, $I^{AA}$ is mCherry fluorescence intensity in the mCherry channel with 561 nm excitation, $I^{DA}$ is eGFP fluorescence intensity in the mCherry channel with 488 nm excitation, and $I^{DD}$ is eGFP fluorescence intensity in the eGFP channel using 488 nm excitation. The FRET samples were transfected with MOR[N190K]-mCherry and Sec24D-eGFP or Rab5-eGFP. Using the AER and DER values calculated in the samples expressing one fluorescent protein, the following equation was used to calculate the corrected FRET intensity, cFRET

$$cFRET = I^{DA} - (DER)(I^{DD}) - (AER)(I^{AA}) \quad (3)$$

where $I^{DA}$, $I^{DD}$, and $I^{AA}$ are measured in the FRET sample using the same parameters as those used in the samples to obtain the AER and DER. Using the cFRET value, we calculated FRET efficiency as:

$$FRET\ Efficiency = \frac{cFRET}{I^{AA}} \quad (4)$$

All five samples were imaged on the same day on the same microscope.

*4.5.5 Image Analysis*

All 2D image analysis was performed using FIJI. To determine the threshold to designate ERES, the 2D image was smoothed three times in FIJI and an ROI was drawn around the entire cell. The top 5% of the most intense pixels that constitute a puncta larger than 0.1 μm$^2$ in the ROI were marked as ERES. This same intensity threshold was used to designate ERES in the 3D images which were analyzed in Imaris (Bitplane). Among the various metrics presented by Imaris, we emphasize the fraction of cytoplasmic volume occupied by ERES, because this volume-integrated metric is relatively insensitive to assumptions about size, shape, and number of individual particles.

*4.5.6 Competitive ELISA for [cAMP] measurement*

SH-SY5Y cells were grown to 90% confluency and transfected with MOR[N190K]. The cells were lysed with 0.1 M HCl 48 h. post-transfection and after the appropriate drug treatment (12 h. with 10 μM Ntx, 15 min. with 10 μM forskolin (positive control for [cAMP] upregulation), or vehicle). Lysates were centrifuged at 15,000 rpm for 10 min at 4 °C on a standard table-top centrifuge to remove

insoluble debris. The supernatant was used for the remainder of the procedure as described by the protocol provided with the cAMP Assay Kit (Abcam, ab65355).

*4.5.7 Statistical Analysis*

All results are presented as mean ± S.E.M. and all statistical analyses were performed using GraphPad Prism. Statistical significance was determined by an unpaired Student's t-test (in comparisons between two samples) or an ANOVA with a post-hoc Tukey test (in comparisons with more than two samples). In comparisons where the p-value < 0.05, these differences were considered significant.

**4.6 References**


1 Keith, D. E. *et al.* μ-opioid receptor internalization: Opiate drugs have differential effects on a conserved endocytic mechanism *in vitro* and in the mammalian brain. *Mol. Pharmacol.* **53**, 377-384, doi:10.1124/mol.53.3.377 (1998).

2 Zhang, X., Bao, L. & Li, S. Opioid receptor trafficking and interaction in nociceptors. *Br. J. Pharmacol.* **172**, 364-374, doi:10.1111/bph.12653 (2015).

3 Wang, Y. L., Van Bockstaele, E. J. & Liu-Chen, L. Y. In vivo trafficking of endogenous opioid receptors. *Life Sci.* **83**, 693-699, doi:10.1016/j.lfs.2008.09.023 (2008).

4 Patel, C. N., Rajashekara, V., Patel, K., Purohit, V. & Yoburn, B. C. Chronic opioid antagonist treatment selectively regulates trafficking and signaling proteins in mouse spinal cord. *Synapse* **50**, 67-76, doi:10.1002/syn.10246 (2003).

5 Ge, X., Loh, H. H. & Law, P.-Y. μ-opioid receptor cell surface expression is regulated by its direct interaction with ribophorin I. *Mol. Pharmacol.* **75**, 1307-1316, doi:10.1124/mol.108.054064 (2009).

6 Cahill, C. M., Holdridge, S. V. & Morinville, A. Trafficking of δ-opioid receptors and other G-protein-coupled receptors: Implications for pain and analgesia. *Trends Pharmacol. Sci.* **28**, 23-31, doi:10.1016/j.tips.2006.11.003 (2007).

7 Williams, J. T. *et al.* Regulation of μ-opioid receptors: desensitization, phosphorylation, internalization, and tolerance. *Pharmacol. Rev.* **65**, 223-254, doi:10.1124/pr.112.005942 (2013).

8 Martini, L. & Whistler, J. L. The role of mu opioid receptor desensitization and endocytosis in morphine tolerance and dependence. *Curr. Opin. Neurobiol.* **17**, 556-564, doi:10.1016/j.conb.2007.10.004 (2007).

9 Machelska, H. & Celik, M. O. Advances in achieving opioid analgesia without side effects. *Front. Pharmacol.* **9**, 22, doi:10.3389/fphar.2018.01388 (2018).

10 Petaja-Repo, U. E. & Lackman, J. J. Targeting opioid receptors with pharmacological chaperones. *Pharmacol. Res.* **83**, 52-62, doi:10.1016/j.phrs.2013.12.001 (2014).

11 Sirohi, S., Kumar, P. & Yoburn, B. C. μ-opioid receptor up-regulation and functional supersensitivity are independent of antagonist efficacy. *J. of Pharmacology and Experimental Therapeutics* **323**, 701-707, doi:10.1124/jpet.107.127019 (2007).

12 Mamede, M. *et al.* Temporal change in human nicotinic acetylcholine receptor after smoking cessation: 5IA SPECT study. *J. Nuclear Medicine : Official Publication, Society of Nuclear Medicine* **48**, 1829-1835, doi:10.2967/jnumed.107.043471 (2007).

13 Minnis, J. G. *et al.* Ligand-induced μ opioid receptor endocytosis and recycling in enteric neurons. *Neuroscience* **119**, 33-42, doi:10.1016/S0306-4522(03)00135-0 (2003).

14 Anselmi, L., Jaramillo, I., Palacios, M., Huynh, J. & Sternini, C. Ligand-induced opioid receptor internalization in enteric neurons following chronic treatment with the opiate fentanyl. *J. Neurosci. Res.* **91**, 854-860, doi:10.1002/jnr.23214 (2013).

15 Bowman, S. L. *et al.* Cell-autonomous regulation of μ-opioid receptor recycling by substance P. *Cell Reports* **10**, 1925-1936, doi:10.1016/j.celrep.2015.02.045 (2015).

16 Subramanian, A. *et al.* Auto-regulation of secretory flux by sensing and responding to the folded cargo protein load in the endoplasmic reticulum. *Cell* **176**, 1461-+, doi:10.1016/j.cell.2019.01.035 (2019).

17 Kosten, T. R. & George, T. P. The neurobiology of opioid dependence: Implications for treatment. *Science & Practice Perspectives* **1**, 13-20 (2002).

18 Leskelä, T. T., Markkanen, P. M. H., Pietilä, E. M., Tuusa, J. T. & Petäjä-Repo, U. E. Opioid receptor pharmacological chaperones act by binding and stabilizing newly synthesized receptors in the endoplasmic reticulum. *J. Biol. Chem.* **282**, 23171-23183, doi:10.1074/jbc.M610896200 (2007).

19 Leidenheimer, N. J. & Ryder, K. G. Pharmacological chaperoning: A primer on mechanism and pharmacology. *Pharmacol. Res.* **83**, 10-19, doi:10.1016/j.phrs.2014.01.005 (2014).

20 Chanoux, R. & Rubenstein, R. Molecular chaperones as targets to circumvent the cftr defect in cystic fibrosis. *Front. Pharmacol.* **3**, doi:10.3389/fphar.2012.00137 (2012).

21 Convertino, M., Das, J. & Dokholyan, N. V. Pharmacological chaperones: design and development of new therapeutic strategies for the treatment of conformational diseases. *ACS Chem. Biol.* **11**, 1471-1489, doi:10.1021/acschembio.6b00195 (2016).

22 Leidenheimer, N. J. in *Targeting Trafficking in Drug Development* Vol. 245 *Handbook of Experimental Pharmacology* (eds A. UlloaAguirre & Y. X. Tao) 135-153 (Springer-Verlag Berlin, 2018).

23 Mazzo, F. *et al.* Nicotine-modulated subunit stoichiometry affects stability and trafficking of α3β4 nicotinic receptor. *J. Neurosci.* **33**, 12316-12328, doi:10.1523/jneurosci.2393-13.2013 (2013).

24 Petaja-Repo, U. E. *et al.* Ligands act as pharmacological chaperones and increase the efficiency of delta opioid receptor maturation. *EMBO J.* **21**, 1628-1637, doi:10.1093/emboj/21.7.1628 (2002).

25 Fortin, J.-P. *et al.* The μ-opioid receptor variant N190K is unresponsive to peptide agonists yet can be rescued by small-molecule drugs. *Mol. Pharmacol.* **78**, 837-845, doi:10.1124/mol.110.064188 (2010).

26 Srinivasan, R. *et al.* Nicotine up-regulates α4β2 nicotinic receptors and ER exit sites via stoichiometry-dependent chaperoning. *The Journal of General Physiology* **137**, 59-79, doi:10.1085/jgp.201010532 (2011).

27 Henderson, B. J. *et al.* Menthol alone upregulates midbrain nAChRs, alters nAChR subtype stoichiometry, alters dopamine neuron firing frequency, and prevents nicotine reward. *J Neurosci* **36**, 2957-2974, doi:10.1523/jneurosci.4194-15.2016 (2016).

28 Heinzer, S., Worz, S., Kalla, C., Rohr, K. & Weiss, M. A model for the self-organization of exit sites in the endoplasmic reticulum. *J. Cell Science* **121**, 55-64, doi:10.1242/jcs.013383 (2008).

29 Elder, A. D. *et al.* A quantitative protocol for dynamic measurements of protein interactions by Förster resonance energy transfer-sensitized fluorescence emission. *J R Soc Interface* **6**, S59-S81, doi:10.1098/rsif.2008.0381.focus (2009).

30 Hu, Y.-B., Dammer, E. B., Ren, R.-J. & Wang, G. The endosomal-lysosomal system: from acidification and cargo sorting to neurodegeneration. *Transl Neurodegener* **4**, 18-18, doi:10.1186/s40035-015-0041-1 (2015).

31 Pasternak, G. W. & Pan, Y.-X. Mu opioids and their receptors: Evolution of a concept. *Pharmacol. Rev.* **65**, 1257-1317, doi:10.1124/pr.112.007138 (2013).

32 Chaipatikul, V., Erickson-Herbrandson, L. J., Loh, H. H. & Law, P. Y. Rescuing the traffic-deficient mutants of rat μ-opioid receptors with hydrophobic ligands. *Mol. Pharmacol.* **64**, 32-41, doi:10.1124/mol.64.1.32 (2003).

33 El Kouhen, R. *et al.* Phosphorylation of Ser363, Thr370, and Ser375 residues within the carboxyl tail differentially regulates μ-opioid receptor internalization. *J. Biol. Chem.* **276**, 12774-12780, doi:10.1074/jbc.M009571200 (2001).

34 Grecksch, G. *et al.* Analgesic tolerance to high-efficacy agonists but not to morphine is diminished in phosphorylation-deficient S375A μ-opioid receptor knock-in mice. *J Neurosci* **31**, 13890-13896, doi:10.1523/jneurosci.2304-11.2011 (2011).

35 Just, S. *et al.* Differentiation of opioid drug effects by hierarchical multi-site phosphorylation. *Mol. Pharmacol.* **83**, 633-639, doi:10.1124/mol.112.082875 (2013).

36 Yousuf, A. *et al.* Role of phosphorylation sites in desensitization of μ-opioid receptor. *Mol. Pharmacol.* **88**, 825-835, doi:10.1124/mol.115.098244 (2015).

37 Li, J. *et al.* Constitutive activation of the μ opioid receptor by mutation of D3.49(164), but not D3.32(147): D3.49(164) is critical for stabilization of the inactive form of the receptor and for its expression. *Biochemistry* **40**, 12039-12050, doi:10.1021/bi0100945 (2001).

38 Divin, M. F., Bradbury, F. A., Carroll, F. I. & Traynor, J. R. Neutral antagonist activity of naltrexone and 6β-naltrexol in naïve and opioid-dependent C6 cells expressing a μ-opioid receptor. *Br. J. Pharmacol.* **156**, 1044-1053, doi:10.1111/j.1476-5381.2008.00035.x (2009).

39 Barlowe, C. *et al.* COPII: A membrane coat formed by set proteins that drive vesicle budding from the endoplasmic reticulum. *Cell* **77**, 895-907, doi:10.1016/0092-8674(94)90138-4 (1994).

40 Stephens, D. J., Lin-Marq, N., Pagano, A., Pepperkok, R. & Paccaud, J. P. COPI-coated ER-to-Golgi transport complexes segregate from COPII in close proximity to ER exit sites. *J. Cell Science* **113**, 2177-2185 (2000).

41 Elsner, M. *et al.* Spatiotemporal dynamics of the COPI vesicle machinery. *EMBO Reports* **4**, 1000-1005, doi:10.1038/sj.embor.embor942 (2003).

42 Arakel, E. C. & Schwappach, B. Formation of COPI-coated vesicles at a glance. *J. Cell Science* **131**, doi:10.1242/jcs.209890 (2018).

43 Henderson, B. J. *et al.* Nicotine exploits a COPI-mediated process for chaperone-mediated up-regulation of its receptors. *The Journal of General Physiology* **143**, 51-66, doi:10.1085/jgp.201311102 (2014).

44 Petaja-Repo, U. E., Hogue, M., Laperriere, A., Walker, P. & Bouvier, M. Export from the endoplasmic reticulum represents the limiting step in the maturation and cell surface expression of the human delta opioid receptor. *J. Biol. Chem.* **275**, 13727-13736, doi:10.1074/jbc.275.18.13727 (2000).

45 Zhang, F. *et al.* Naja atra venom peptide reduces pain by selectively blocking the voltage-gated sodium channel Nav1.8. *J. Biol. Chem.* **294**, 7324-7334, doi:10.1074/jbc.RA118.007370 (2019).

46 Knowland, D. *et al.* Functional α6β4 acetylcholine receptor expression enables pharmacological testing of nicotinic agonists with analgesic properties. *The Journal of Clinical Investigation* **130**, 6158-6170, doi:10.1172/JCI140311 (2020).

47 Zadina, J. E., Chang, S. L., Ge, L. J. & Kastin, A. J. μ opiate receptor down-regulation by morphine and up-regulation by naloxone in SH-SY5Y human neuroblastoma cells. *J. Pharmacology and Experimental Therapeutics* **265**, 254 (1993).

48 Lester, H. A. *et al.* Nicotine is a Selective Pharmacological Chaperone of Acetylcholine Receptor Number and Stoichiometry. Implications for Drug Discovery. *Aaps J.* **11**, 167-177, doi:10.1208/s12248-009-9090-7 (2009).

49 Bailey, C. P. & Connor, M. Opioids: cellular mechanisms of tolerance and physical dependence. *Curr. Opin. Pharmacol.* **5**, 60-68, doi:10.1016/j.coph.2004.08.012 (2005).

50 Stoeber, M. *et al.* A Genetically Encoded Biosensor Reveals Location Bias of Opioid Drug Action. *Neuron* **98**, 963-+, doi:10.1016/j.neuron.2018.04.021 (2018).

51 Henderson, B. J. & Lester, H. A. Inside-out neuropharmacology of nicotinic drugs. *Neuropharmacology* **96**, 178-193, doi:10.1016/j.neuropharm.2015.01.022 (2015).

52 Yoburn, B. C., Shah, S., Chan, K. W., Duttaroy, A. & Davis, T. Supersensitivity to opioid analgesics following chronic opioid antagonist treatment - relationship to receptor selectivity. *Pharmacology Biochemistry and Behavior* **51**, 535-539, doi:10.1016/0091-3057(94)00375-s (1995).

53 Yoburn, B. C., Purohit, V., Patel, K. & Zhang, Q. Y. Opioid agonist and antagonist treatment differentially regulates immunoreactive mu-opioid

receptors and dynamin-2 in vivo. *Eur. J. Pharmacol.* **498**, 87-96, doi:10.1016/j.ejphar.2004.07.052 (2004).

54 Foss, J. F., Bass, A. S. & Goldberg, L. I. Dose-related antagonism of the emetic effect of morphine by methylnaltrexone in dogs. *J Clin Pharmacol* **33**, 747-751, doi:10.1002/j.1552-4604.1993.tb05618.x (1993).

55 Srinivasan, R. *et al.* Forster resonance energy transfer (FRET) correlates of altered subunit stoichiometry in cys-loop receptors, exemplified by nicotinic α4β2. *Int J Mol Sci* **13**, 10022-10040, doi:10.3390/ijms130810022 (2012).

56 Srinivasan, R. *et al.* Pharmacological chaperoning of nicotinic acetylcholine receptors reduces the endoplasmic reticulum stress response. *Mol Pharmacol* **81**, 759-769, doi:10.1124/mol.112.077792 (2012).

# Chapter 5: Agonist-induced μ-opioid receptor endocytosis is dependent on phosphorylation at the C-terminus

## 5.1 Abstract

The opioid crisis is largely a result of the addictive nature of opioids. The relatively rapid initiation of dependence and tolerance to opioids results from various actions, one of which being μ-opioid receptor (MOR) endocytosis following activation. Activation will usually lead to various phosphorylation events on the C-terminus, and some of these are important for receptor internalization. Experiments to determine the dependence on C-terminal phosphorylation for endocytosis were done using DAMGO binding assays to determine the amount of MORs on the plasma membrane. Here, we decide to expand on some of these measurements using an endosome localization assay following morphine and fentanyl treatment. Currently, the data regarding morphine-induced internalization is conflicted, and precise experiments regarding fentanyl and the C-terminal's phosphorylation status are lacking. Here, we find that both morphine and fentanyl induce increases in MOR-endosome colocalization, suggesting that both drugs increase endocytosis. We do not observe MOR-endosome colocalization increases after morphine treatment if the S375 residue is mutated to alanine. These results are similar to what has been observed in other labs where the MOR[S375A] mutant did not undergo endocytosis following DAMGO treatment. We do not observe MOR-endosome colocalization increases after fentanyl treatment if most C-terminal phosphorylation sites (T354, S355, S356, T357, S363, S364, T370, S375, T376, and T379) are mutated to alanine. These results continue the narrative that C-terminal phosphorylation is important for developing dependence and tolerance.

## 5.2 Introduction

The previous chapter delved into the supersensitivity induced by opioid antagonists that resulted from increases in the MOR density on the plasma membrane. The inverse is true for many agonists where they induce internalization and decrease the MOR plasma membrane density.[1-8] Unfortunately, unlike pharmacological chaperoning, which mostly relies on the protein and the small molecule, MOR internalization involves many factors. The opioid receptors are G-protein coupled receptors (GPCR), and as such, they will interact with many different cytosolic proteins.[9] The two proteins that get the most attention are the β-arrestins and the G proteins.[10] These protein classes have been studied extensively because the β-arrestins are generally responsible for most of the negative effects of opioid use (respiratory depression, tolerance, and receptor desensitization) while G-protein coupling is associated with the desired analgesic effects.[11] Some agonists will induce more β-arrestin coupling than G-protein coupling or vice versa; the preference between one or the other is the foundation of biased agonism.[12,13] Biased agonists are one of the most popular directions scientists have taken to find safer analgesics. Unfortunately, morphine and other opioids remain the “gold standard” for pain relief medications.[14-16] Unfortunately, with over 30% of all Americans suffering from some form of chronic pain, opioids are one of the most prescribed substances, and along with the ease of which to acquire illicit opioids, there is an overabundance of opioids in the public that make the opioid crisis a major problem.[17]

One can say that the chief issue with opioids is the downstream effects of β-arrestin binding. In many GPCRs, β-arrestin follows after receptor phosphorylation.[18] While the crucial phosphorylation sites will vary between

353-CIPTSSNIEQQNSTRIRQNTRDHPSTA
NTVDRTNHQLENLEAETAPLP-400

**Figure 5.1 C-terminal sequence of the human MOR according to UNIPROT.** Residues highlighted are putative phosphorylation sites. The serine highlighted in red is S375

different GPCRs, the key phosphorylation sites in the MOR for receptor internalization are in the C-terminus (**Figure 5.1**).[4,19,20] The site that has gotten special interest is the S375 site. Studies show that S375 is the first residue phosphorylated, it will be selectively phosphorylated by morphine, and prevention of S375 phosphorylation will inhibit DAMGO-induced endocytosis.[20-22] In terms of further phosphorylation, there is some debate on what sites are only phosphorylated in the presence of agonists.[23-25] Nevertheless, there is agreement that there is a strong link between phosphorylation and internalization.

Here we decide to expand on these studies by conducting fluorescence-based experiments investigating how phosphorylation at the C-terminus influences morphine- and fentanyl-induced endocytosis. Our experiments will measure the colocalization between the MOR and the early endosome. As opposed to binding assays, this measurement will specifically look at endocytosis and will not depend on potential complications from various states of the MOR that may inhibit DAMGO binding. For example, prolonged exposure to agonists can induce desensitization, which can change the binding properties of the receptor.[26] Since we are only dependent on fluorescence, the conformation of the MOR is not important in our assay. Further, our assay is specific for endocytosis, while binding assays examine general decreases in the MOR plasma membrane density. We found that both morphine and fentanyl increase MOR colocalization with early endosomes

following a 30 minute treatment compared to untreated cells. However, there were no morphine-induced increases in MOR-early endosome colocalization if there was an S375A mutation. Conversely, we needed to mutate T354, S355, S356, T357, S363, S364, T370, S375, T376, and T379 to alanine to prevent fentanyl-induced increases in MOR-early endosome colocalization. These results continue to support the importance of C-terminal phosphorylation to endocytosis.

### *5.3 Results and Discussion*

#### *5.3.1 Morphine and fentanyl induce endocytosis of MORs in SH-SY5Y cells*

While most researchers are convinced that fentanyl will induce endocytosis, morphine-induced endocytosis appears very dependent on the system used.[1,5,27,28] Here, we overexpress the MOR-mCherry via transfection of cDNA. We also used CellLight™ Early Endosome GFP to visualize early endosomes. We used a Zeiss LSM 880 with "Fast Airyscan" to image the MOR-mCherry and CellLight™ Early Endosome GFP. The Pearson's correlation coefficient was calculated using a FIJI plug-in. We acknowledge that there are certain advantages and disadvantages to this method, but we are confident that these experiments will shed light on how the MOR C-terminus influences agonist-induced endocytosis. We also decided to use equally efficacious doses of fentanyl (0.2 μM) and morphine (10 μM) instead of equal molar concentrations of the agonists.[29]

Here, we find that both fentanyl and morphine will increase the colocalization of MORs and early endosomes (**Figure 5.2**). Both of these observations agree with results from other labs and suggest that our assay can detect increases in agonist-induced endocytosis.

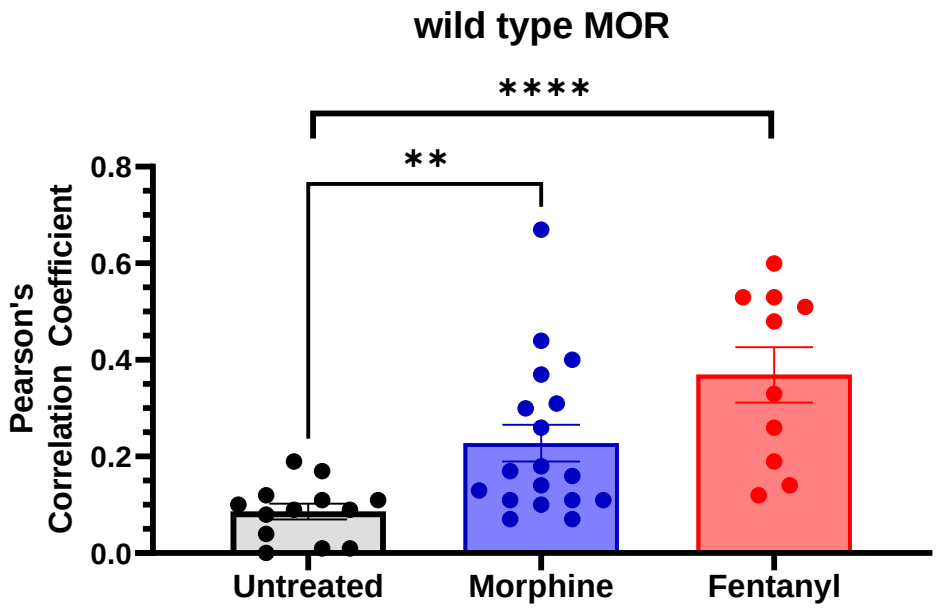


**Figure 5.2** Both morphine and fentanyl increase endocytosis of wild-type MOR.

*5.3.2 Fentanyl will, but morphine will not increase endocytosis of MOR[S375A]*

Next, we decided to start mutating some of the C-terminal phosphorylation sites to alanine so that phosphorylation would become impossible. This strategy has been used extensively for similar purposes and the receptors remained functional.[22,30] We start with arguably the most important phosphorylation site, S375. Compared to vehicle-treated samples, we find that morphine does not increase endocytosis, but fentanyl still does (**Figure 5.3**). These results are consistent with observations that morphine only phosphorylates S375 and that phosphorylation is important for MOR endocytosis.[11,22,24] Meanwhile, we know that fentanyl will phosphorylate sites other than S375, which appears sufficient to recruit β-arrestin and induce endocytosis.[21]

Next, we tested the single mutant, MOR[T370A], to see if morphine depends specifically on S375 phosphorylation. Here, we find that both morphine

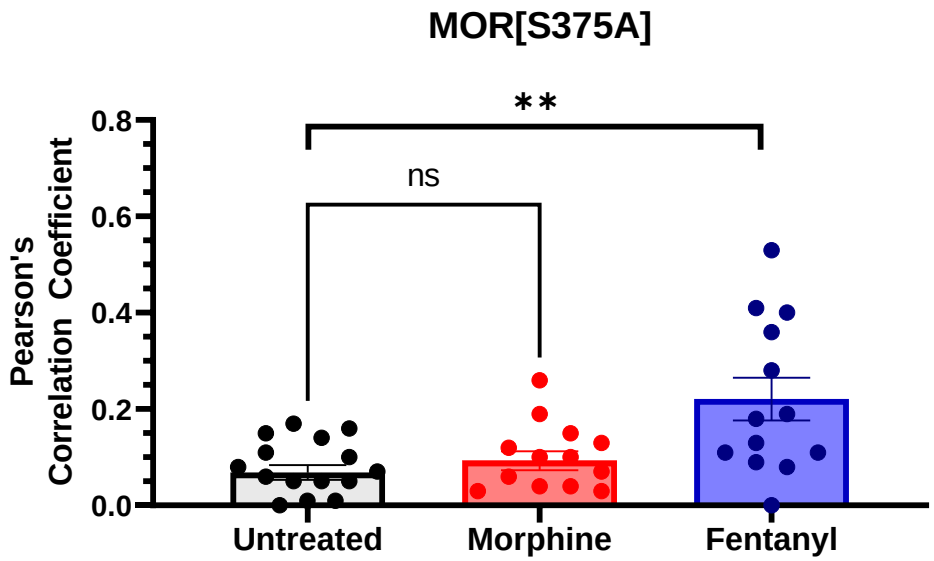


**Figure 5.3** The S375A mutation prevents morphine-induced endocytosis, but not fentanyl induced endocytosis.

and fentanyl will increase endocytosis of MOR[T370A] (**Figure 5.4**). These results suggest that the T370 site is not as critical to morphine's ability to induce endocytosis as the S375 site is. Indeed, this is consistent with other reports that emphasize that the S375 site is the only one phosphorylated by morphine.

*5.3.3 Inhibiting fentanyl-induced endocytosis requires the abolition of several C-terminal phosphorylation sites*

We next progressively mutated phosphorylation sites to alanine and continued to test both fentanyl- and morphine-induced endocytosis. Significance was determined by comparing to untreated samples using a Student's t-test. Consistent with S375 residue's importance to morphine-induced MOR endocytosis, all subsequent MOR mutants were not endocytosed significantly more when treated with morphine over the vehicle (**Figure 5.5**). In contrast, we observed increases in endocytosis after fentanyl treatment for all mutants except for when we mutated T354, S355, S356, T357, S363, S364, T370, S375, T376,

and T379 to alanine. These results suggest that fentanyl-induced endocytosis will not occur if most of the C-terminal serine and threonine residues cannot be phosphorylated.

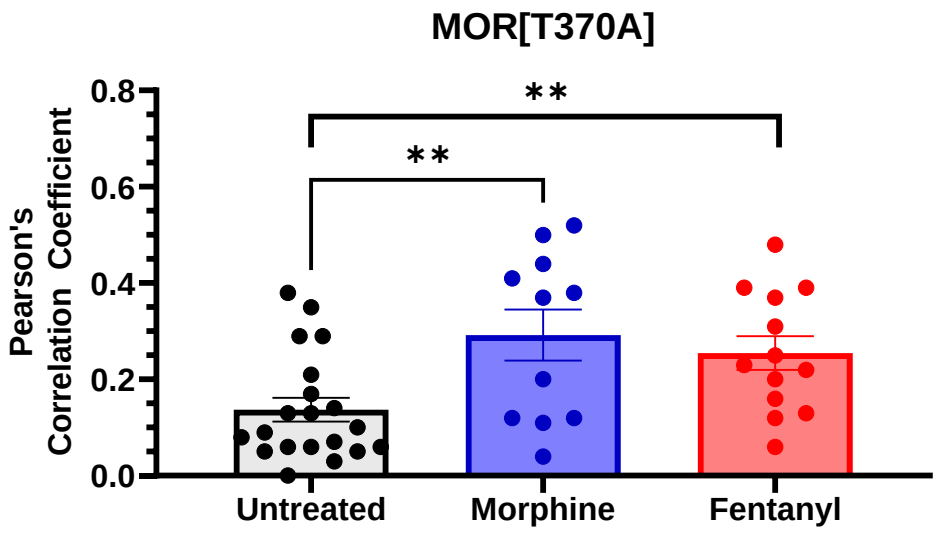


**Figure 5.4** The T370A mutation does not prevent morphine-induced or fentanyl-induced endocytosis.

### *5.4 Conclusions*

MOR endocytosis plays a critical role in developing tolerance to opioids.[2,30,31] The field has made tremendous progress in this area, where we are quite sure that β-arrestin coupling to the MOR promotes endocytosis.[6,7,12,32] Presently, we are still not sure what some of the most important opioids do regarding endocytosis. Here, we expand on these studies by observing the colocalization of MORs and early endosomes following morphine or fentanyl treatment. Consistent with other experiments, our assay suggests that morphine and fentanyl induce endocytosis in SH-SY5Y cells expressing MOR-mCherry.[5,8,27] We no longer observe morphine-induced endocytosis if the S375 residue is mutated to alanine, but we need to mutate T354, S355, S356, T357, S363, S364,

T370, S375, T376, and T379 to alanine in order to inhibit fentanyl-induced endocytosis.

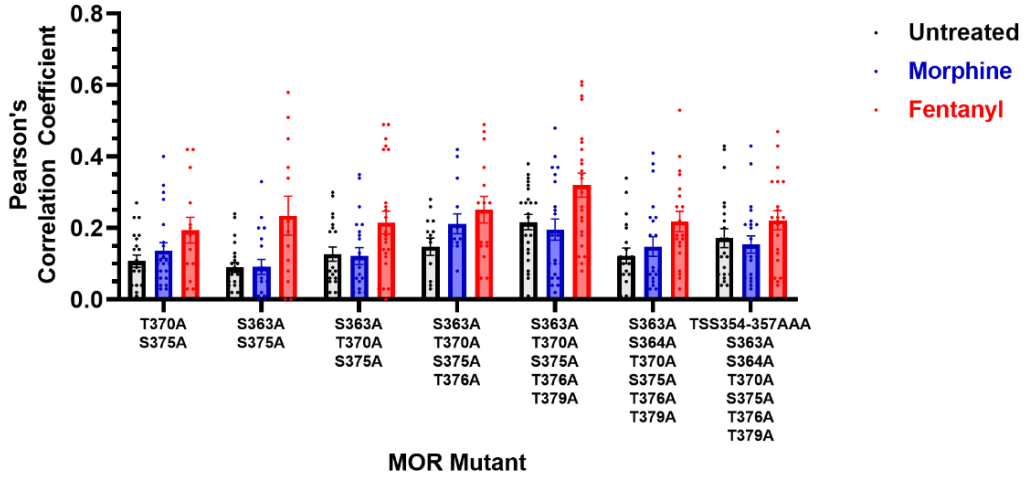


| P-values (compared to untreated) | Morphine | Fentanyl |
|---|---|---|
| T370A, S375A | 0.3 | 0.02 |
| S363A, S375A | 0.9 | 0.003 |
| S363A, S375A, T370A | 0.9 | 0.03 |
| S363A, S375A, T370A, T376A | 0.09 | 0.03 |
| S363A, S375A, T370A, T376A, T379A | 0.6 | 0.01 |
| S363A, S375A, T370A, T376A, T379A, S364A | 0.4 | 0.01 |
| S363A, S375A, T370A, T376A, T379A, S364A, TSS354-357AAA | 0.6 | 0.2 |

**Figure 5.5 MOR mutants and their Pearson's correlation co-efficients with early endosomes after agonist treatment.** None of the mutants here were endocytosed significantly more after morphine treatment. Only the S363A, S375A, T370A, T376A, T379A, S364A, TSS354-357AAA mutants did not have increased endocytosis after fentanyl treatment.

Future efforts in this study will require orthogonal experiments to validate our microscopy observation. Since this is a novel means of measuring MOR endocytosis, these orthogonal experiments are critical. We did some preliminary immunoblots to evaluate MOR levels, but the results are inconclusive. Further attempts may turn to binding assays or other biochemical experiments to evaluate MOR density on the plasma membranes.

## *5.5 Materials and Methods*

### *5.5.1 Reagents, materials, and plasmids*

All reagents were obtained from Sigma-Aldrich (St. Louis, MO). The MOR plasmid was a gift from Dr. Brigitte Kieffer. The MOR-mCherry plasmid was purchased from VectorBuilder (the vector ID is VB181109-1086uuu, which can be used to retrieve detailed information about the vector on vectorbuilder.com). Mutations were made using a QuikChange protocol (Stratagene). CellLight™ Early Endosome GFP was purchased from ThermoFisher.

### *5.5.2 SH-SY5Y cell culture and transfection*

SH-SY5Y cells were purchased from the ATCC® (CRL-2266™). Cells were cultured according to the protocols specified by the ATCC, except Opti-Mem was used instead of EMEM/F12. Cells were cultured in MatTek® 1.5 coverslip-14C-35 mm glass bottom dishes and allowed to reach 90% confluency before transfection. Transfection was carried out using Lipofectamine™ 3000 (Thermo Fisher) using the standard protocols. Typical DNA loads were between 0.5 and 1.0 µg per dish. Transfection media was replaced 24 hours post-transfection with 3 mL of growth media and 2 µL of CellLight™ Early Endosome GFP. Drugs were added to the cell media to give a total drug concentration of 10 µM for morphine or 0.2 µM for fentanyl, 30 minutes before imaging. Before imaging, the cells were washed once with phosphate-buffered saline (PBS), and then remained in fresh PBS for imaging.

*5.5.3 Imaging and analysis*

Imaging was performed on a Zeiss LSM 880 with “Fast Airyscan.” Fast Airyscan improves the signal-to-noise ratio by incorporating the photons that traditionally get rejected by the confocal pinhole to help reconstitute the image. Image dimensions varied to ensure ideal “Fast Airyscan” conditions. Pixel dwell time was ~2 µs.

The top 5% most intense pixels in each channel were used to calculate the Pearson’s correlation coefficient. The calculation was performed using the “Coloc 2” plug-in in FIJI. The “Pearson’s R Values (no threshold)” were recorded and used for further analysis. The “Pearson’s R Values” were compiled into a GraphPad Prism file for statistical analysis. A Student’s t-test was used to compare each drug-treated sample to the untreated control. Any pair where $p < 0.05$ was considered to be significantly different.

***5.6 References***


1 Sternini, C. *et al.* Agonist-selective endocytosis of µ opioid receptor by neurons in vivo. *PNAS* **93**, 9241-9246 (1996).

2 Whistler, J. L., Chuang, H. H., Chu, P., Jan, L. Y. & von Zastrow, M. Functional dissociation of µ opioid receptor signaling and endocytosis: implications for the biology of opiate tolerance and addiction. *Neuron* **23**, 737-746, doi:10.1016/s0896-6273(01)80032-5 (1999).

3 Finn, A. K. & Whistler, J. L. Endocytosis of the µ opioid receptor reduces tolerance and a cellular hallmark of opiate withdrawal. *Neuron* **32**, 829-839, doi:10.1016/s0896-6273(01)00517-7 (2001).

4 Koch, T. *et al.* C-terminal splice variants of the mouse µ-opioid receptor differ in morphine-induced internalization and receptor resensitization. *J. Biol. Chem.* **276**, 31408-31414, doi:10.1074/jbc.M100305200 (2001).

5 Minnis, J. G. *et al.* Ligand-induced µ opioid receptor endocytosis and recycling in enteric neurons. *Neuroscience* **119**, 33-42, doi:10.1016/S0306-4522(03)00135-0 (2003).

6 Martini, L. & Whistler, J. L. The role of µ opioid receptor desensitization and endocytosis in morphine tolerance and dependence. *Curr. Opin. Neurobiol.* **17**, 556-564, doi:10.1016/j.conb.2007.10.004 (2007).

7 Williams, J. T. *et al.* Regulation of µ-opioid receptors: Desensitization, phosphorylation, internalization, and tolerance. *Pharmacol. Rev.* **65**, 223-254, doi:10.1124/pr.112.005942 (2013).

8 Anselmi, L., Jaramillo, I., Palacios, M., Huynh, J. & Sternini, C. Ligand-induced opioid receptor internalization in enteric neurons following chronic treatment with the opiate fentanyl. *J. Neurosci. Res.* **91**, 854-860, doi:10.1002/jnr.23214 (2013).

9 Jean-Alphonse, F. & Hanyaloglu, A. C. Regulation of GPCR signal networks via membrane trafficking. *Molecular and Cellular Endocrinology* **331**, 205-214, doi:10.1016/j.mce.2010.07.010 (2011).

10 Schmid, C. L. *et al.* Bias factor and therapeutic window correlate to predict safer opioid analgesics. *Cell* **171**, 1165-1175.e1113, doi:10.1016/j.cell.2017.10.035 (2017).

11 Bohn, L. M., Gainetdinov, R. R., Lin, F. T., Lefkowitz, R. J. & Caron, M. G. μ -opioid receptor desensitization by beta-arrestin-2 determines morphine tolerance but not dependence. *Nature* **408**, 720-723, doi:10.1038/35047086 (2000).

12 Molinari, P. *et al.* Morphine-like opiates selectively antagonize receptor-arrestin interactions. *J. Biol. Chem.* **285**, 12522-12535, doi:10.1074/jbc.M109.059410 (2010).

13 Kenakin, T., Watson, C., Muniz-Medina, V., Christopoulos, A. & Novick, S. A simple method for quantifying functional selectivity and agonist bias. *ACS Chem. Neurosci.* **3**, 193-203, doi:10.1021/cn200111m (2012).

14 Gabriel, R. A. *et al.* State of the art opioid-sparing strategies for post-operative pain in adult surgical patients. *Expert Opin. Pharmacother.* **20**, 949-961, doi:10.1080/14656566.2019.1583743 (2019).

15 Kaye, A. D. *et al.* New opioid receptor modulators and agonists. *Best Practice & Research. Clinical Anaesthesiology* **32**, 125-136, doi:10.1016/j.bpa.2018.06.009 (2018).

16 Livingston, K. E. & Traynor, J. R. Disruption of the $Na^+$ ion binding site as a mechanism for positive allosteric modulation of the μ-opioid receptor. *PNAS* **111**, 18369-18374, doi:10.1073/pnas.1415013111 (2014).

17 Volkow, N. D. & McLellan, A. T. Opioid abuse in chronic pain — misconceptions and mitigation strategies. *NEJM* **374**, 1253-1263, doi:10.1056/NEJMra1507771 (2016).

18 Mayer, D. *et al.* Distinct G protein-coupled receptor phosphorylation motifs modulate arrestin affinity and activation and global conformation. *Nat. Commun.* **10**, 1261, doi:10.1038/s41467-019-09204-y (2019).

19 Yu, Y. K. *et al.* μ opioid receptor phosphorylation, desensitization, and ligand efficacy. *J. Biol. Chem.* **272**, 28869-28874, doi:10.1074/jbc.272.46.28869 (1997).

20 El Kouhen, R. *et al.* Phosphorylation of Ser363, Thr370, and Ser375 residues within the carboxyl tail differentially regulates μ-opioid receptor internalization. *J. Biol. Chem.* **276**, 12774-12780, doi:10.1074/jbc.M009571200 (2001).

21 Just, S. *et al.* Differentiation of opioid drug effects by hierarchical multi-site phosphorylation. *Mol. Pharmacol.* **83**, 633-639, doi:10.1124/mol.112.082875 (2013).

22 Grecksch, G. *et al.* Analgesic tolerance to high-efficacy agonists but not to morphine is diminished in phosphorylation-deficient S375A μ-opioid receptor knock-in mice. *J Neurosci* **31**, 13890-13896, doi:10.1523/jneurosci.2304-11.2011 (2011).

23 Lau, E. K. *et al.* Quantitative encoding of the effect of a partial agonist on individual opioid receptors by multisite phosphorylation and threshold detection. *Sci. Signal.* **4**, 12, doi:10.1126/scisignal.2001748 (2011).

24 Doll, C. *et al.* Deciphering μ-opioid receptor phosphorylation and dephosphorylation in HEK293 cells. *Br. J. Pharmacol.* **167**, 1259-1270, doi:10.1111/j.1476-5381.2012.02080.x (2012).

25 Miess, E. *et al.* Multisite phosphorylation is required for sustained interaction with GRKs and arrestins during rapid μ-opioid receptor desensitization. *Sci. Signal.* **11**, 15, doi:10.1126/scisignal.aas9609 (2018).

26 Shahoei, R. & Tajkhorshid, E. Menthol binding to the human α4β2 nicotinic acetylcholine receptor, facilitated by its strong partitioning in membrane. *The Journal of Physical Chemistry B*, doi:10.1021/acs.jpcb.9b10092 (2020).

27 Zadina, J. E., Chang, S. L., Ge, L. J. & Kastin, A. J. μ opiate receptor down-regulation by morphine and up-regulation by naloxone in SH-SY5Y human neuroblastoma cells. *Journal of Pharmacology and Experimental Therapeutics* **265**, 254 (1993).

28 Keith, D. E. *et al.* Morphine activates opioid receptors without causing their rapid internalization. *The Journal of Biological Chemistry* **271**, 19021-19024, doi:10.1074/jbc.271.32.19021 (1996).

29 Chen, J. C., Smith, E. R., Cahill, M., Cohen, R. & Fishman, J. B. The opioid receptor binding of dezocine, morphine, fentanyl, butorphanol and nalbuphine. *Life Sci.* **52**, 389-396, doi:10.1016/0024-3205(93)90152-s (1993).

30 Grecksch, G. *et al.* Development of tolerance and sensitization to different opioid agonists in rats. *Psychopharmacology* **186**, 177-184, doi:10.1007/s00213-006-0365-8 (2006).

31 Dang, V. C. & Christie, M. J. Mechanisms of rapid opioid receptor desensitization, resensitization and tolerance in brain neurons. *Br. J. Pharmacol.* **165**, 1704-1716, doi:10.1111/j.1476-5381.2011.01482.x (2012).

32 Weinberg, Z. Y., Zajac, A. S., Phan, T., Shiwarski, D. J. & Puthenveedu, M. A. Sequence-specific regulation of endocytic lifetimes modulates arrestin-mediated signaling at the μ opioid receptor. *Mol. Pharmacol.* **91**, 416-U216, doi:10.1124/mol.116.106633 (2017).

# Chapter 6: Regulation of epithelial sodium channel activity by SARS-CoV-1 and SARS-CoV-2 proteins

**This chapter is adapted from*: Stephen N. Grant and Henry A. Lester. Regulation of epithelial sodium channel activity by SARS-CoV-1 and SARS-CoV-2 proteins *Biophysical Journal*, **2021.**

## 6.1 Abstract

Severe acute respiratory syndrome (SARS) coronavirus (CoV) 2 (SARS-CoV-2), which causes the coronavirus disease 2019 (COVID-19), encodes several proteins whose roles are poorly understood. We tested their ability either to directly form plasma membrane ion channels or to change the functions of two mammalian plasma membrane ion channels, the epithelial sodium channel (ENaC) and the α3β4 nicotinic acetylcholine receptor (nAChR). In mRNA-injected *Xenopus* oocytes, none of nine SARS-CoV-2 proteins or two SARS-CoV-1 proteins produced conductances, nor did co-injection of several combinations. Immunoblots for ORF8, spike (S), and envelope (E) proteins revealed that the proteins are expressed at appropriate molecular weights. In experiments on co-expression with ENaC, three tested SARS proteins (SARS-CoV-1 E, SARS-CoV-2 E, and SARS-CoV-2 S) markedly decrease ENaC currents. SARS-CoV-1 S protein decreases ENaC currents modestly. Coexpressing the E proteins, but not the S proteins, with α3β4 nAChRs significantly reduces acetylcholine-induced currents. ENaC inhibition does not occur if the SARS-CoV protein mRNAs are injected 24 h after the ENaC mRNAs, suggesting that SARS-CoV proteins affect early step(s) in functional expression of channel proteins. Consistent with the hypothesis that the SARS-CoV-2 S protein-induced ENaC inhibition involves

competition for available protease, mutating the furin cleavage site in SARS-CoV-2 S protein partially relieves inhibition of ENaC currents. Extending previous suggestions that SARS proteins affect ENaC currents via protein kinase C (PKC) activation, PKC activation via phorbol 12-myristate 13-acetate (PMA) decreases ENaC and α3β4 activity. PMA application reduced membrane capacitance ~ 5%, presumably via increased endocytosis, but this decrease is much smaller than the SARS proteins' effects on conductances. Also, incubating oocytes in Gö-6976, a PKCα and PKCβ inhibitor, did not alter E or S protein-induced channel inhibition. We conclude that SARS-CoV-1 and SARS-CoV-2 proteins alter the function of human plasma membrane channels, via incompletely understood mechanisms. These interactions may play a role in COVID-19 pathophysiology.

**6.2 Introduction**

The coronavirus disease 2019 (COVID-19) has caused a massive global public health crisis. As of April 19, 2021, over 140 million people have been infected and over three million lives have been lost to COVID-19, according to the Johns Hopkins Coronavirus Resource Center. The pandemic has spurred drastic changes throughout the world in every part of life. Understanding this virus gives the global community its best chance to return to relatively standard practices. However, much like the pandemic it elicited, SARS-CoV-2 is an unprecedented virus that requires study from various approaches.

We sought to contribute to COVID-19 research by systematically studying membrane-relevant SARS-CoV-2 proteins, both by themselves and in various combinations with host proteins, and comparing homologous proteins from SARS-CoV-1 and SARS-CoV-2. Plasma membrane viroporins are important for many

viruses,[1-5] and we tested for their presence in SARS-CoV-2 by expressing SARS-CoV-1 and SARS-CoV-2 proteins in *Xenopus* oocytes.

It is important to understand how the various proteins encoded by SARS-CoV-2 interact with endogenous human proteins.[2,6,7] SARS-CoV-2 must interact with host proteins to replicate.[8] These interactions begin when the SARS-CoV-2 S protein binds to the human angiotensin-converting enzyme 2 (ACE2) protein; this interaction leads to viral entry.[9-11] Many subsequent interactions have been studied between SARS-CoV-2 and human proteins. Studies using mass spectrometry and *in silico* methods identified many protein-protein interactions between SARS-CoV-2 and humans.[7,12] Additionally, researchers have looked to work done on SARS-CoV-1, the related beta-coronavirus responsible for the SARS epidemic in 2002 and 2003.[13]

We are also interested in how the E and S proteins from SARS-CoV-2 affect ENaC function. Ji *et al*. used electrophysiology to suggest that both SARS-CoV-1 E and S proteins markedly decreased ENaC activity in *Xenopus laevis* oocytes.[14] After pharmacological experiments to probe the cause of this inhibition, Ji *et al*. suggested that the E and S protein decreased ENaC protein levels via a protein kinase C (PKC)-dependent mechanism.[14] ENaC helps regulate fluid levels in the lung, and if this function is inhibited, pulmonary edema can develop.[15] Pulmonary edema has been observed in COVID-19 patients, so inhibition of ENaC via E and S protein expression may have been conserved in SARS-CoV-2.[16,17] Other ion channels may be affected by SARS-CoV-2 proteins, so we tested the generality of our results by studying how the SARS-CoV-1 and SARS-CoV-2 proteins affect α3β4 nAChR activity. Finally, we begin mechanistic work to explain

how the SARS-CoV-1 and SARS-CoV-2 proteins affect ENaC and α3β4 nAChR currents.

## 6.3 Results

### *6.3.1 SARS-CoV proteins do not form ion channels in the plasma membrane*

Many viruses rely on the function of viroporins, including viruses in the coronavirus family.[2,4,6,18,19] The ORF3a and E protein are postulated to be viroporins.[20] Furthermore, there are viral protein-protein interactions such that the individual protein, do not create a pore, but together they do so.[21] Here we find that the injection of SARS-CoV-1 S and E and SARS-CoV-2 Nsp2, Nsp3, Nsp4, Nsp6, ORF3a, ORF8, M, E, and S protein mRNA, all simultaneously or individually, into *Xenopus* oocytes does not produce conductances in the plasma membrane (**Figure 6.1**).

### *6.3.2 SARS proteins are expressed following mRNA injection*

Although most properly transcribed mRNA is translated into proteins when injected into oocytes, there are exceptions. Here, we made immunoblots to determine whether a subset of these SARS proteins are translated in oocytes. We specifically studied the S, E, and SARS-CoV-2 ORF8 proteins. Each SARS protein was only observed in oocytes injected with their respective mRNA (**Figure 6.2**). These results suggest that S, E, and SARS-CoV-2 ORF8 proteins are expressed in the oocytes following mRNA injection; inadequate protein translation or protein degradation does not underlie the lack of plasma membrane conductances.

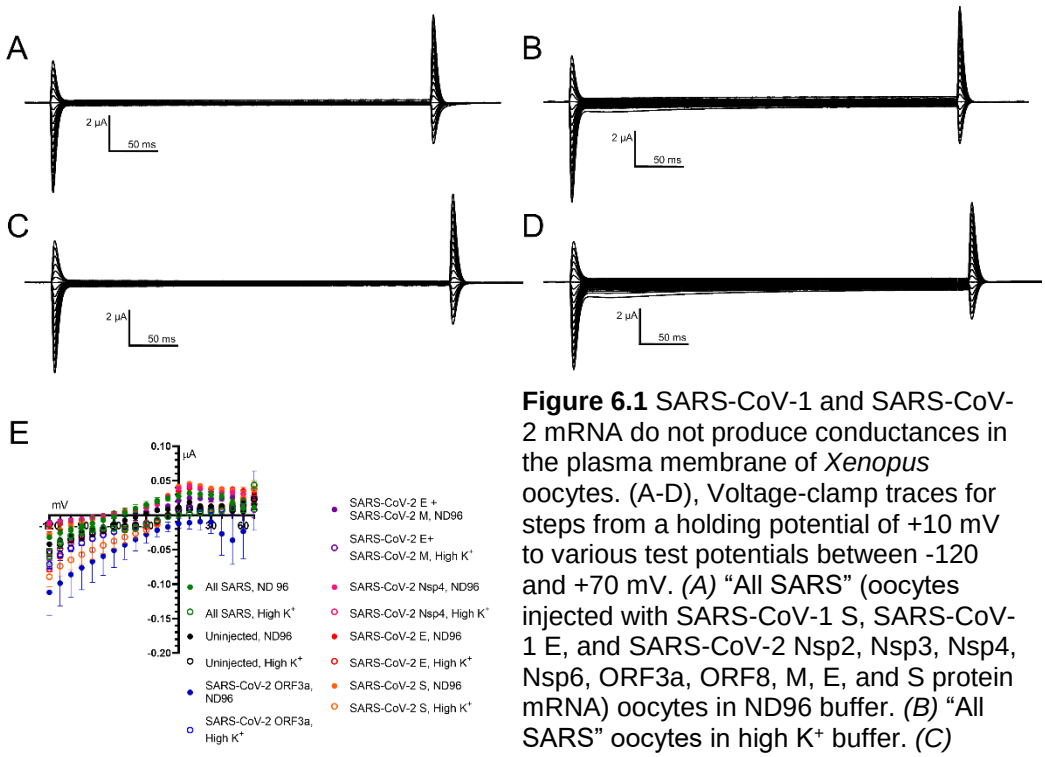


**Figure 6.1** SARS-CoV-1 and SARS-CoV-2 mRNA do not produce conductances in the plasma membrane of *Xenopus* oocytes. (A-D), Voltage-clamp traces for steps from a holding potential of +10 mV to various test potentials between -120 and +70 mV. *(A)* "All SARS" (oocytes injected with SARS-CoV-1 S, SARS-CoV-1 E, and SARS-CoV-2 Nsp2, Nsp3, Nsp4, Nsp6, ORF3a, ORF8, M, E, and S protein mRNA) oocytes in ND96 buffer. *(B)* "All SARS" oocytes in high $K^+$ buffer. *(C)* Uninjected oocytes in ND96 buffer. *(D)* Uninjected oocytes in high $K^+$ buffer. *(E)* I-V relationship for all samples with error bars representing the S.E.M. N = 12 (All SARS in ND 96), 13 (All SARS in High $K^+$), 5 (uninjected in ND 96), 11 (uninjected in High $K^+$), 18 (ORF3a ND96), 43 (ORF3a, High $K^+$), 8 (E+M, ND96), 8 (E+M, High $K^+$), 37 (Nsp4, ND96), 45 (Nsp4, High $K^+$), 15 (E, ND96), 23 (E, High $K^+$), 64 (S, ND96), and 19 (S, High $K^+$).

### *6.3.3 SARS-CoV-1 E, SARS-CoV-2 E, and SARS-CoV-2 S proteins decrease ENaC currents*

Protein-protein interactions between the virus and host are crucial for viral entry, replication, maturation, transport, and secretion. Ji *et al*. investigated the SARS-CoV-1 E and S protein interactions with ENaC.[14] Here, we repeated these experiments and included the SARS-CoV-2 proteins (**Figure 6.3**). We use SARS-CoV-2 ORF8 as a negative control plasmid since ORF8 does not produce viroporins in the plasma membrane and is not expected to interact with ENaC.[20]

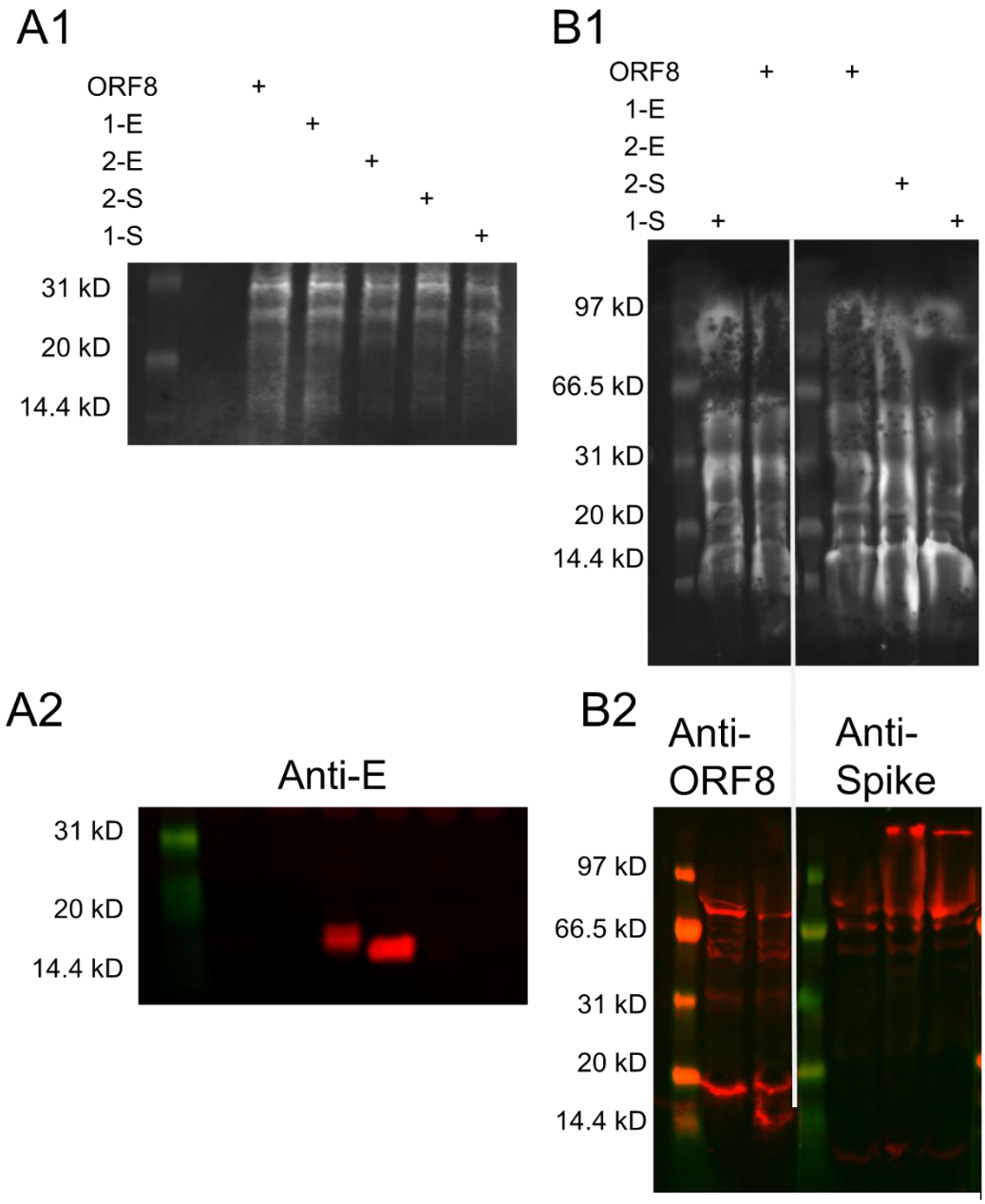


**Figure 6.2** SARS proteins are expressed in *Xenopus* oocytes. *(A1)* Total protein stain for the immunoblot that would be probed with E protein antisera. *(A2)* Immunoblots probed with the E protein antisera. The oocytes in each lane were injected with ENaC and the SARS proteins designated at the top of the total protein stain. *(B1)* Total protein stain for the immunoblots that would be probed with anti-ORF8 and anti-spike protein. *(B2)* Immunoblots probed with the antibodies designated at the top of each immunoblot. The oocytes in each lane were injected with ENaC and the SARS proteins designated at the top of their respective total protein stain.

Compared to  oocytes injected with ORF8, oocytes injected with SARS-CoV-1 E,

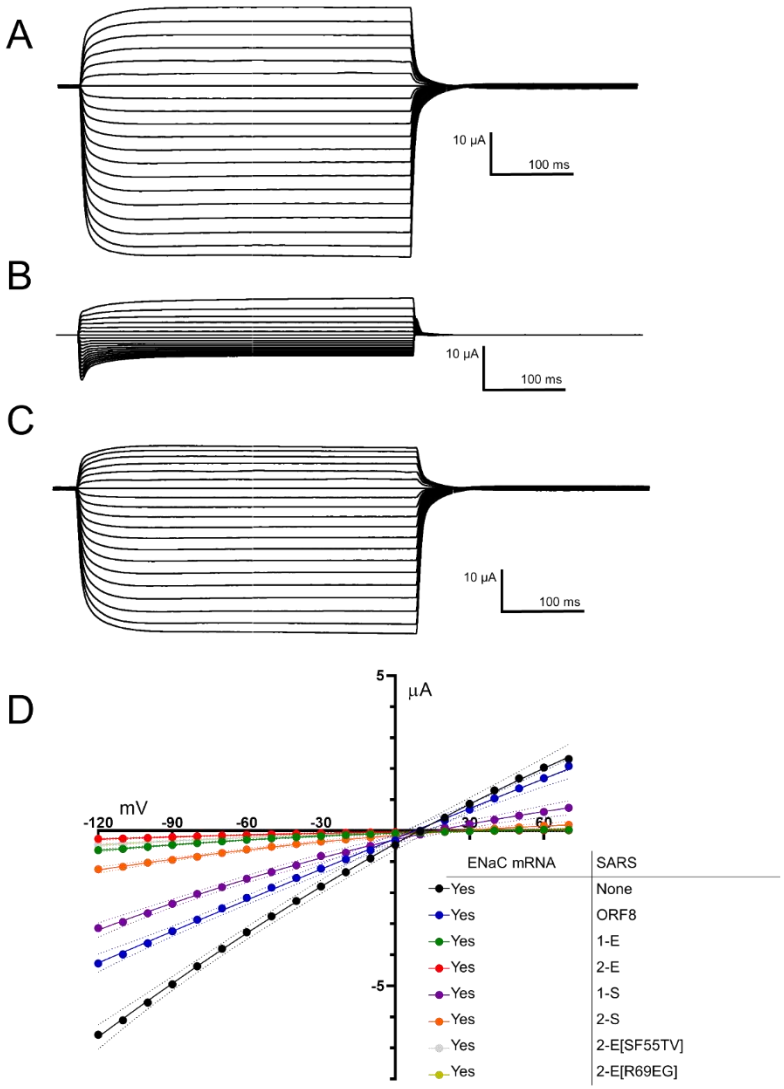


**Figure 6.3** Representative voltage-clamp currents. Membrane potential was held at +10 mV, then stepped to test potentials from -120 mV to +70 mV at 10 mV intervals. *(A)* buffer. *(B)* 10 µM amiloride. *(C)* subtraction of the amiloride traces from the buffer traces, produce the amiloride-sensitive currents and are used to determine ENaC currents. *(D)* I-V relationships for oocytes injected with ENaC mRNA and SARS proteins. "ORF8" = SARS-CoV-2 ORF 8. "1-E" = SARS-CoV-1 E protein. "2-E" = SARS-CoV-2 E protein. "2-S" = SARS-CoV-2 S protein. "1-S" = SARS-CoV-1 S protein. "2-E[SF55TV]" refers to the chimera-like E protein with the partial P**TV**YVYSRVKNLNSS**R**-V sequence. "2-E[R69EG]" refers to the chimera-like E protein with the partial P**SF**YVYSRVKNLNSS**EG**V sequence (this protein is one amino acid longer than wild-type SARS-CoV-2 E protein). The dotted line represents the 95% confidence interval. n=18 (ENaC only), 49 (ORF8), 52 (1-S), 51 (2-S), 35 (1-E), 40 (2-E), 30 (2-E[SF55TV]), and 30 (2-E[R69EG]).

SARS-CoV-2 E, and SARS-CoV-2 S protein decrease ENaC currents, with the E proteins having a greater effect than SARS-CoV-2 S proteins. Furthermore, we find that the SARS-CoV-2 E protein inhibits ENaC more than the SARS-CoV-1 E protein. Although Ji *et al*. report that SARS-CoV-1 S protein also decreases ENaC current, we find that this is true compared to oocytes injected

only with ENaC, the control Ji *et al*. used. However, when the control is oocytes co-injected with ORF8, there is no significant difference between oocytes co-injected with SARS-CoV-1 S or the control mRNA. Altogether, we find that the E and S proteins from SARS-CoV-2 have a greater inhibitory effect on ENaC than their SARS-CoV-1 counterparts.

The SARS-CoV-1 and -2 E proteins differ at two sequence regions, positions 55-56 and 69-70. We constructed two chimera-like E proteins in which either the 55-56 or 69-70 sequences differ, but not both. Proteins with the SARS-CoV-1 E protein residues at 69-70 are one amino acid longer than proteins with the SARS-CoV-2 E protein residues at 69-70 because this sequence is Glu-Gly in SARS-CoV-1 and Arg-(Δ) in SARS-CoV-2. Like both unmutated E proteins, both of these chimera-like proteins markedly decreased ENaC current.

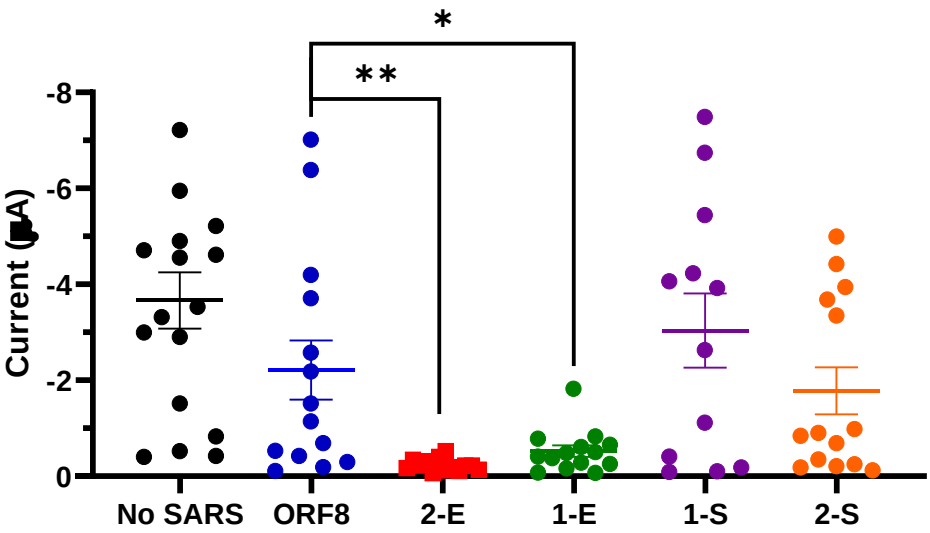


**Figure 6.4** Currents induced by 100 μM ACh in oocytes expressing mouse α3β4 and SARS mRNA. "ORF8" = SARS-CoV-2 ORF 8. "1-E" = SARS-CoV-1 E protein. "2-E" = SARS-CoV-2 E protein. "2-S" = SARS-CoV-2 S protein. "1-S" = SARS-CoV-1 S protein. The error bars represent the S.E.M. p-values were calculated from an unpaired t-test where * denotes $p < 0.05$ and ** denotes $p < 0.005$.

*6.3.4 SARS-CoV-1 and SARS-CoV-2 E proteins inhibit α3β4 nAChR currents*

Next, we were interested in the SARS proteins' general effect on ion channels. We studied the α3β4 nAChR as it is readily expressed in *Xenopus* oocytes and plays a role in several respiratory diseases.[22] Once again, we find that α3β4 currents are significantly reduced when oocytes are co-injected with either E protein (**Figure 6.4**). However, in contrast to our ENaC experiments, SARS-CoV-2 S protein does not significantly reduce α3β4 currents.

*6.3.5 Inhibition does not occur if the SARS-CoV protein mRNAs are injected 24 h after ENaC mRNA*

The individual ENaC subunits must be translated, folded, assembled into mature channels, and trafficked to the plasma membrane. ENaC currents are observed 24 hours after mRNA injection, suggesting that these steps occur within that time. To understand whether the SARS-CoV proteins affect ENaC during these steps, we injected ENaC mRNA, and waited 24 hours before injecting the SARS-CoV mRNA. We find that if the SARS-CoV mRNA is injected 24 hours after the ENaC mRNA, there is no ENaC inhibition (**Figure 6.5**).

We interpret the experiment of **Figure 6.5** as follows. On the one hand, delaying ORF8 injection by 24 h significantly increases ENaC conductance by 2-3 fold, at $V < -30$ mV and $V > +40$ mV. This effect may indicate that ORF8 inhibits ENaC expression or function modestly during the first 24 h after co-injection. On the other hand, delaying the SARS-CoV-2 S, SARS-CoV-1 E, or SARS-CoV-2 E mRNA injection by 24 h produces more dramatic increases. Quantitative comparisons are vitiated by the very small currents produced by co-injection; but the increase is > 10-fold. Therefore, we conclude that the severe block of ENaC

by SARS-CoV-1 E, SARS-CoV-2 S, or SARS-CoV-2 E proteins all occur at early steps in the functional expression of channel proteins. The relatively modest block by SARS-CoV-1 S protein presents an intermediate case. Delaying SARS-CoV-1 S co-injection by 24 h produces a ~ 4- fold increase in ENaC conductance when measured at all voltages outside the -20 mV to + 20 mV range.

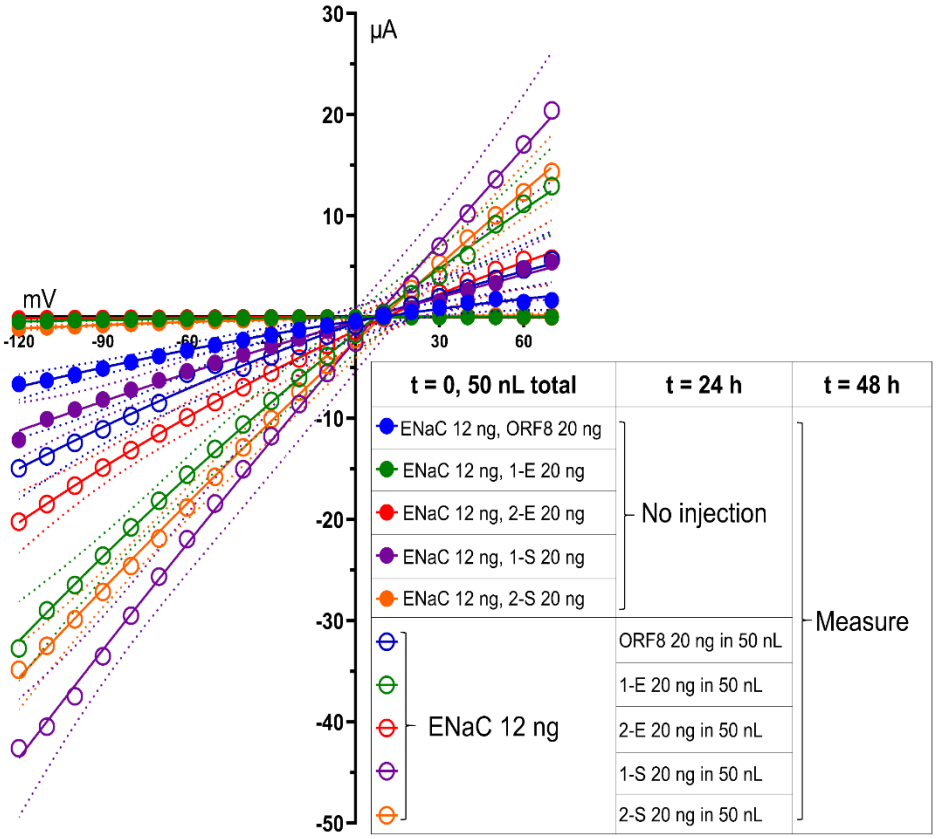


**Figure 6.5** Injecting oocytes with the SARS mRNA 24 hours after ENaC mRNA injection does not result in ENaC inhibition. The filled circles represent samples where both ENaC and SARS mRNA were injected at the same time. The open circles represent samples that had the SARS mRNA injected after the ENaC mRNA. The dotted line represents the 95% confidence interval. n = 4 (48h (ENaC + ORF8)), 12 (48h (ENaC + 1-E)), 13 (48h (ENaC + 2-E)), 8 (48h (ENaC + 1-S)), 11 (48h (ENaC + 2-S)), 6 (ENaC then ORF8), 8 (ENaC then 1-E), 10 (ENaC then 10), 5 (ENaC then 1-S), and 6 (ENaC then 2-S).

*6.3.6 Mutating the furin cleavage site in SARS-CoV-2 S protein improves ENaC function*

ENaC function is dependent on a furin cleavage event, while α3β4 does not depend on furin cleavage.[23] The ability of SARS-CoV-2 S protein to inhibit ENaC, but not α3β4, could be explained by the furin cleavage site in SARS-CoV-2 S protein that may compete for available furin. Indeed, several others have proposed this mechanism for possible ENaC inhibition via SARS-CoV-2 S protein expression.[24-26] We mutated the $^{682}$RRAR$^{685}$ motif to $^{682}$AAAR$^{685}$ to destroy the furin cleavage site. In oocytes expressing ENaC, there was greater current when we expressed the SARS-CoV-2 S [$^{682}$AAAR$^{685}$] mutant instead of the wild-type SARS-CoV-2 S protein (**Figure 6.6**). However, the currents were not completely restored, suggesting that other factors influence ENaC inhibition by SARS-CoV-2 S protein.

*6.3.7 PKC activation decreases ENaC and α3β4 currents*

PKC helps regulate many cellular functions, including net endocytosis.[27] Ji *et al.* suggested that PKC activation is the cause for decreased ENaC currents due to SARS-CoV-1 S or E protein expression. They hypothesized that as endocytosis occurs, the number of ENaC channels on the plasma membrane decreases, and the total ENaC current decreases *pari passu*. Here, we verify that PKC activation decreases ENaC and α3β4 currents after a 15-minute treatment in 10 μM PMA, a PKC activator.[28] We find that compared to vehicle, currents are significantly lower after PMA treatment, consistent with Ji *et al*.'s hypothesis that PKC activation decreases plasma membrane currents (**Figure 6.7**). Additionally, based on our

capacitance measurements, net endocytosis increased (membrane area decreased ~5%) following PMA treatment (**Figure 6.8**).

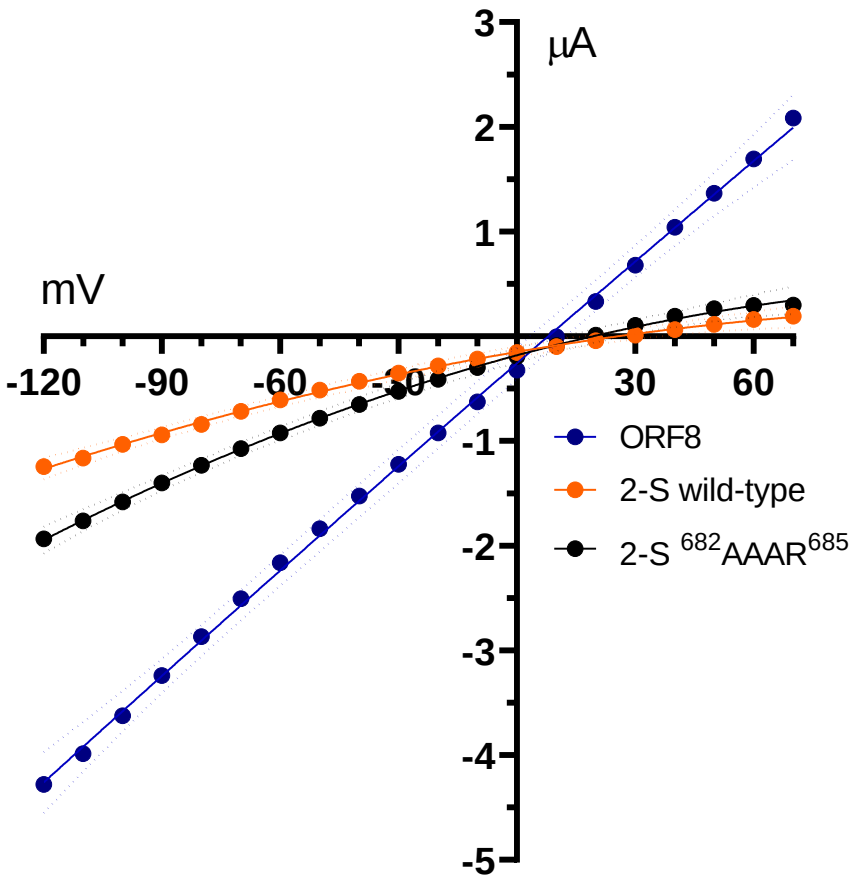


**Figure 6.6** Mutating the SARS-CoV-2 S protein furin cleavage site ($^{682}$RRAR$^{685}$) to $^{682}$AAAR$^{685}$ improves ENaC function after coinjection. The dotted line represents the 95% confidence interval. n = 49 (ORF8), 51 (2-S wild-type), and 30 (2-S $^{682}$AAAR$^{685}$).

### 6.3.8 *PKC inhibition does not abolish SARS-CoV-1 E, SARS-CoV-2 E, or SARS-CoV-2 S protein-induced reductions in ENaC currents*

We tried to inhibit PKC activation with Gö-6976, a known PKC inhibitor.[29] We hypothesized that if we can prevent PKC activation with Gö-6976, then the effects of SARS-CoV-1 E, SARS-CoV-2 S, and SARS-CoV-2 E will be abolished. However, after incubating oocytes in 1 μM Gö-6976 following mRNA injection, we found no differences between Gö-6976-treated and vehicle-treated cells (**Figure**

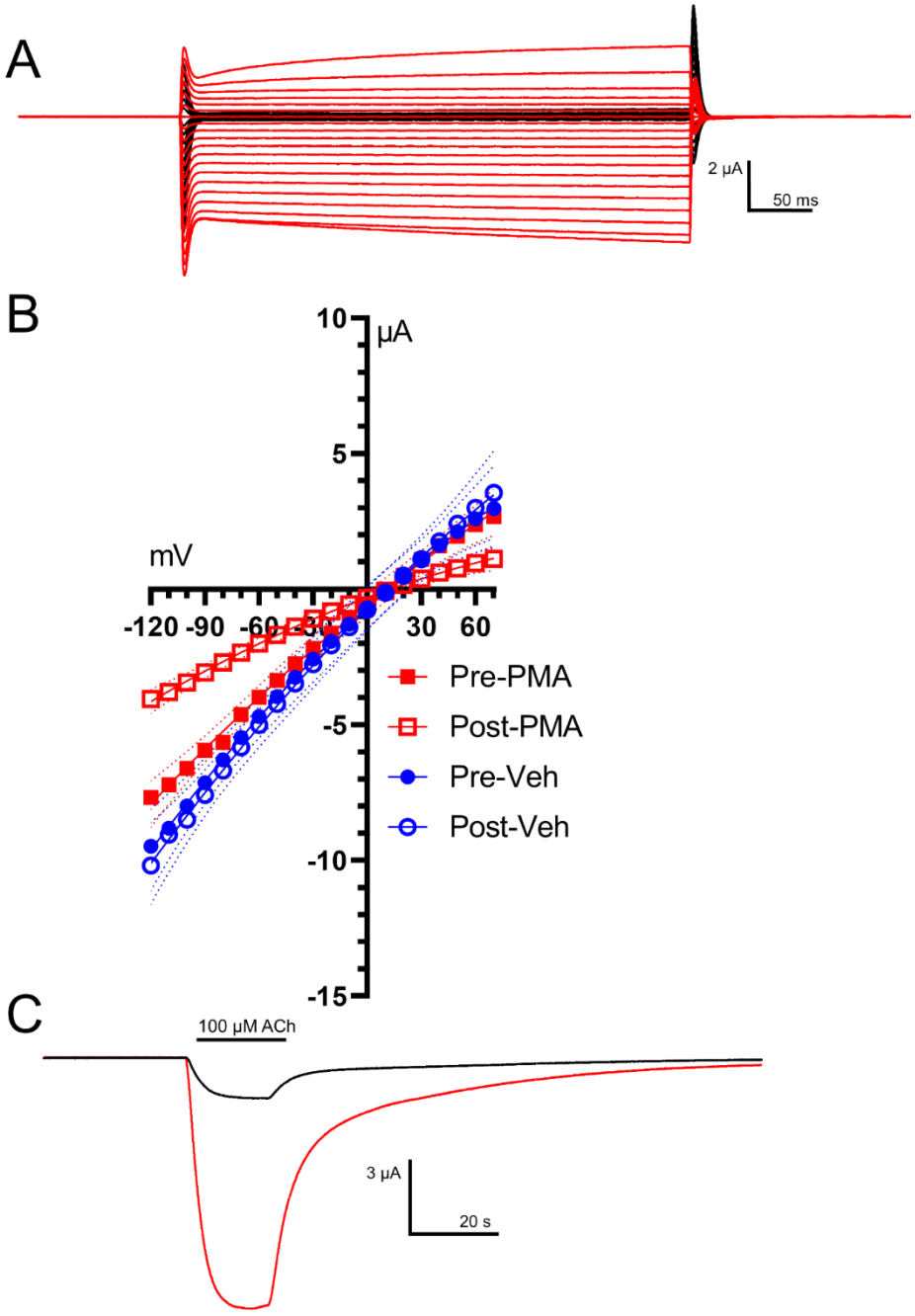


**Figure 6.7** PKC activation via 10 µM PMA treatment decreases ENaC and α3β4 currents. Oocyte currents were measured before (Pre-) and after (Post-) a 15-minute treatment with vehicle or 10 µM PMA. *(A)* Traces for oocytes expressing ENaC. Red traces represent before PMA ("Pre-PMA") and the black traces are after PMA ("Post-PMA"). This oocyte showed unusually large suppression of ENaC currents by PMA *(B)* I-V relationships for oocytes expressing ENaC before or after vehicle or PMA treatment. The dotted line represents the 95% confidence interval. n = 10 (Pre-Veh), 10 (Post-Veh), 12 (Pre-PMA), 13 (Post-PMA). *(C)* Traces for oocytes expressing α3β4; 100 µM ACh was present as noted by the horizontal bar. Red traces represent before PMA ("Pre-PMA") and the black traces are after PMA ("Post-PMA").

**6.9**). Once again, this is somewhat consistent with Ji *et al*.'s data in that Gö-6976 treatment did not completely recover ENaC currents, although our data suggest a much less impressive improvement with Gö-6976 treatment. Nonetheless, both Ji *et al.* and we suggest that although PKC activation can decrease ENaC currents, the SARS proteins appear to be utilizing other mechanisms as well.

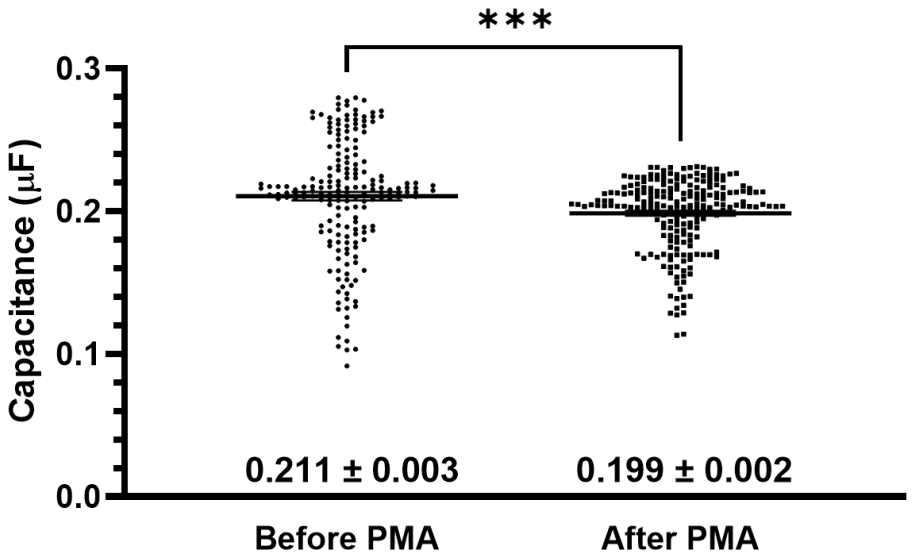


**Figure 6.8** PKC activation via PMA treatment decreases membrane capacitance. The error bars represent the S.E.M. p-values were calculated from an unpaired t-test where *** denotes $p < 0.001$.

**6.4 Discussion**

COVID-19 has wreaked havoc on the world in unprecedented ways. We show that the SARS-CoV-1 and SARS-CoV-2 proteins, expressed either singly or in combination, do not produce conductance at the plasma membrane (**Figure 6.1**). This contrasts with reports suggesting that SARS-CoV-1 and SARS-CoV-2 may produce viroporins on the plasma membrane.[30-32] We verify that proteins are being translated by detecting E, S, and ORF8 proteins via immunoblots (**Figure 6.2**) and by observing inhibition of other channels. Whereas these results do not

prove the absence of ion channels in other intracellular regions, the plasma membrane's lack of ion channels complicates some therapeutic strategies.[5]

Caveats include that a *Xenopus* oocytes differ markedly from human epithelial cells, so further work must be done on other model systems to produce a more comprehensive understanding of SARS-CoV-2 proteins' roles in COVID-

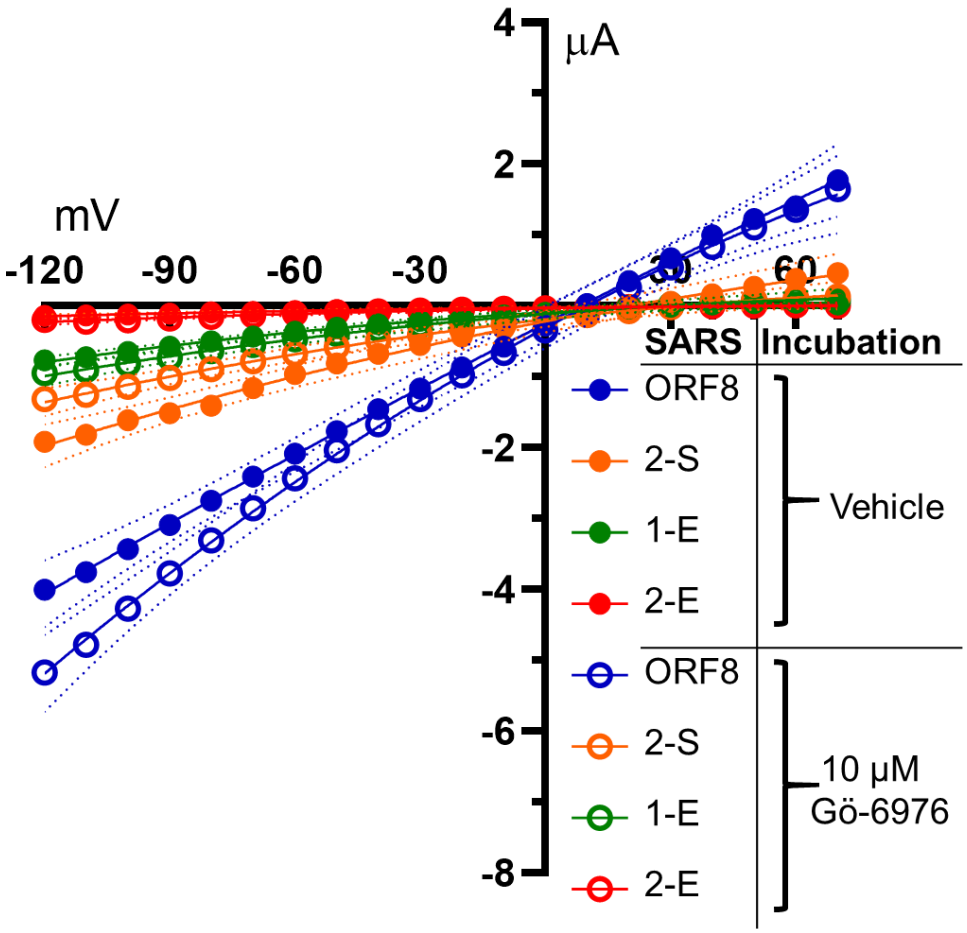


**Figure 6.9** PKC inhibition with 1 μM Gö-6976 does not prevent E protein or SARS-CoV-2 S protein-related decreases in ENaC activity. For each coinjection, there is no significant difference between the oocytes treated with vehicle or Gö-6976. "ORF8" = SARS-CoV-2 ORF8, "1-E" = SARS-CoV-1 E protein. "2-E" = SARS-CoV-2 E protein. "2-S" = SARS-CoV-2 S protein. Error bars represent S.E.M. The dotted line represents the 95% confidence interval. n = 11 (ORF Veh), 11 (1-E Veh), 12 (2-E Veh), 10 (2-S Veh), 14 (ORF8 + Gö-6976), 13 (1-E + Gö-6976), 7 (2-E + Gö-6976), and 11 (2-S + Gö-6976).

19. Also, the intracellular life cycle of a coronavirus involves several steps in organelles; if the SAR-CoV proteins produce channels in organelles, these might not traffic to the plasma membrane and might therefore escape detection in our experiments.

As in many viral diseases, viral protein-host protein interactions underlie the pathophysiology of COVID-19. Therefore, we have studied interactions that include the effects of E or S protein expression on ENaC or α3β4 activity. In SARS-CoV-1, Ji *et al*. found that E and S protein expression decreased ENaC activity.[14] Our observations suggest that the inhibitory properties are greater for the SARS-CoV-2 E protein and S protein (**Figure 6.3**). We found that in α3β4-expressing oocytes, both E proteins decreased α3β4 currents (**Figure 6.4**). For S protein, Ji *et al*. found that SARS-CoV-1 S protein decreased ENaC activity.[14] In contrast, our results suggest that SARS-CoV-2 S protein, but not SARS-CoV-1 S protein, has this effect. This difference is likely due to a difference in our control experiments. On the one hand, Ji *et* al. compared their currents to samples only injected with ENaC; on the other hand, we compared our results to samples co-injected with ORF8, a protein that is not expected to interact with ENaC. Therefore, we hypothesize that the decreased ENaC currents that we observe for SARS-CoV-1 S protein (that do not significantly differ from samples injected with ORF8) are due to occlusion of translational or trafficking pathways instead of a selective effect from the translated proteins.[33] However, oocytes co-injected with SARS-CoV-2 S protein did have significantly lower ENaC currents compared to our controls. We show that the inhibitions do not occur if the SARS-CoV protein mRNAs are injected 24 h after ENaC mRNAs, suggesting that SARS-CoV proteins affect early step(s) in the functional expression of channel proteins (**Figure 6.5**).

Previous studies show that some viral fusion proteins are activated by proteolysis.[34] The increased inhibition with SARS-CoV-2 S protein is consistent with the appearance of a furin cleavage site.[35] This site is identical to the furin cleavage site in the ENaC-α subunit, so SARS-CoV-2 S protein may be competing for available furin, thereby decreasing the proteolytic activation of ENaC-α and thus decreasing ENaC activity.[26,36,37] SARS-CoV-2 S protein competing for furin would also explain how α3β4 currents do not change with SARS-CoV-2 S protein expression: α3β4 does not depend on furin cleavage for activity. Our experiments with the SARS-CoV-2 S [$^{682}$AAAR$^{685}$] mutant support this hypothesis, although it does not completely explain SARS-CoV-2-induced ENaC inhibition as uninhibited ENaC currents were not observed. (**Figure 6.6**).

We hypothesized, similarly to Ji *et al.*, that PKC activation may partly underlie the decreased currents.[14] When PKC is activated, net endocytosis increases.[27] Decreasing the number of channels on the membrane via endocytosis is expected to decrease currents. When we examined this relationship quantitatively in oocytes treated with PMA, we observed only a modest (~5%) decrease in membrane area (as a decrease in capacitance) along with a much larger decrease in membrane currents through ENaC and α3β4 (**Figure 6.7 and Figure 6.8**). Furthermore, when we blocked PKC activation with Gö-6976 treatment, we did not block the inhibitory effects of SARS-CoV-1 E, SARS-CoV-2 E, or SARS-CoV-2 S proteins (**Figure 6.9**). While these SARS proteins may be activating PKC, there appear to be other mechanisms that inhibit ENaC activity as well.

Both chimera-like E protein constructs suppressed ENaC currents like the parent proteins. Although we could not directly probe events in the Golgi (where

the E protein is expected to localize)[38], this result suggests that combining the two regions conferred no selective advantage to SARS-CoV-2, at least as measured by our assay of ENaC suppression. Among the presently known SARS-CoV-2 variant lineages, we have noted no mutations at the 55-56 and 69-70 positions. Several members of the B.1.351 lineage have a P71L mutation; this position is near the 69-70 sequence and immediately upstream from a candidate PDZ domain binding motif at the C-terminus.

**6.5 Conclusion**

Unfortunately, COVID-19 will not be the last virus to cross over into humans and strain public health resources. While the COVID-19 vaccine will greatly help the world recover from this pandemic, basic research into SARS-CoV-2 will improve our response when the next viral infection emerges.

Because SARS and COVID-19 are different diseases, one expects to note differences between the proteins from SARS-CoV-1 and SARS-CoV-2. Here, we show that the E and S proteins inhibit ENaC and are more potent at inhibiting ENaC than their SARS-CoV-1 counterparts. ENaC participates in lung fluid homeostasis, so an improperly functioning ENaC may result in pulmonary edema.[14,15] If ENaC is inhibited more in COVID-19 than in SARS, this may help us predict the course of future viral diseases. Indeed, if pulmonary edema is more prominent in COVID-19 patients than SARS patients, the different S and E proteins may be responsible. Additionally, the SARS-CoV-2 variants are troubling. Most researchers emphasize that any differential virulence or lethality of variant S proteins may arise via differential interactions with antibodies—induced either by host infection or by vaccines. This report presents quantitative data on another S protein effect: consequences of interactions with host non-antibody proteins. One such

interaction, not studied here, is binding to the ACE2 receptor. Measuring the interactions made by the S and E proteins with human proteins may be crucial to understanding COVID-19 and the SARS-CoV-2 variants. We are still in the early stages of understanding SARS-CoV-2 and COVID-19. Although our findings may be meaningful and important, they represent only part of the required knowledge about SARS-CoV-2 and COVID-19.

## 6.6 Materials and Methods

### *6.6.1 cDNA and mRNA*

Human ENaC subunit cDNAs h-alpha-ENaC, h-beta-ENaC, and h-gamma-ENaC Myc were gifts from Christie Thomas.[37] pLVX-EF1alpha-SARS-CoV-2-orf8-2xStrep-IRES-Puro, pLVX-EF1alpha-SARS-CoV-2-nsp2-2xStrep-IRES-Puro, pLVX-EF1alpha-SARS-CoV-2-nsp4-2xStrep-IRES-Puro, pLVX-EF1alpha-SARS-CoV-2-orf3a-2xStrep-IRES-Puro, and pLVX-EF1alpha-SARS-CoV-2-M-2xStrep-IRES-Puro were gifts from Nevan Krogan.[7] pDONR223 SARS-CoV-2 NSP6 and pDONR207 SARS-CoV-2 NSP3 were gifts from Fritz Roth. pUC57-2019-nCoV-S plasmid was purchased from MolecularCloud. pcDNA3.1-SARS-Spike was a gift from Fang Li.[39] The SARS-CoV-2 E protein plasmid was constructed and packaged by VectorBuilder. The vector ID, VB200324-4348fzb, provides information about the vector on vectorbuilder.com. SARS-CoV-1 E protein was produced by introducing point mutations in the SARS-CoV-2 E protein plasmid. All SARS-CoV-1 and SARS-CoV-2 proteins were cloned into the pGEMHE vector for optimal *Xenopus* oocyte expression. The mouse α3 and β4 nicotinic acetylcholine receptor mRNAs have been described previously.[40] mRNA was produced using the mMessage mMachine T7 transcription kit (Invitrogen) and purified with the RNeasy Mini Kit (Qiagen).

*6.6.2 Protein expression in oocytes*

*Xenopus laevis* stage V and VI oocytes were harvested via standard protocols.[41] For each ENaC subunit, 12 ng of mRNA was injected into oocytes. For mouse α3β4 nAChR expression, 10 ng of mRNA for each subunit were injected into each oocyte. For the SARS-CoV-1 or SARS-CoV-2 proteins, 20 ng of mRNA were injected into oocytes along with the ENaC or α3β4 nAChR mRNA. For oocytes injected with a single SARS-CoV-2 protein mRNA, each oocyte received 20 ng of mRNA. For oocytes injected with nine SARS-CoV-2 and two SARS-CoV-1 protein mRNAs, 3 ng of each were injected into each oocyte. The final mRNA injection took place 24 hours before electrophysiological recording or 48 hours before lysis for immunoblotting.

*6.6.3 Immunoblotting*

48 hours post-injection, oocyte lysates were prepared by lysing oocytes osmotically in a 20 mM 4-(2-hydroxyethyl)-1-piperazineethanesulfonic acid (HEPES), pH 7.3 solution (20 µL per oocyte).[42] Lysates were centrifuged for 5 minutes at 10,000 rpm. The supernatant was used to probe for E protein. The pellets were resuspended in 50 mM Tris, 150 mM NaCl, 1% NP-40, pH 7.3 buffer, and these solutions were used to probe for ORF8 and S protein. 12% Mini-PROTEAN® TGX™ Precast Protein Gels (Bio-Rad) were used for electrophoresis and wet-transferred onto an Immun-Blot® LF PVDF membrane (Bio-Rad). E protein was probed using rabbit antiserum that responds to the C-terminus of SARS-CoV-1 E protein at 1:1000 concentration. The antiserum was a gift from Carolyn Machamer.[18] The ORF8 was probed using a primary antibody at 1:500 concentration (GeneTex, Cat#: GTX135591). S protein was probed using a

primary antibody at 1:500 concentration (Invitrogen, Cat#: PA581795). The primary antibodies were visualized using IRDye® 800 CW donkey anti-rabbit antibody (Li-Cor, Cat#: 926-32213) at 1:1000 concentration.

*6.6.4 Electrophysiology*

Oocyte recordings were performed in two-electrode voltage-clamp mode using the OpusXpress 6000A instrument (Axon Instruments). Oocyte equilibration and washes were performed with ND96 [96 mM NaCl, 2 mM KCl, 1.8 mM CaCl2, 1 mM MgCl2, and 5 mM HEPES (pH 7.4)] or High $K^+$ buffer [2 mM NaCl, 96 mM KCl, 1.8 mM CaCl2, 1 mM MgCl2, and 5 mM HEPES (pH 7.4)]. Microelectrodes were fabricated from borosilicate glass (BF150-117-15, Sutter Instrument Company, Novato, CA) using a one-stage horizontal pull (P-87, Sutter Instrument Co., Novato, CA) and filled with 3 M KCl. Pipette resistances ranged from 0.3 to 3.0 MΩ. The initial holding potential was +10 mV for ENaC expressing oocytes or -60 mV for α3β4 expressing oocytes. For ENaC expressing oocytes, voltages were sampled from -120 mV to +70 mV at 10 mV intervals and the currents through the oocyte membrane were recorded. For α3β4 expressing oocytes, the potential was held at -60 mV throughout the experiment, and the currents were measured during 100 µM acetylcholine (ACh) application. Data were sampled at 50 Hz. Traces were processed in Clampfit 11.1. In ENaC expressing oocytes, amiloride-sensitive currents were calculated by subtracting currents measured in the presence of 10 µM amiloride (an ENaC inhibitor) from the average currents measured in ND96 taken before amiloride treatment and after amiloride wash-out. For PMA experiments, oocyte currents were measured before and after 15 minute incubation in the vehicle or 10 µM PMA. For Gö-6976 experiments, the oocytes

were incubated in 1 μM Gö-6976 right after injection until electrophysiology experiments were performed.

Analysis and curve fitting was performed using Prism (GraphPad Software, La Jolla, CA). For the ENaC experiments in Figures 6.3, 6.5, 6.6, 6.7, and 6.8, we fitted a second-order polynomial to each current-voltage dataset (> 10 oocytes, except where noted), to account for the nonlinear ENaC conductance. For control currents (for instance, co-injection with ORF8), the reversal potential ($V_0$) varied < 5 mV within each experiment; however, the much smaller currents resulting from co-injection of other SARS-Cov-1 and SARS-CoV-2 proteins vitiated a meaningful estimate of $V_0$. The data plots show the 95% confidence limits of these fitting functions at each voltage between -120 mV and +70 mV. “Significant differences” between current-voltage relations in a particular voltage range mean that the 95% confidence limits do not overlap in that voltage range. This presentation has the physiological and pathophysiological relevance (a) that ENaC is expressed primarily in epithelial cells—a likely site of SARS-Cov-2 infection and proliferation[43-45] and (b) where possible, we extend the analysis to the > -60 mV resting potentials typical of epithelial cells.

Membrane capacitance was measured on oocytes for each voltage jump. The capacitive charge $\Delta Q$ was calculated by temporally integrating the transient capacitive current ($\Delta Q = \int \Delta I$) during the 20 ms following the command voltage jump. Figures 6.3A and 6.3C show how relatively large conductive currents challenge the voltage-clamp circuitry, the current amplifier’s compliance, and the linearity of the current electrode so that $\Delta Q$ becomes distorted by the presence of a large conductance. An example of the resulting artifact is our lab’s erroneous overestimate of the decreases in oocyte capacitance that accompany large

decreases in $K^+$ currents.[46] To minimize such artifacts in the present experiments, we measured capacitance during the blockade of most ENaC currents by amiloride (10 mM). We also subtracted remaining time-independent conductive currents by extrapolating such currents back to the time of the jump in the command voltage. We verified that the capacitive transient $\Delta Q$ showed a linear dependence on the voltage jump $\Delta V$, allowing us to measure $C = \Delta V/\Delta Q$.

In analyses of data that emphasized currents at a single potential, an unpaired t-test was used to determine statistical significance between results with ORF8 coinjection vs each other coinjection (**Figure 6.4**). A p-value of 0.05 or less was considered to be statistically significant.

### 6.7 References


1 Zhang, R. *et al.* The ORF4a protein of human coronavirus 229E functions as a viroporin that regulates viral production. *Biochimica Et Biophysica Acta* **1838**, 1088-1095, doi:10.1016/j.bbamem.2013.07.025 (2014).

2 To, J. & Torres, J. Chapter 15 in *Virus Protein and Nucleoprotein Complexes* Vol. 88 *Subcellular Biochemistry* (eds J. R. Harris & D. Bhella) 329-377 (Springer, 2018).

3 Farag, N. S., Breitinger, U., Breitinger, H. G. & El Azizi, M. A. Viroporins and inflammasomes: A key to understand virus-induced inflammation. *Int. J. Biochem. Cell Biol.* **122**, 11, doi:10.1016/j.biocel.2020.105738 (2020).

4 Wang, C., Takeuchi, K., Pinto, L. H. & Lamb, R. A. Ion-channel activity of influenza-A virus M(2) protein - characterization of the amantadine block. *J. Virology* **67**, 5585-5594, doi:10.1128/jvi.67.9.5585-5594.1993 (1993).

5 Cabrera-Garcia, D., Bekdash, R., Abbott, G. W., Yazawa, M. & Harrison, N. L. The envelope protein of SARS-CoV-2 increases intra-Golgi pH and forms a cation channel that is regulated by pH. *The Journal of Physiology* doi:10.1113/JP281037 (2021).

6 Torres, J., Surya, W., Li, Y. & Liu, D. X. Protein-protein interactions of viroporins in coronaviruses and paramyxoviruses: New targets for antivirals? *Viruses-Basel* **7**, 2858-2883, doi:10.3390/v7062750 (2015).

7 Gordon, D. E. *et al.* A SARS-CoV-2 protein interaction map reveals targets for drug repurposing. *Nature* **583**, 459–468, doi:10.1038/s41586-020-2286-9 (2020).

8 Chen, Y., Liu, Q. Y. & Guo, D. Y. Emerging coronaviruses: Genome structure, replication, and pathogenesis. *J. Medical Virology* **92**, 418-423, doi:10.1002/jmv.25681 (2020).

9 Yan, R. *et al.* Structural basis for the recognition of the SARS-CoV-2 by full-length human ACE2. *Science*, eabb2762, doi:10.1126/science.abb2762 (2020).

10 Wrapp, D. *et al.* Cryo-EM structure of the 2019-nCoV spike in the prefusion conformation. *Science* **367**, 1260-1263, doi:10.1126/science.abb2507 (2020).

11 Hoffmann, M. *et al.* SARS-CoV-2 cell entry depends on ACE2 and TMPRSS2 and is blocked by a clinically proven protease inhibitor. *Cell*, doi:10.1016/j.cell.2020.02.052 (2020).

12 Guzzi, P. H., Mercatelli, D., Ceraolo, C. & Giorgi, F. M. Master regulator analysis of the SARS-CoV-2/Human interactome. *bioRxiv*, 2020.2003.2015.992925, doi:10.1101/2020.03.15.992925 (2020).

13 Ng, M. L., Tan, S. H., See, E. E., Ooi, E. E. & Ling, A. E. Proliferative growth of SARS coronavirus in Vero E6 cells. *The Journal of General Virology* **84**, 3291-3303, doi:10.1099/vir.0.19505-0 (2003).

14 Ji, H. L. *et al.* SARS-CoV proteins decrease levels and activity of human ENaC via activation of distinct PKC isoforms. *American Journal of Physiology. Lung Cellular and Molecular Physiology* **296**, L372-383, doi:10.1152/ajplung.90437.2008 (2009).

15 Fronius, M. Treatment of pulmonary edema by ENaC activators/stimulators. *Current Molecular Pharmacology* **6**, 13-27, doi:10.2174/1874467211306010003 (2013).

16 Valtueña, J., Ruiz-Sánchez, D., Volo, V., Manchado-López, P. & Garayar-Cantero, M. Acral edema during the COVID-19 pandemic. *International Journal of Dermatology* **59**, 1155-1157, doi:10.1111/ijd.15025 (2020).

17 Zwaveling, S., Gerth van Wijk, R. & Karim, F. Pulmonary edema in COVID-19: Explained by bradykinin? *Journal of Allergy and Clinical Immunology*, doi:10.1016/j.jaci.2020.08.038 (2020).

18 Cohen, J. R., Lin, L. D. & Machamer, C. E. Identification of a golgi complex-targeting signal in the cytoplasmic tail of the severe acute respiratory syndrome coronavirus envelope protein. *J. Virology* **85**, 5794-5803, doi:10.1128/jvi.00060-11 (2011).

19 Shimbo, K., Brassard, D. L., Lamb, R. A. & Pinto, L. H. Viral and cellular small integral membrane proteins can modify ion channels endogenous to Xenopus oocytes. *Biophysical journal* **69**, 1819-1829, doi:10.1016/s0006-3495(95)80052-4 (1995).

20 Castaño-Rodriguez, C. *et al.* Role of severe acute respiratory syndrome coronavirus viroporins E, 3a, and 8a in replication and pathogenesis. *mBio* **9**, e02325-02317, doi:10.1128/mBio.02325-17 (2018).

21 Wolff, G. *et al.* A molecular pore spans the double membrane of the coronavirus replication organelle. *Science*, eabd3629, doi:10.1126/science.abd3629 (2020).

22 Mazzo, F. *et al.* Nicotine-modulated subunit stoichiometry affects stability and trafficking of α3β4 nicotinic receptor. *J. Neurosci.* **33**, 12316-12328, doi:10.1523/jneurosci.2393-13.2013 (2013).

23 Harris, M., Garcia-Caballero, A., Stutts, M. J., Firsov, D. & Rossier, B. C. Preferential assembly of epithelial sodium channel (ENaC) subunits in Xenopus oocytes: role of furin-mediated endogenous proteolysis. *The Journal of Biological Chemistry* **283**, 7455-7463, doi:10.1074/jbc.M707399200 (2008).

24 Anand, P., Puranik, A., Aravamudan, M., Venkatakrishnan, A. J. & Soundararajan, V. SARS-CoV-2 strategically mimics proteolytic activation of human ENaC. *eLife* **9**, e58603, doi:10.7554/eLife.58603 (2020).

25 Gentzsch, M. & Rossier, B. C. A pathophysiological model for COVID-19: Critical importance of transepithelial sodium transport upon airway infection. *Function* **1**, doi:10.1093/function/zqaa024 (2020).
26 Szabó, G. T., Kiss, A., Csanádi, Z. & Czuriga, D. Hypothetical dysfunction of the epithelial sodium channel may justify neurohumoral blockade in coronavirus disease 2019. *ESC Heart Failure* **8**, 171-174, doi:10.1002/ehf2.13078 (2021).
27 Alvi, F., Idkowiak-Baldys, J., Baldys, A., Raymond, J. R. & Hannun, Y. A. Regulation of membrane trafficking and endocytosis by protein kinase C: emerging role of the pericentrion, a novel protein kinase C-dependent subset of recycling endosomes. *Cellular and Molecular Life Sciences : CMLS* **64**, 263-270, doi:10.1007/s00018-006-6363-5 (2007).
28 Vasilets, L. A., Schmalzing, G., Mädefessel, K., Haase, W. & Schwarz, W. Activation of protein kinase C by phorbol ester induces downregulation of the Na+/K(+)-ATPase in oocytes of Xenopus laevis. *The Journal of Membrane Biology* **118**, 131-142, doi:10.1007/bf01868470 (1990).
29 Martiny-Baron, G. *et al.* Selective inhibition of protein kinase C isozymes by the indolocarbazole Gö 6976. *The Journal of Biological Chemistry* **268**, 9194-9197 (1993).
30 Sarkar, M. & Saha, S. Structural insight into the putative role of novel SARS CoV-2 E protein in viral infection: a potential target for LAV development and therapeutic strategies. *bioRxiv*, 2020.2005.2011.088781, doi:10.1101/2020.05.11.088781 (2020).
31 Dey, D., Borkotoky, S. & Banerjee, M. In silico identification of Tretinoin as a SARS-CoV-2 envelope (E) protein ion channel inhibitor. *Comput Biol Med* **127**, 104063-104063, doi:10.1016/j.compbiomed.2020.104063 (2020).
32 Kern, D. M. *et al.* Cryo-EM structure of the SARS-CoV-2 3a ion channel in lipid nanodiscs. *bioRxiv*, 2020.2006.2017.156554, doi:10.1101/2020.06.17.156554 (2020).
33 Richter, J. D., Evers, D. C. & Smith, L. D. The recruitment of membrane-bound mRNAs for translation in microinjected Xenopus oocytes. *The Journal of Biological Chemistry* **258**, 2614-2620 (1983).
34 Chen, J. *et al.* Structure of the hemagglutinin precursor cleavage site, a determinant of influenza pathogenicity and the origin of the labile conformation. *Cell* **95**, 409-417, doi:10.1016/s0092-8674(00)81771-7 (1998).
35 Anand, P., Puranik, A., Aravamudan, M., Venkatakrishnan, A. & Soundararajan, V. SARS-CoV-2 selectively mimics a cleavable peptide of human ENaC in a strategic hijack of host proteolytic machinery. *bioRxiv*, 2020.2004.2029.069476, doi:10.1101/2020.04.29.069476 (2020).
36 Kumar, A. *et al.* SARS-CoV-2-specific virulence factors in COVID-19. *Journal of Medical Virology*, 8, doi:10.1002/jmv.26615 (2020).
37 Raikwar, N. S. & Thomas, C. P. Nedd4-2 isoforms ubiquitinate individual epithelial sodium channel subunits and reduce surface expression and function of the epithelial sodium channel. *American Journal of Physiology. Renal Physiology* **294**, F1157-1165, doi:10.1152/ajprenal.00339.2007 (2008).

38 Gordon, D. E. *et al.* Comparative host-coronavirus protein interaction networks reveal pan-viral disease mechanisms. *Science* **370**, eabe9403, doi:10.1126/science.abe9403 (2020).
39 Shang, J. *et al.* Structural basis of receptor recognition by SARS-CoV-2. *Nature* **581**, 221-224, doi:10.1038/s41586-020-2179-y (2020).
40 Blom, A. E. M., Campello, H. R., Lester, H. A., Gallagher, T. & Dougherty, D. A. Probing binding interactions of cytisine derivatives to the α4β2 nicotinic acetylcholine receptor. *J Am Chem Soc* **141**, 15840-15849, doi:10.1021/jacs.9b06580 (2019).
41 Henderson, B. J. *et al.* Menthol stereoisomers exhibit different effects on α4β2 nAChR upregulation and dopamine neuron spontaneous firing. *eNeuro* **5**, eneuro.0465-0418.2018, doi:10.1523/eneuro.0465-18.2018 (2018).
42 Lin-Moshier, Y. & Marchant, J. S. A rapid Western blotting protocol for the Xenopus oocyte. *Cold Spring Harbor Protocols* **2013**, 10.1101/pdb.prot072793 pdb.prot072793, doi:10.1101/pdb.prot072793 (2013).
43 Mulay, A. *et al.* SARS-CoV-2 infection of primary human lung epithelium for COVID-19 modeling and drug discovery. *Cell Reports* **35**, 109055, doi:10.1016/j.celrep.2021.109055 (2021).
44 Melms, J. C. *et al.* A molecular single-cell lung atlas of lethal COVID-19. *Nature*, doi:10.1038/s41586-021-03569-1 (2021).
45 Delorey, T. M. *et al.* COVID-19 tissue atlases reveal SARS-CoV-2 pathology and cellular targets. *Nature*, doi:10.1038/s41586-021-03570-8 (2021).
46 Tong, Y. *et al.* Tyrosine decaging leads to substantial membrane trafficking during modulation of an inward rectifier potassium channel. *The Journal of General Physiology* **117**, 103-118, doi:10.1085/jgp.117.2.103 (2001).

# Appendix 1: Investigating protein-protein interactions in the estrogen receptor α with photocrosslinking amino acids

*This work was done in collaboration with Dr. Matthew Rienzo, Dr. Richard Mosesso, and Gabrielle Tender*

## A1.1 Abstract

The estrogen receptor α (ERα) is one of the most investigated proteins due to its role in breast cancer. ERα is a nuclear transcription factor whose function is dependent on hormones and several protein-protein interactions (PPIs). Many of these PPI studies used mass spectrometry and immunoblot experiments that relied on maintaining non-covalent interactions between the proteins. Unfortunately, these methods would miss some of the transient or weak PPIs that might not survive some of the harsh conditions utilized in mass spectrometry and immunoblots. Here, we incorporate a photocrosslinking amino acid, azidophenylalanine ($N_3$Phe), to help capture these weak or transient PPIs. We first investigated the dimerization event required for ERα activation as a proof-of-concept of our technique. We incorporated $N_3$Phe in the dimerization interface and observed an increase in dimerization with increasing concentration of the ERα agonist, estradiol (E2). Next, we attempted to observe a decrease in dimerization with ERα antagonists, tamoxifen and fulvestrant. Surprisingly, both of these antagonists induced dimerization, demonstrating that these antagonists are not inhibiting dimerization. Finally, we moved the $N_3$Phe to the hinge region of the ERα to look for non-dimer PPIs. We found that the ERα will interact with some unknown protein when the $N_3$Phe is incorporated at residue 275. Despite our best attempts

to identify the unknown protein partner, we could never get enough protein to get a definitive identification via protein gel or mass spectrometry. We attempted stable isotope labeling using amino acids in cell culture (SILAC), but it did not give satisfactory results.

**A1.2 Introduction**

Nuclear transcription factors are vital to a cell's development as they are responsible for turning certain genes on and off. Many of these transcription factors are controlled by hormones. Proper function of both the hormones and transcription factors is critical to the health of the organism. One example of how a malfunctioning transcription factor can lead to disastrous results is ERα's role in breast cancer. Breast cancer is the most common form of cancer in women, affecting approximately one in eight women in the United States.[1] Due to the prevalence of breast cancer, some of the biggest drugs on the market target ERα. The prime example is tamoxifen, which has made billions of dollars and saved many lives for over two decades.[2]

ERα has several regions that depend on conformational changes to occur for action as a transcription factor.[3] The major components are the ligand-binding domain (LBD), the DNA-binding domain (DBD), and a hinge domain between the LBD and DBD (**Figure A1.1**).[4,5] The LBD includes the dimerization interface and is the binding site for most agonists and antagonists. Following ligand binding, several conformation changes occur that "cap" the ligand-binding site, induce dimerization, and cause dissociation from its chaperone proteins.[6,7] Activation may cause ERα to bind to estrogen response elements (EREs) as a dimer in the nucleus and induce transcription at nearby DNA sequences. Alternatively, ERα may bind to other transcription factors after activation to promote transcription. In

addition to activation, dimerization, and binding to EREs or transcription factors, several factors will affect ERα function.[8] For example, tamoxifen, which is great at stopping breast cancer cell growth, can increase one's risk of endometrial cancer because tamoxifen is an ERα antagonist in breast tissue but an agonist in bone and uterus tissue.[8]

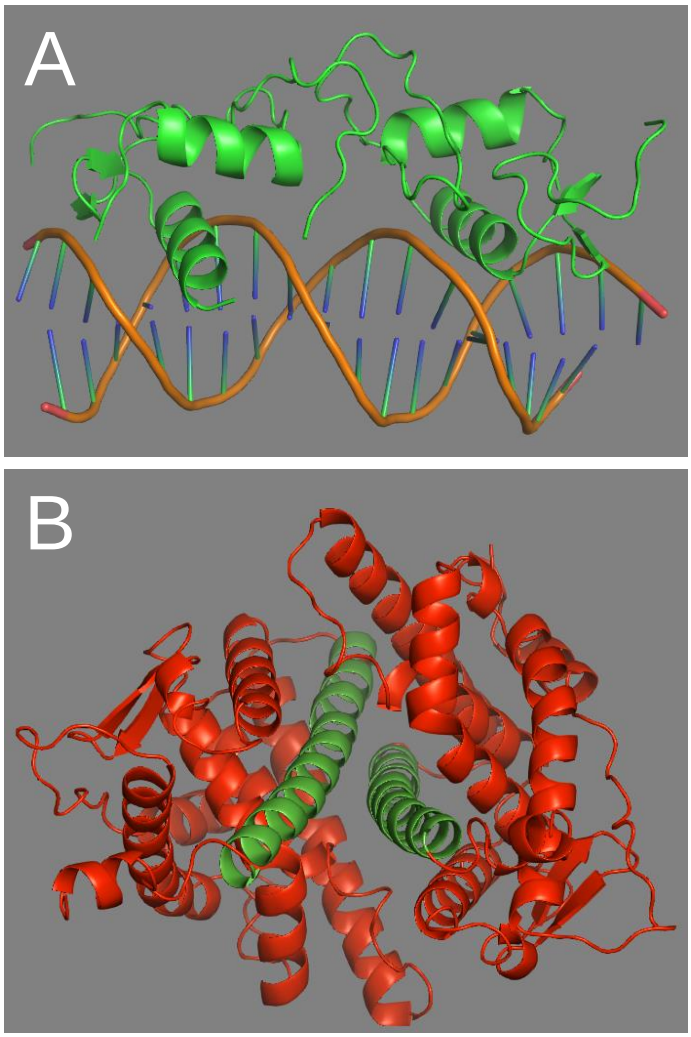


**Figure A1.1** Structures of the ERα. (*A)* The DNA binding domain (PDB: 1HCQ) and *(B)* the ligand binding domain. The green helicies respresent the dimerization interface (PDB: 1A52).

Many of these questions involve the hinge region. The hinge region is a largely disordered region between the DBD and the LBD that is important for relaying the effects of the LBD to the DBD and is responsible for some of the differences between ERα and estrogen receptor β (ERβ).[9] The hinge region is also responsible for coordinating the actions of the two activation functions, AF-1 and AF-2, whose synergy is greater in ERα than ERβ.[9] Furthermore, the hinge region is the location of some important phosphorylation and PPI sites in addition to the nuclear localization sequence.[10] Nevertheless, partly due to the lack of structural information, our

understanding of the hinge region and the location of some of the PPI interfaces is lacking.

Here, we go in a new direction to investigate ERα PPIs using a photocrosslinking amino acid, $N_3$Phe, to precisely determine where certain PPIs occur. $N_3$Phe is a non-canonical amino acid (NCAA) that, after UV irradiation, will generate a nitrene that will capture transient PPIs (**Figure A1.2**). These interactions may break during standard immunoblot or mass spectrometry and may therefore go undetected. Since we will be capturing these interactions with a covalent bond, we can observe these PPIs using the harsh conditions inherent in protein gels and mass spectrometry. First, we start observing homodimerization and only observe a dimer band if we incorporate $N_3$Phe, activate ERα, and irradiate the cells with UV light, thus providing a proof-of-concept for our PPI assay. Next, we moved to several sites in the hinge region. We found a novel, non-dimer band when we incorporated $N_3$Phe at either residue 265 or 275. In order to identify the protein binding to the ERα hinge region, we attempted SILAC mass spectrometry and were unsuccessful. Unfortunately, crosslinked protein yields were insufficient to get an identification.

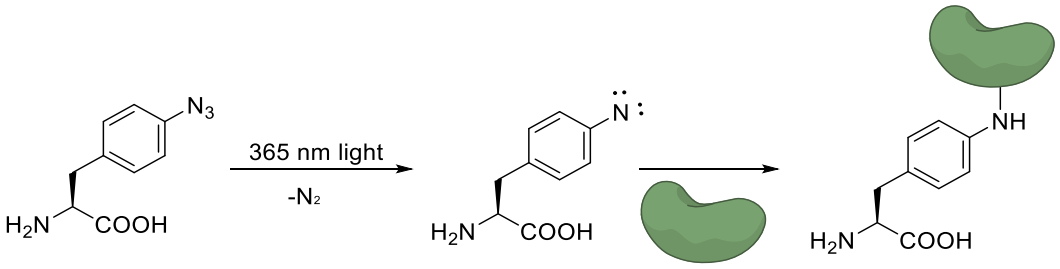


**Figure A1.2** Nitrene formation and covalent capture of PPIs following UV irradiation of $N_3$Phe

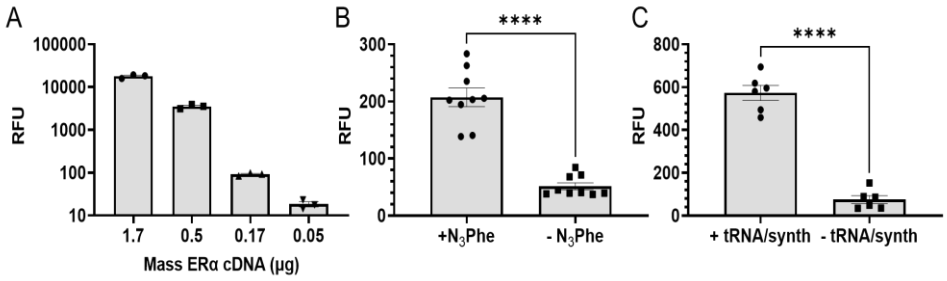


**Figure A1.3 Verifying the presence of functional ERα**. *(A)* Intensity from the luciferase assay is directly dependent on the amount of ERα transfected into the HEK193T cells. In this assay, wild-type ERα was used. *(B)* When cells are transfected with ERα[H516TAG] and the $N_3$Phe tRNA/synthetase, the presence of $N_3$Phe in the cell media significantly increases ERα activity. *(C)* In cells treated with $N_3$Phe and transfected with ERα[H516TAG], there is a dependence on also transfecting the $N_3$Phe tRNA and synthetase. P-values are calculated from a Student's t test. ****, $p < 0.0001$

## A1.3 Results and Discussion

### *A1.3.1 Incorporating $N_3$Phe into functional ERα*

As mentioned in the introduction of this thesis, NCAAs can be incorporated into proteins by providing the system with an orthogonal tRNA that will recognize a stop codon and an orthogonal synthetase to charge the tRNA with the desired NCAA.[11] However, there are instances (similar to the difficulties detailed in Chapter 2) where regions of proteins will not accept NCAAs, or the protein will cease to function with certain mutations. Since $N_3$Phe is an aromatic amino acid and we wished to probe the dimerization interface, we decided to test His516. His516 is on helix 12 on ERα, which spans the dimerization interface (**Figure A1.1**). To incorporate $N_3$Phe at the 516 residue, we mutated this codon to TAG so that our orthogonal synthetase could incorporate $N_3$Phe at this position.[12]

To verify that our mutated ERα was functional, we also expressed a luciferase protein that depended on ERα binding to an ERE on the luciferase vector for expression. In experiments where we tranfected wild-type ERα, luciferase intensity was directly related to the amount of ERα plasmid used (**Figure A1.3A**). In cells transfected with ERα[His516TAG], we found that cells treated with media

spiked with $N_3$Phe had greater intensity than those not supplied with the NCAA (**Figure A1.3B**). Finally, we found significantly greater chemiluminescence from cells transfected with ERα[His516TAG] and the $N_3$Phe tRNA/synthetase over those not transfected with the tRNA/synthetase (**Figure A1.3C**). We note that the luciferase measurements were orders-of-magnitude higher with the wild-type ERα than the $N_3$Phe incorporated ERα. This suggests that NCAA incorporation is rather inefficient.

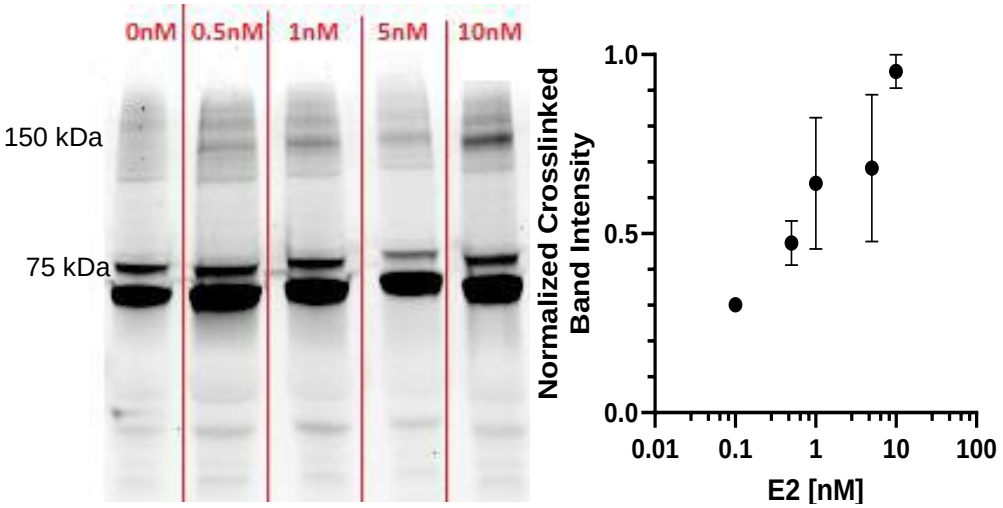


**Figure A1.4 Dimerization increases with increasing concentrations of E2.** HEK293T cells were transfected with ERα[His516TAG] and the $N_3$Phe tRNA/synthetase. 24 hours after transfection, 10 nM E2 was added. 24 hours post E2 addition, cells were irradiated with 365 nm light to induce crosslinking, lysed, and ran on a protein gel. Bands were detected by exciting and capturing GFP fluorescence. *(A)* Representative protein gel demonstrating that dimerization (as represented by the 150 kDa band) increases with increasing concentrations of E2. *(B)* Quantification of these protein gels.

*A1.3.2 Observing ERα dimer bands in protein gels following photocrosslinking*

After determining that we were able to generate functional ERα with $N_3$Phe, we decided to move into crosslinking assays, more specifically, using protein gels to detect higher molecular weight species of ERα (i.e., dimers). We used a vector encoded for ERα[His516TAG] with a green fluorescent protein (GFP) at its N-terminal. We decided to attach GFP at the N-terminal to understand how much

protein got truncated at the TAG codon and see the dimers without immune reagents. We continued with our preliminary experiments by looking at the dependence on the [E2] for dimerization (**Figure A1.4**). One major concern going into these experiments was how GFP would behave in the gel and if we could quantify the data. Fortunately, the data from our assay was consistent with literature precedence.[13-15]

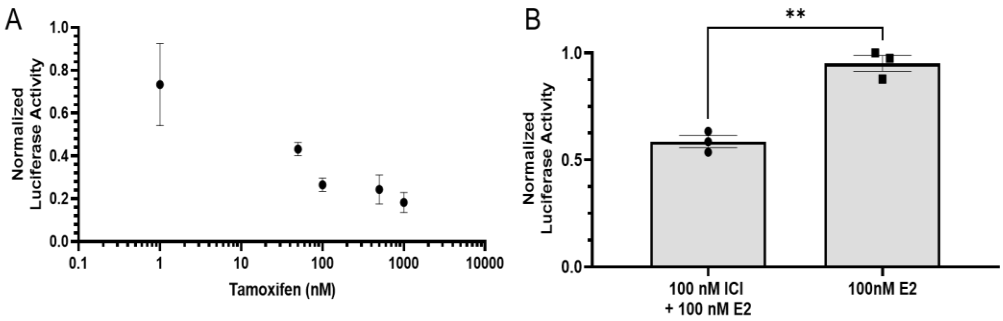


**Figure A1.5** Luciferase activity assays demonstrating that both *(A)* tamoxifen and *(B)* fulvestrant (ICI) inhibit ERα. HEK293T cells were transfected with ERα and a luciferase plasmid whose expression is dependent on ERα activity. P-values were calculated from an unpaired Student's t-test. **, p = 0.001

*A1.3.3 Tamoxifen and fulvestrant induce dimerization*

There have been hypotheses that some of the ERα antagonists inhibit activation by preventing dimerization.[19] Alternately, these ligands may induce dimerization and inhibit ERα's transcriptional activity in other ways.[3,20,21] Here, we decided to use our assay on two of the most popular ERα antagonists, tamoxifen and fulvestrant.

First, we ensured that both antagonists prevent ERα activation via a luciferase assay (**Figure A1.5**). Both antagonists decreased ERα activity, consistent with what we expected to see from these drugs. Next, we decided to put both fulvestrant and tamoxifen through our dimerization assay. Interestingly, we see dimer bands from samples treated with either tamoxifen or fulvestrant (**Figure A1.6**). Both of these results suggest that some downstream step is

inhibited following dimerization. This conclusion is consistent with what others have found regarding activation or inactivation mediated by these antagonists. Arao *et al*. found that a mutation in the C-terminal region (outside the dimerization helix) would change fulvestrant and tamoxifen into agonists.[22] Dimerization via tamoxifen or fulvestrant has been observed before in bioluminescence resonance energy transfer (BRET) experiments.[24] Altogether, we find that both agonists and antagonists are capable of inducing ERα dimerization.

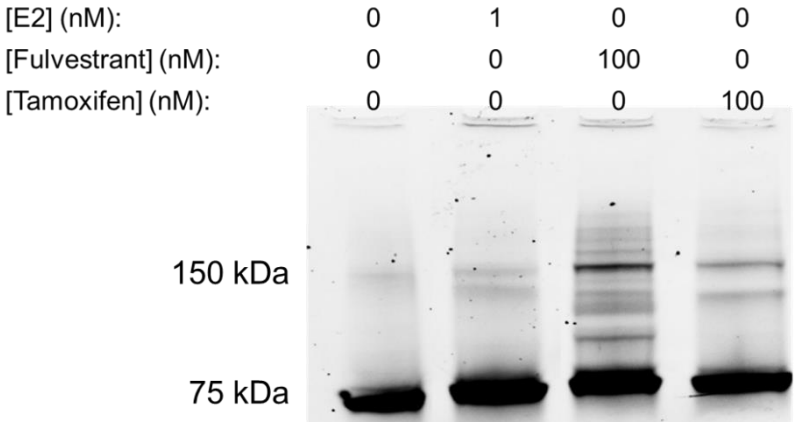


**Figure A1.6** Both tamoxifen and fulvestrant induce dimerization.

*A1.3.4 Observing a non-dimer PPI in the ERα hinge region*

Following the proof-of-concept experiments demonstrating that we can covalently capture PPIs with $N_3$Phe, we decided to move the $N_3$Phe incorporation site to the hinge region. Compared to the DBD and the LDB, the hinge region has garnered less attention, but it is still worthy of investigation.[9,16-18] The hinge region consists of residues between 255-305, and at the moment, there are no complete structures of this region. We tested four different sites within the hinge region and observed PPIs when we incorporated $N_3$Phe at residues 265 or 275 (**Figure A1.7**). We decided to go through with the 275 site since it was closer to the middle of the

hinge region. These protein gels were reproducible, suggesting that this is a real PPI.

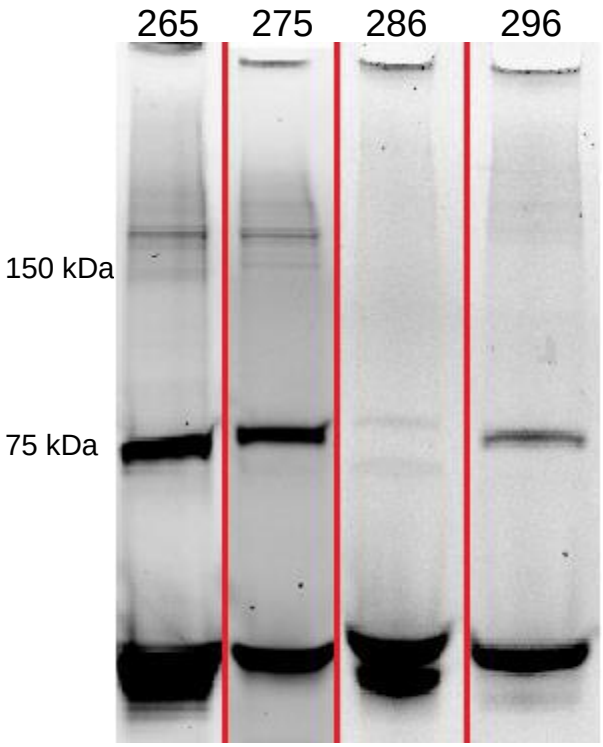


**Figure A1.7 PPIs observed by crosslinking certain residues in the hinge region.** We incorporated $N_3$Phe at residues 265, 275, 285, and 296. We observed bands with $N_3$Phe at 265 and 275 that are slightly above where we observe dimer bands. Bands below the 75 kDa bands are truncated ERα.

We next decided to investigate whether this PPI was a dimerization event. Although the molecular weight of the hinge region PPI would suggest that it is binding to something heavier than ERα, we needed to validate this inference. We decided to generate two ERα plasmids: a GFP-ERα with no TAG mutations and ERα[E275TAG] without GFP (**Figure A1.8**). Under these conditions, we should be able to observe dimerization, but not a non-dimer PPI. Compared to experiments using GFP-ERα[E275TAG], we do not see the same higher molecular weight band when we separate GFP and E275TAG, suggesting that we are not observing a dimerization event.

*A1.3.5 Attempts to identify hinge region PPI using mass spectrometry and immunoblots*

Traditionally, the proteins within a PPI are identified by mass spectrometry, and then their identities are validated via immunoblots. We attempted to use a similar workflow to generate promising candidates via mass spectrometry and test them using immunoblots.

Our initial attempts extended the experiments depicted in **Figure A1.7** by performing an in-gel digest of the bands with the crosslinked ERα. Unfortunately, due to the nature of NCAA mutagenesis and photocrosslinking, the yields from these bands were quite low, and a confident detection could not be made. Even the ERα was fairly low compared to the other proteins identified by mass spectrometry. A major issue is that there was no enrichment, so the gel band contained everything in the cell that migrated at the molecular weight.

For subsequent attempts, we utilized SILAC to help improve the

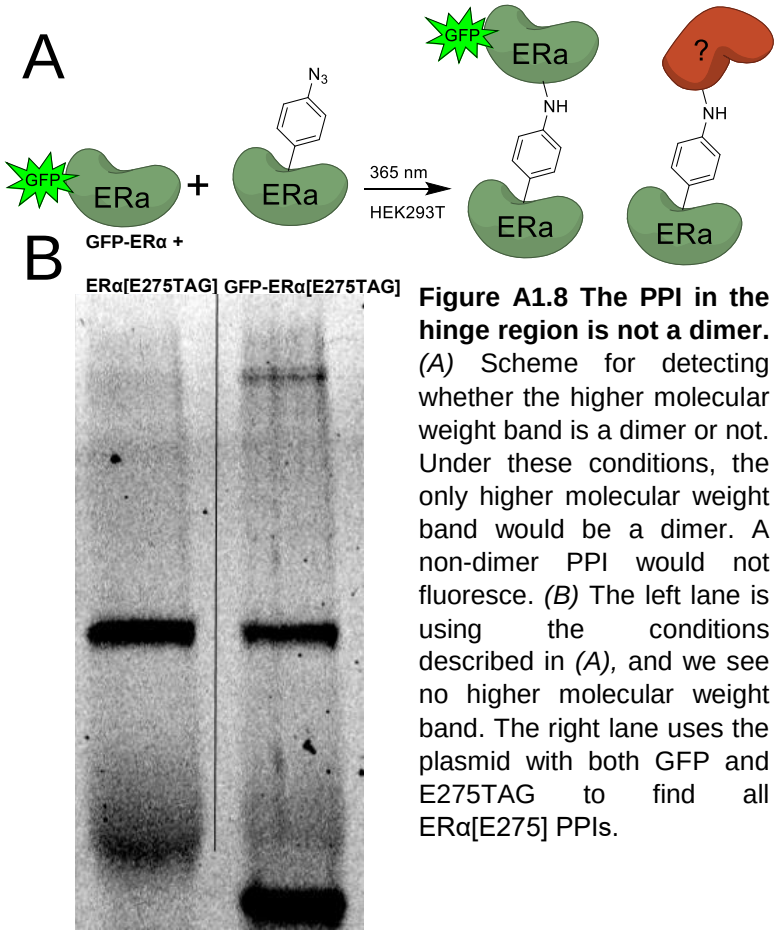


**Figure A1.8 The PPI in the hinge region is not a dimer.** *(A)* Scheme for detecting whether the higher molecular weight band is a dimer or not. Under these conditions, the only higher molecular weight band would be a dimer. A non-dimer PPI would not fluoresce. *(B)* The left lane is using the conditions described in *(A),* and we see no higher molecular weight band. The right lane uses the plasmid with both GFP and E275TAG to find all ERα[E275] PPIs.

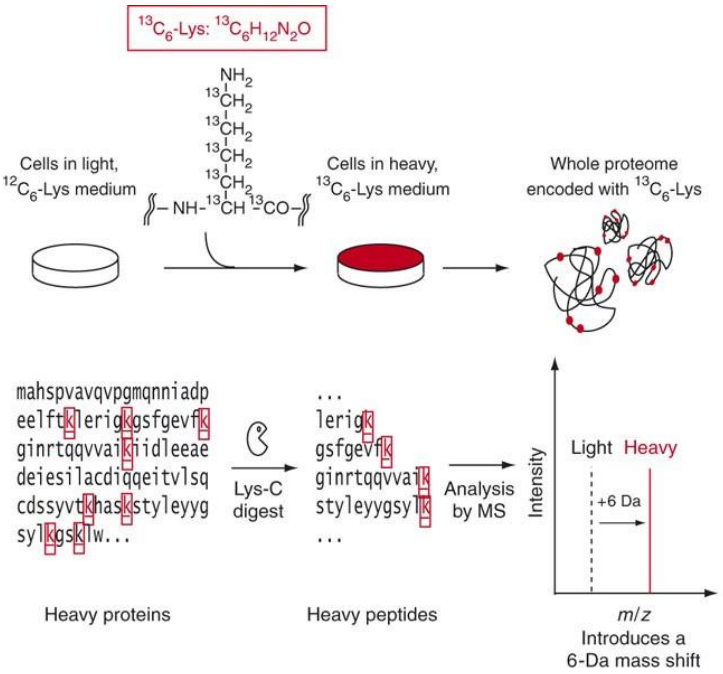


**Figure A1.9** Brief summary of SILAC protocol to differentiate proteins within a sample. Adopted from Ong 2006.

signal-to-noise ratio. In unlabeled experiments, we had no way to know what proteins were "background" and which could be targets due to the low concentrations of the proteins in the band. [25] One can run controls, but this requires cutting another band, and it is nearly impossible to perfectly repeat the gel electrophoresis (protein migration will differ from lane to lane) and the gel cutting. In SILAC experiments, one sample is grown in "heavy" media, which contains some amino acids made with $^{15}N$ and $^{13}C$ (**Figure A1.9**). Since these amino acids will contain heavier proteins, the peptides detected in the mass spectrometer can be differentiated from the peptides produced from cells incubated in standard media. We utilize this technique in order to use one lane for both the experimental and the control samples. SILAC experiments will allow us to have perfect replication between the gel electrophoresis and gel cutting steps with both the experimental and control sample.

We were able to get strong incorporation of the heavy amino acids into our experimental samples (>98% of proteins had heavy amino acids), but it did not significantly improve our ability to identify hits. One small exception was the heat

shock protein 90 (Hsp90), which consistently showed up in our experimental samples. We were further encouraged to evaluate Hsp90 because Hsp90 is a chaperone for ERα.[26,27] Unfortunately, when we probed a protein blot with anti-Hsp90, we only observed a band corresponding to the Hsp90 monomer, suggesting that the antibodies worked and the ERα[E275TAG] PPI partner was not Hsp90.

**A1.4 Conclusion**

We made some strides in developing a new dimerization assay that is not directly dependent on mass spectrometry, immunoblots, or resonance energy transfer assays. The innovation in our approach is that we know the product of the photocrosslinking by selectively placing the $N_3$Phe in a place where only dimerization can occur. Indeed, we only observed dimerization as the major bands we could identity were the truncated ERα, full-length ERα, and dimerized ERα. We envision that this strategy could be applied to many other dimerization events since dimerization is a common step in various activation mechanisms.

We could also do more conventional photocrosslinking experiments where we discovered a potentially unknown PPI in the ERα hinge region. Unfortunately, the concentration of the crosslinked product was insufficient for definitive identification of the protein partner, even in our SILAC experiments. Future efforts will probably go into a different biological system where protein yields can be greater. Precedence suggests moving into bacteria for these experiments to get significantly more protein since bacteria is easier to grow than human cells. Alternately, we could attempt other enrichment strategies. We briefly attempted to use a 6xHis tag to selectively pull-down ERα, but our purification was unsatisfactory. This is again likely a result of poor protein yields. Lastly, we can

move to another protein that has behaved better in photocrosslinking experiments. We believe that identifying PPIs via photocrosslinking NCAAs is an interesting and precise method that we hope to use in the future.

## A1.5 Materials and Methods

### *A1.5.1 Transfection and protein gels*

eGFP-ERα was expressed in pcDNA3.1(+), and mutations were accomplished via QuikChange (Stratagene). The orthogonal aminoacyl-tRNA synthetase/tRNA pair was encoded in a pU6 plasmid (a gift from Professor Michelle Krogsgaard). Transfections were conducted when cells were 50% confluent in a 35 mm-petri dish using 3 μL Xfect polymer(Takara), 7.5 ng ERα plasmid, 2.5 ng synthetase plasmid, and Xfect buffer up to 100 μL in 1 mL DMEM media (with 10% FBS, 100 U/mL penicillin and 100 U/mL streptomycin). Three hours after the addition of the Xfect solution, the media was replaced with 3 mL DMEM (with 10% FBS, 100 U/mL penicillin, 100 U/mL streptomycin) and 0.5 mM $N_3$Phe. Cells were incubated for 24 hours before the addition of E2 and were incubated for another 24 hours. Next, the media was replaced with media that did not contain $N_3$Phe, and the plates were subjected to a 365 nm LED illumination rated for 1 W for 20 min. The media was then removed, and the cells were lysed with 1% SDS or Luciferase Lysis Buffer (Promega) and sonicated. These cell lysates were then used without purification on MiniProtean TGX Any kD PAGE precast gels (Bio-Rad). Gels were run for 1 hour at 150 V and then imaged on a Typhoon FLA 9000 (General Electric) with 473 nm laser excitation and an LPB (510LP) detection filter to detect eGFP fluorescence.

*A1.5.2 Mass spectrometry*

After visualizing the desired band on a protein gel, the band was cut from the gel. The proteins were reduced by incubating the gel piece in 10 mM dithiothreitol (DTT) in 100 mM ammonium bicarbonate for 30 minutes at 50 °C. The reducing solution was then removed, and the proteins were alkylated by incubating the gel piece in 55 mM iodoacetamide in 100 mM ammonium bicarbonate for twenty minutes in the dark. The alkylating solution was then removed. The gel piece was dehydrated by washing the gel in 50 mM ammonium bicarbonate and then with acetonitrile until the gel piece became opaque white. The gel piece was further evaporated under vacuum for 3 minutes. Next, the proteins were digested with a 6 ng/µL trypsin solution. The gel piece was incubated in this solution for 20 minutes before the excess solution was removed, and the gel piece was kept in a minimal volume of 50 mM ammonium bicarbonate to digest overnight at 37 °C. The supernatant was collected and the peptides were further extracted by adding, then removing, 1% formic acid/2% acetonitrile, 1:1 acetonitrile/water, and then 1% formic acid in acetonitrile. The pooled extracted peptides were dried under vacuum and desalted using a ZipTip® (MilliporeSigma). Samples were run on an OrbiTrap Elite (Thermo).

## *A1.6 References*


1 Alkabban, F. M. & Ferguson, T. *Breast Cancer* in *StatPearls* (StatPearls Publishing Copyright © 2021, StatPearls Publishing LLC., 2021).

2 Crew, K. D., Albain, K. S., Hershman, D. L., Unger, J. M. & Lo, S. S. How do we increase uptake of tamoxifen and other anti-estrogens for breast cancer prevention? *NPJ Breast Cancer* **3**, 20, doi:10.1038/s41523-017-0021-y (2017).

3 Arao, Y. & Korach, K. S. The F domain of estrogen receptor α is involved in species-specific, tamoxifen-mediated transactivation. *J. Biological Chemistry* **293**, 8495-8507, doi:10.1074/jbc.RA117.001212 (2018).

4 Schwabe, J. W., Chapman, L., Finch, J. T. & Rhodes, D. The crystal structure of the estrogen receptor DNA-binding domain bound to DNA: how receptors discriminate between their response elements. *Cell* **75**, 567-578, doi:10.1016/0092-8674(93)90390-c (1993).

5 Tanenbaum, D. M., Wang, Y., Williams, S. P. & Sigler, P. B. Crystallographic comparison of the estrogen and progesterone receptor's ligand binding domains. *PNAS* **95**, 5998-6003, doi:10.1073/pnas.95.11.5998 (1998).

6 Fratev, F. Activation helix orientation of the estrogen receptor is mediated by receptor dimerization: evidence from molecular dynamics simulations. *Phys. Chem. Chem. Phys.* **17**, 13403-13420, doi:10.1039/c5cp00327j (2015).

7 Klinge, C. M. Estrogen receptor interaction with estrogen response elements. *Nucleic Acids Res.* **29**, 2905-2919, doi:10.1093/nar/29.14.2905 (2001).

8 Motlagh, H. N. & Hilser, V. J. Agonism/antagonism switching in allosteric ensembles. *PNAS* **109**, 4134-4139, doi:10.1073/pnas.1120519109 (2012).

9 Zwart, W. *et al.* The hinge region of the human estrogen receptor determines functional synergy between AF-1 and AF-2 in the quantitative response to estradiol and tamoxifen. *J. Cell Sci.* **123**, 1253-1261, doi:10.1242/jcs.061135 (2010).

10 Burns, K. A., Li, Y., Liu, L. W. & Korach, K. S. Research resource: Comparison of gene profiles from wild-type ERα and ERα hinge region mutants. *Molecular Endocrinology* **28**, 1352-1361, doi:10.1210/me.2014-1122 (2014).

11 Ellman, J., Mendel, D., Anthonycahill, S., Noren, C. J. & Schultz, P. G. Biosynthetic method for introducing unnatural amino acids site-specifically into proteins. *Method Enzymol.* **202**, 301-336, doi:10.1016/0076-6879(91)02017-4 (1991).

12 Wang, W. *et al.* Quantitative analysis of T cell receptor complex interaction sites using genetically encoded photo-cross-linkers. *ACS Chemical Biology* **9**, 2165-2172, doi:10.1021/cb500351s (2014).

13 Rich, R. L. *et al.* Kinetic analysis of estrogen receptor/ligand interactions. *PNAS* **99**, 8562-8567, doi:10.1073/pnas.142288199 (2002).

14 D'Auria, S. *et al.* Tumor-specific protein human galectin-1 interacts with anticancer agents. *Mol. Biosyst.* **5**, 1331-1336, doi:10.1039/b905921k (2009).

15 Petrova, L. *et al.* Binding of antitumor compounds to wheat protein. *Biotechnol. Biotechnol. Equip.* **27**, 3857-3860, doi:10.5504/bbeq.2013.0025 (2013).

16 Burns, K. A., Li, Y., Arao, Y., Petrovich, R. M. & Korach, K. S. Selective mutations in estrogen receptor α D-domain alters nuclear translocation and non-estrogen response element gene regulatory mechanisms. *J. Biological Chemistry* **286**, 10, doi:10.1074/jbc.M110.187773 (2011).

17 Carlier, L. *et al.* Biophysical studies of the interaction between calmodulin and the R-287-T-311 region of human estrogen receptor α reveals an atypical binding process. *Biochem. Biophys. Res. Commun.* **419**, 356-361, doi:10.1016/j.bbrc.2012.02.028 (2012).

18 Leiber, D. *et al.* The sequence Pro(295)-Thr(311) of the hinge region of oestrogen receptor α is involved in ERK1/2 activation via GPR30 in leiomyoma cells. *Biochem. J.* **472**, 97-109, doi:10.1042/bj20150744 (2015).

19 Robertson, J. F. ICI 182,780 (Fulvestrant)--the first oestrogen receptor down-regulator--current clinical data. *British Journal of Cancer* **85 Suppl 2**, 11-14, doi:10.1054/bjoc.2001.1982 (2001).

20 Tamrazi, A., Carlson, K. E., Daniels, J. R., Hurth, K. M. & Katzenellenbogen, J. A. Estrogen receptor dimerization: Ligand binding regulates dimer affinity and dimer dissociation rate. *Molecular Endocrinology* **16**, 2706-2719, doi:10.1210/me.2002-0250 (2002).

21 Carlson, R. W. The history and mechanism of action of fulvestrant. *Clinical Breast Cancer* **6 Suppl 1**, S5-8, doi:10.3816/cbc.2005.s.008 (2005).

22 Arao, Y., Hamilton, K. J., Coons, L. A. & Korach, K. S. Estrogen receptor α L543A,L544A mutation changes antagonists to agonists, correlating with the ligand binding domain dimerization associated with DNA binding activity. *J. Biological Chemistry* **288**, 21105-21116, doi:10.1074/jbc.M113.463455 (2013).

23 Arnal, J. F. *et al.* Membrane and nuclear estrogen receptor α actions: from tissue specificity to medical implications. *Physiol. Rev.* **97**, 1045-1087, doi:10.1152/physrev.00024.2016 (2017).

24 Powell, E. & Xu, W. Intermolecular interactions identify ligand-selective activity of estrogen receptor α/β dimers. *PNAS* **105**, 19012-19017, doi:10.1073/pnas.0807274105 (2008).

25 Ong, S. E. *et al.* Stable isotope labeling by amino acids in cell culture, SILAC, as a simple and accurate approach to expression proteomics. *Mol. Cell. Proteomics* **1**, 376-386, doi:10.1074/mcp.M200025-MCP200 (2002).

26 Powell, E., Wang, Y., Shapiro, D. J. & Xu, W. Differential requirements of Hsp90 and DNA for the formation of estrogen receptor homodimers and heterodimers. *J. Biological Chemistry* **285**, 16125-16134, doi:10.1074/jbc.M110.104356 (2010).

27 Dhamad, A. E., Zhou, Z. Q., Zhou, J. H. & Du, Y. C. Systematic proteomic identification of the heat shock proteins (Hsp) that interact with estrogen receptor α (ERα) and biochemical characterization of the ERα-Hsp70 interaction. *PLoS One* **11**, 19, doi:10.1371/journal.pone.0160312 (2016).